Aalto University
School of chemical engineering

ATTE-MAINIO HARRIKARI

MULTIVARIATE ANALYSIS OF HEAT TRANSFER IN ICE RINKS WITH CARBON DIOXIDE AS A REFRIGERANT

Submitted for examination as a thesis for a master's degree in engineering.

31.07.2020

Tekijä Atte-Mainio Harrikari

Työn nimi LÄMMÖN SIIRTYMISEN MONIMUUTTUJA-ANALYYSI JÄÄKENTISSÄ HYÖDYNTÄEN HIILIDIOKSIDIA JÄÄHDYTYSFLUIDINA

Maisteriohjelma Advanced Energy Solutions – Industrial Energy Processes and Sustainability   **Koodi** CHEM26

Työn valvoja Professori Mika Järvinen

Työn ohjaaja(t) Diplomi-insinööri Santeri Siren

Päivämäärä 31.07.2020   **Sivumäärä** 90 + 13   **Kieli** Englanti

Tämän diplomityön tavoitteena on rakentaa työkalu, jolla voidaan optimoida hiilidioksidia jäähdytysfluidina käytettäviä luistinratoja. Aihetta lähestytään pumppukiertoisen jäädytysjärjestelmän tarkastelulla, jäähän kohdistuvan lämpörasitteen määrittelyllä sekä yksityiskohtaisella jääkentän rakenteen kuvailulla.

Työkalu ja diplomityö on jaettu kolmeen osioon, jotka kuvaavat lämmön johtumista 2D-tasossa, märkähöyrysteisen hiilidioksidin sekä glykoliseoksen käyttäytymistä putkissa, ja materiaalien termodynaamisia ominaisuuksia. Työ esittelee kattavan teoreettisen pohjan, joiden avulla osiot rakennetaan Microsoft EXCEL® ja COMSOL Multiphysics® alustoille VBA-ohjelmointikielen avulla. Työn toteutusosio sisältää yli 2700 riviä ohjelmointikoodia, mutta työ esittelee vain pääpiirteet työkalun toteutuksesta.

Lämmön johtuminen 2D-tasossa mallinnetaan lämpövastusverkkoja (TRN) sekä numeerista simulaatiota hyödyntäen kahden eri konfiguraation kautta. Lisäksi nesteiden käyttäytymistä putkissa tarkastellaan monimuuttuja-analyysin avulla tehokkaita iteratiivisia funktioita käyttäen. Lopuksi materiaalien termodynaamisten ominaisuuksien määritelmistä rakennettua materiaalikirjastoa arvioidaan kriittisesti eri näkökulmista.

Tuloksista ilmenee, että työkalua voidaan käyttää jäähallien suunnittelussa erittäin tarkasti. Toteutusvaiheen muuttuvia sekä kiinteitä kustannuksia voidaan vähentää merkittävästi ja niiden ratkaisut voidaan perustella teoreettisen viitekehyksen kautta. Esimerkiksi numeerisen simulaation ja lämpövastusverkkojen tulos poikkeaa $0.068\ K$ jään pinnalla, jos lämpövuo jäähän on $112.7\ W/m^2$. Lisäksi työkalu kykenee minimoimaan routasulatusputkien tarvittavan lämpötehon 5.43 kilowattiin. Tulokset riippuvat voimakkaasti muiden parametrien arvoista ja siksi tämä diplomityön kirjallinen osio ei anna suoria vastauksia ihanteellisiin ratkaisuihin mutta kertoo, minkälaiset ratkaisut olisivat tulevaisuudessa eduksi.

Avainsanat #icerink #refrigerant #COMSOL #CO2 #brine #pipe #module #vba #flow #conduction #convection #multivariate #analysis #heat #programming #optimization

Author Atte-Mainio Harrikari

Title of thesis MULTIVARIATE ANALYSIS OF HEAT TRANSFER IN ICE RINKS WITH CARBON DIOXIDE AS A REFRIGERANT

This thesis aims to build a tool which can be used to design and optimize CO_2-based ice rinks. The topic is approached by the introduction of a direct-controlled refrigeration system, the definition of heat load on the ice, and a detailed description of the structure of the ice rink.

The tool and the thesis are divided into three modules, which describe the conduction of heat in the 2D plane, the behavior of carbon dioxide and brines in pipes, and the thermodynamic properties of materials. The work presents a comprehensive theoretical framework for building the modules constructed on Microsoft EXCEL® and COMSOL Multiphysics® platforms using the VBA programming language. The implementation of the work contains more than 2,700 lines of code. However, the work presents only the main features of the implementation.

Heat conduction is modeled by thermal resistance networks (TRN) and a numerical simulation through two different configurations. Besides, the behavior of fluids is examined using multivariate analysis utilizing efficient functions and a constant heat approach. Finally, a material library constructed by the definitions of the thermodynamic properties is critically examined from alternate perspectives.

The results show that the tool can be used to design ice rinks with high accuracy. The variable and fixed costs can be significantly reduced, and the solutions can be justified through a robust theoretical framework. For example, the results of the numerical simulation and thermal resistance networks deviate only $0.068\ K$ on top of the ice with the heat flux of $112.7\ W/m^2$. Moreover, the tool is capable of minimizing the required heat of the heating pipes to $5.43\ kW$. The presented results are dependent on other parameters. Therefore, this paper does not give direct answers to the ideal solutions but tells in which direction the development should continue.

PREFACE

This thesis acts for a master's degree in engineering, which has been funded by Ramboll Finland Oy. Furthermore, the thesis is done in the school of Chemical Engineering at Aalto University.

First, I want to thank Ramboll Finland Oy and Aalto university for all the help I have gained during the study. The company has delivered some critical perspectives from experience concerning the subject, which I have identified as valuable information. For example, it has been a pleasure to discuss the topic with Timo Reikko, Onni Ojala, and Jani Visunen, whom all three work with a refrigerator system in various projects. Furthermore, I want to thank Juho Ruotamäki, Juhana Mikkola, and Toni Wasenius. Discussion with them at the early stages of the study made it possible. Moreover, I would also like to thank my supervisor, Professor Mika Järvinen from Aalto University, and my advisor Santeri Siren from Ramboll Finland, for the invaluable feedback and support throughout the entire process.

Corona epidemic has given me much time to write. My primary motivation for writing has been the idea of an added value to the company and helping those who design ice rinks in their everyday life. Most of all, I want to thank my friends, family, and girlfriend, Erika, who have believed in me and my project through frustrating and challenging times.

Helsinki 31.7.2020

Atte-Mainio Harrikari

CONTENT

NOMENCLATURE

Symbol	Description	SI Unit
A	Surface area	m^2
C	Thermal conductance, the inverse of thermal resistance R	K/W
D	Diameter	m
G	Flow rate per surface area	$kg/(s \cdot m^2)$
H	Enthalpy	J/kg
ΔH	Change in enthalpy	J/kg
K	A factor for minor pressure loss	—
M	Molar mass	kg/mol
P	Perimeter	m
Q	Heat	J
$\dot{Q}$	Rate of heat	J/s
R	Thermal resistance, the inverse of thermal conductance C	W/K
S	Shape factor for heat conduction	—
T	Temperature	K
$\bar{T}$	Mean temperature	
ΔT	Temperature difference	K
W	Work	J/s
X	Indicator for a thermophysical property. Can be ρ, c_p or λ, for example.	
a	Parameter of the thermophysical function	—
b	Parameter of the thermophysical function	—
c	Parameter of the thermophysical function	—
c_p	Specific isobaric heat capacity	$J/(kg \cdot K)$
d	Distance	m
h	Height	m
l	Length	m
m	Mass	kg
$\dot{m}$	Mass flow rate	kg/s
n	Number of datapoints	—
p	Pressure	Pa
$\dot{q}$	Heat flux	$J/(s \cdot m^2)$
r	Radius	m
s	Slip factor, a ratio of velocities between vapor and liquid	—
v	Velocity	m/s
$\bar{v}$	Mean velocity	m/s

x	Vapor quality or mass fraction	—
y	Mole fraction of a component	—
z	Distance from the beginning of the pipe	m

Constants

Constant	Description	Value	SI Unit
g	Gravitational constant	9.80665	m/s^2
$\tilde{R}$	Universal gas constant	8.31446262	$J/(mol \cdot K)$
π	Pi	3.14159265	—

Greek letters

Symbol	Description	SI Unit
Φ_{L0}^2	A two-phase multiplier for pressure	—
α	Heat transfer coefficient	$W/(m \cdot K)$
ε	Void fraction	—
ϵ	The roughness of the pipe	—
η	Viscosity	$Pa \cdot s$
γ	A linear parameter in transition flow	—
λ	Thermal conductivity	$W/(m \cdot K)$
ρ	Density	kg/m^3
ϕ	Porosity of concrete	—
φ	Relative humidity of humid air	—
σ	Surface tension	N/m
τ	Shear stress	$N \cdot m^2$
θ	Degree of branching of polyethylene	—
ζ	Darcy Friction factor	—

Subscripts

Symbol	Description
ac	Acceleration
C	Convection
c	Characteristic; refers to the characteristic length L_c
CP	Cooling pipe
cr	Critical point or state
DA	Dry air
eq	Equilibrium
f	Fluid
fr	Friction
GL	Glycol; denotes ethylene glycol MEG or propylene glycol PEG
gr	Gravity
HA	Humid air
HP	Heating pipe
i	Index or value at a given index
in	Into the system
L	Liquid
$L0$	The fluid is treated as if only the liquid is flowing through the tube
mix	Mixture
nb	Nucleate boiling
NVG	Net vapor generation point
NWC	Normal weight concrete
ONB	The onset of nucleation boiling point
out	Out from the system
PC	Porous concrete
r	Relative
RS	Reinforcement steel/rebar
s	Steam
sat	Saturation state or region
sub	Subcooled state or region
tr	Triple point
us	Unsaturated state or region
V	Vapor
$V0$	The fluid is treated as if only the vapor is flowing through the tube
vap	Vaporization; refers to the enthalpy of vaporization
w	Value at the tube wall
W	Water
z	At length z

Abbreviations

Symbol	Description
HFC	Hydrofluorocarbon
PFC	Perfluorocarbon
EOS	Equation of state
SFS	Finnish Standards Association
GWP	Global Warming Potential
HTC	Heat transfer coefficient
LHTC	Local heat transfer coefficient
LDPE	Low-density polyethylene
HDPE	High-density polyethylene
NWC	Normal weight concrete
RRR	Residual resistivity ratio
TRN	Thermal resistance network
XLPE	Cross-linked polyethylene
ONB	The onset of nucleate boiling
NVG	Net vapor generation

Dimensionless numbers

Symbol	Description	Equation	Alternatives
Fr	Froude number	$\dfrac{G^2}{\rho^2 g l_c}$	$Fr_{L0} = \dfrac{G^2}{\rho_L^2 g D}$
We	Weber number	$\dfrac{G^2 l_c}{\rho \sigma}$	$We_L = \dfrac{G^2 D}{\rho_L \sigma}$
Bo	Boiling number	$\dfrac{\dot{q}}{G \Delta H_{vap}}$	
Re	Reynolds number	$\dfrac{\rho v l_c}{\eta}$	$Re_L = \dfrac{(1-x)GD}{\eta_L}$
Nu	Nusselt number	$\dfrac{h l_c}{\lambda}$	
Pr	Prandtl number	$\dfrac{c_p \eta}{\lambda}$	$Pr_L = \dfrac{c_{pL} \eta_L}{\lambda_L}$
Bd	Bond number	$\dfrac{g(\rho_L - \rho_V) l_c^2}{\sigma}$	
La	Laplace number	$\sqrt{\dfrac{\sigma}{g(\rho_L - \rho_V)}} \cdot l_c^{-1}$	

1   INTRODUCTION

Designing multipurpose halls with ice rinks requires special attention paid to energy systems. Building an ice rink involves a refrigeration system which maintains the surface at a constant temperature, while an external heat is applied. The system involves high investment, manufacturing, and operating costs and needs a proper design to operate.

Using a direct-controlled refrigeration system with carbon dioxide has gained interest in recent years. The system offers excellent energy efficiency and simplicity compared to the traditional indirect refrigeration system. However, it has higher fixed costs and needs professional skills to install. Moreover, carbon dioxide is safe, friendly to the environment, and it has a low cost. If the system is optimized correctly, it will lead to lower costs, better energy management, and improved safety.

This thesis aims to construct a tool which can be used to optimize direct-controlled ice rinks when carbon dioxide is used as a refrigerant. This introduction defines the overall heat load to the ice and presents the principle of the direct-controlled refrigeration system. The structure of the ice rink is visualized in more detail, and the suitability of carbon dioxide as a refrigerant is discussed. Finally, the scope and structure of the thesis are presented.

1.1   Energy systems of the ice rink

A simplified arrangement of a multipurpose hall with ice rink is presented in Figure 1 with various heat loads. Convection of air, radiation by various surfaces, lightning, condensation of water by humid air, and resurfacing of the ice are primary contributors of heat load to the ice. Additionally, work by the pump, the heat of people, and accumulation of frost on headers compile a small portion of the required energy by the refrigerator system.
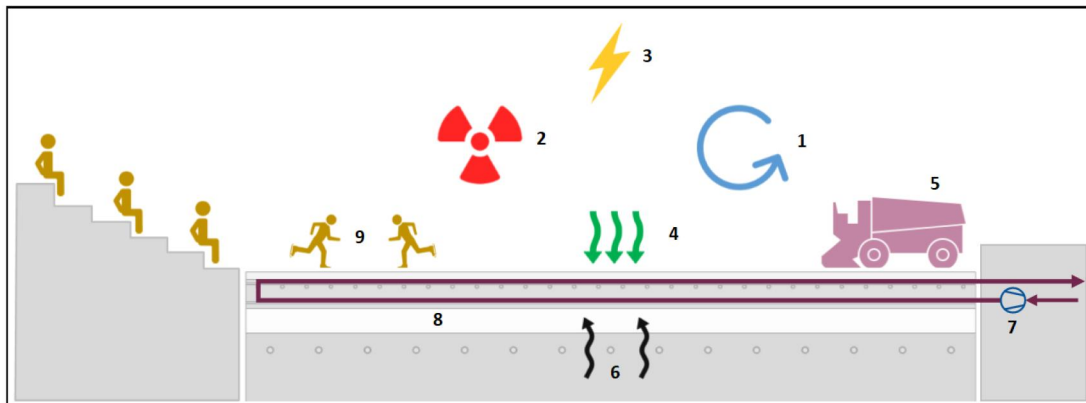

Figure 1. Heat loads of ice-rinks. 1: Convection, 2: Radiation, 3: Lightning, 4: Condensation of water by humid air, 5: Ice resurfacing, 6: Heat by heating pipes and ground conduction, 7: Pump work, 8: Accumulation of frost on headers, 9: Excess heat by people.

A total heat load of ice consists of several factors. Fortunately, the research suggests many approaches to estimate the overall heat loads on the ice rinks (See Bellache, Ouzzane, and Galanis, 2005; Daoud, Galanis, and Bellache, 2008; Seghouani, Daoud and Galanis, 2009; Karampour, 2011). Figure 2 illustrates the average seasonal shares of heat load by two indoor ice rinks located in Edmonton and Pittsburgh (Sunyé et al., 2007; ASHRAE Handbook: Refrigeration. SI Edition, 2018, chap. 44: Ice rinks). Radiation and convection contribute most of the load. Furthermore, the effect of condensation becomes a more substantial factor when the outdoor temperature rises. The geographical location of the ice rink plays a vital role as well.
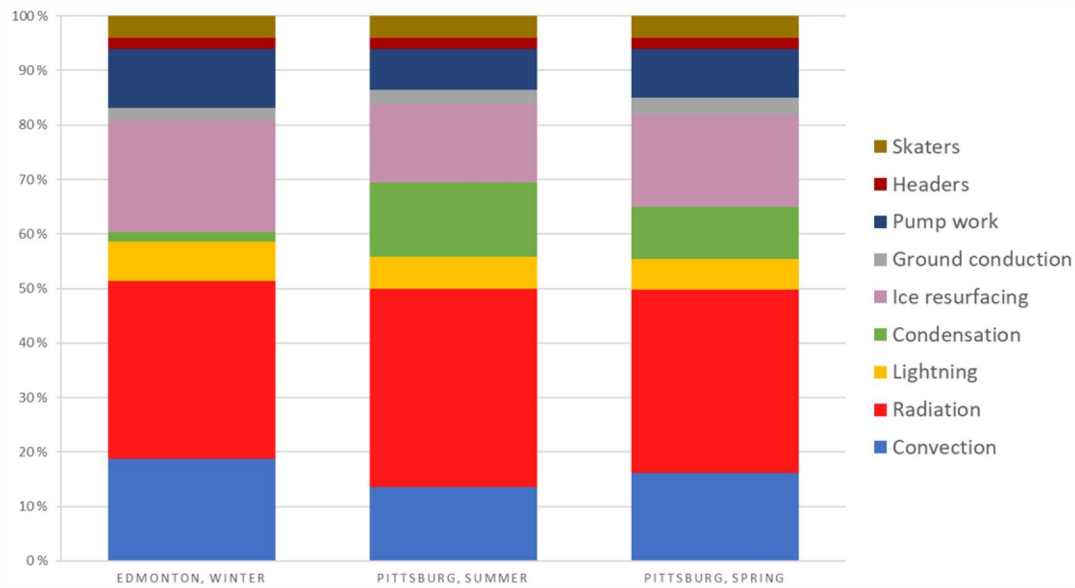
Figure 2. Estimation of heat loads by shares on ice rinks during winter, summer, and spring.

The ice rink requires a refrigeration system that can be characterized by an inverse Rankine cycle, the operation principle of which is illustrated in Figure 3. The compressor uses work to increase the pressure of the vapor in phase $(1 \rightarrow 2)$. The vapor moves to a condenser unit in which releases heat as the vapor condenses back to liquid $(2 \rightarrow 3)$. Furthermore, the liquid migrates into the expansion unit in which the pressure is reduced, partially vaporizing the liquid $(3 \rightarrow 4)$. Finally, the vapor-liquid mixture is fully evaporated by the evaporator unit, and the heat is absorbed from the environment $(4 \rightarrow 1)$. The cycle starts again while the fluid moves into the compressor.

Figure 3. Operation principle of fundamental inverse Rankine cycle.
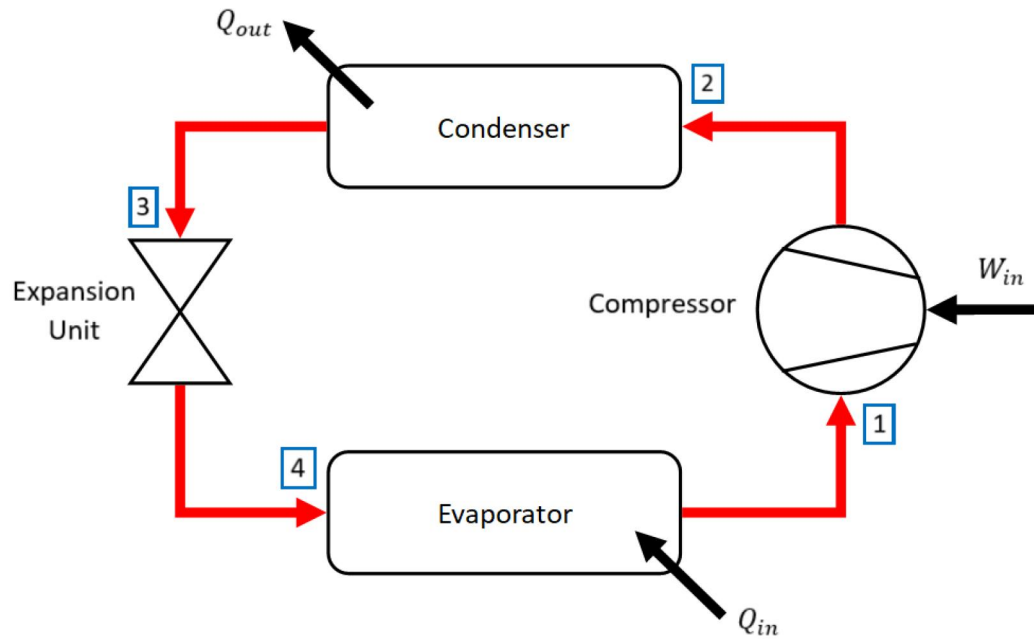Q_{in} *indicates the overall heat load on the evaporator.*

Most of the ice rinks use an indirect refrigeration system. The secondary refrigerant maintains the ice, and the primary refrigerant never leaves from the refrigeration unit. Only heat is transferred between the refrigerants. However, in the direct-controlled system, the secondary refrigerant is eliminated. The primary refrigerant is pumped directly under the ice, which circulates through the refrigeration unit as well.

The principle of a direct-controlled circulation system is illustrated in Figure 4.[1] After the expansion $(3 \rightarrow 4)$ the vapor-liquid mixture is directed to a vapor-liquid separator known as a chiller where the mixture is separated into liquid and vapor. The liquid is directed to the pump $(4 \rightarrow 5)$ and the vapor is directed to the compressor $(4 \rightarrow 1)$. Moreover, the liquid is pumped into the ice rink where the evaporation occurs $(5' \rightarrow 6)$. The increase in pressure by the pump from point (5) to point $(5')$ is usually measured to compensate for the pressure loss of the pipes inside the ice rink. (Hakala and Kaappola, 2007, p. 189)

---

[1] The operation principle of Figure 3 is included in Figure 4. For clearance, the operation of inverse Rankine cycle is presented with **red arrows** in Figures 3, 4, 5, and 6. Additionally, the **blue arrows** marks the inlet to the ice rink, and **green arrows** indicates the flow out and inside the ice rink.
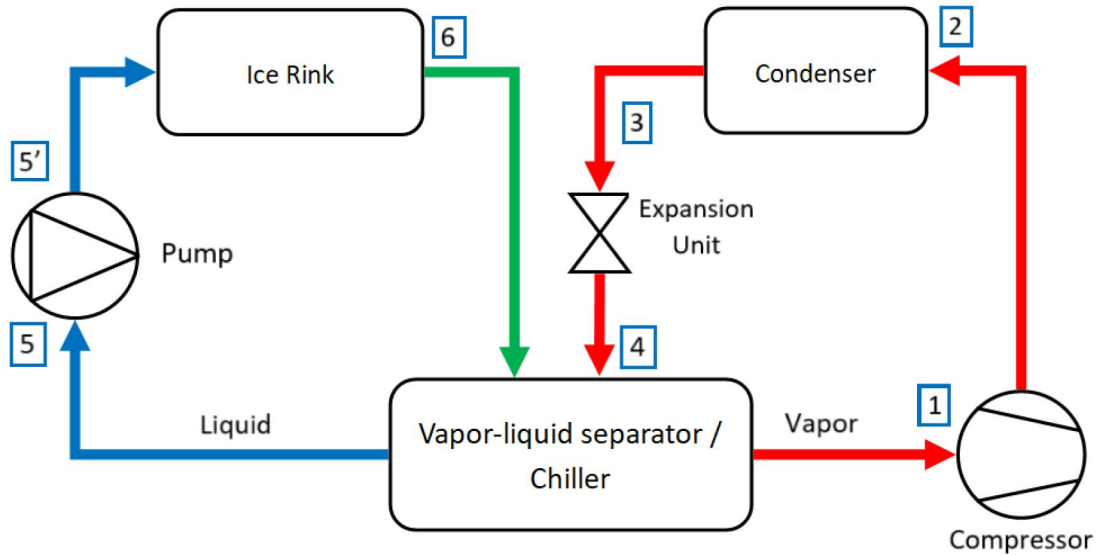
Figure 4. Operation principle of the controlled circulation system.

Figure 5 visualizes a logarithmic phase diagram by functions of pressure and enthalpy, which is specific for carbon dioxide. The purpose of the diagram is to describe the enthalpy changes in different parts of the circulation system. The red arrows represent the basic operation cycle of the inverse Rankine cycle, which were also portrayed in Figure 3 and Figure 4. The extension of the direct-controlled circulation system with points (5), (5'), and (6) are illustrated as well. (Hakala and Kaappola, 2007, pp. 189–190)

Figure 5. pH-diagram of carbon dioxide and the operation cycle. s is the constant entropy, v is the constant volume, and T is the constant temperature. Black lines present the boundaries of the phases. The operation stages are numbered from 1 to 6. The condensation can be performed by a supercritical phase or subcritical phase (dashed red line).

1.2   Structure of the ice rink

A typical arrangement of a longitudinal evaporator system is presented below. The purpose of Figure 6 is to present how the l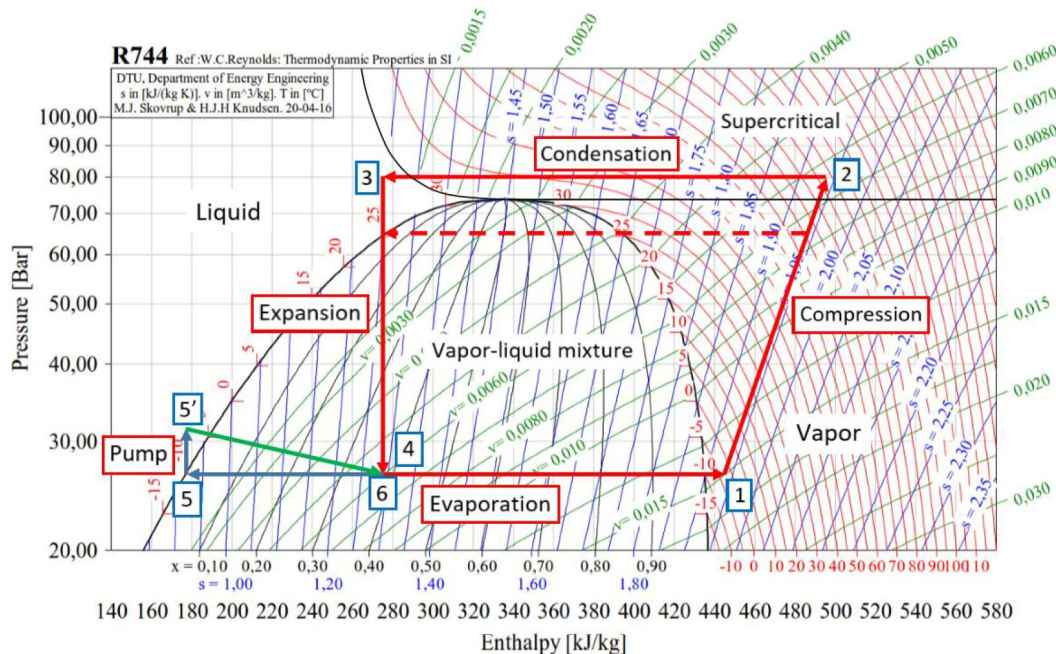iquid refrigerant moves into an inlet header, circulates in a loop beneath the ice, and finally exits through the outlet header.[2] The transverse option or arrangement is also available but rarely used (International Ice Hockey Federation (IIHF), 2016; ASHRAE Handbook: Refrigeration. SI Edition, 2018, chap. 44: Ice rinks).

Outlet   Inlet
header   header
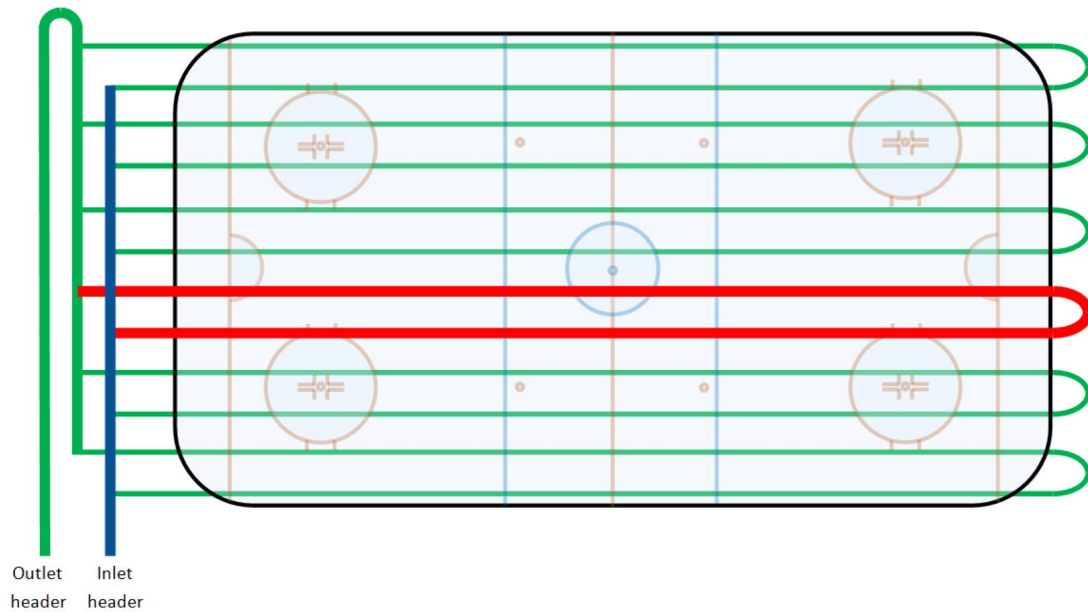
Figure 6. Typical longitudinal arrangement of the evaporation unit and loops beneath the ice. The red line illustrates one loop. The headers connect the loops in series.

Figure 7 dives into the detailed structure of an ice rink. The cooling pipes absorb the incoming heat. Furthermore, the heating pipes prevent the ground from freezing. The heating pipes use brine as a standard fluid, which are solutions of water-ethylene glycol (MEG) or water-propylene glycol (PEG). Moreover, the insulation reduces the heat transfer between the pipes. (International Ice Hockey Federation (IIHF), 2016; *ASHRAE Handbook: Refrigeration*. SI Edition, 2018, chap. 44: Ice rinks; Ferrantelli, Viljanen and Kurnitski, 2019).


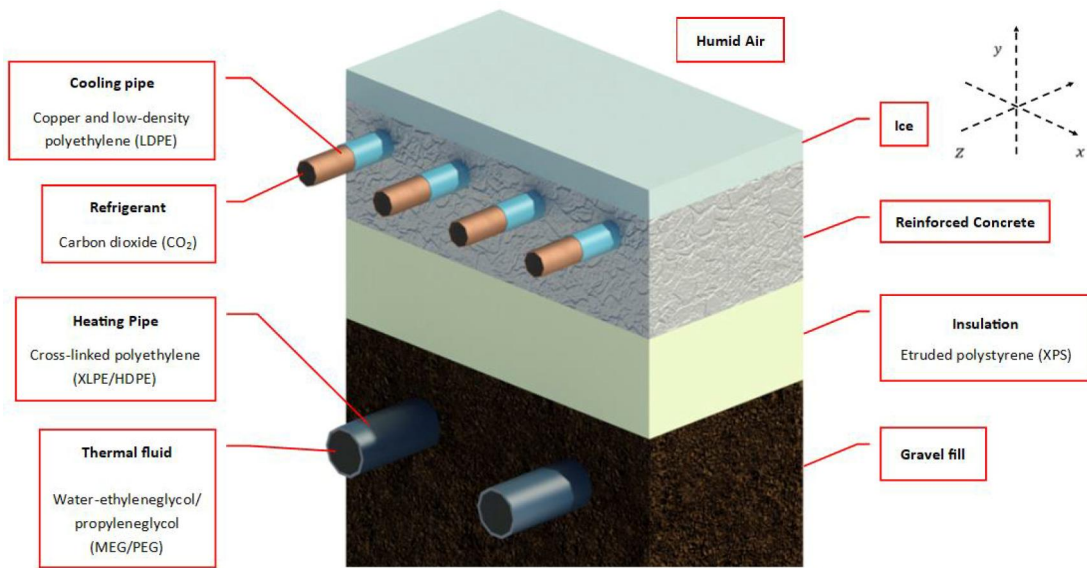[2] Figure 6 only visualizes the type of arrangement, and ice rink usually consists around 150 loops.

Figure 7. The layered structure of the ice rink. 3D-model created with Autodesk® Revit®.

1.3 Carbon dioxide as a refrigerant

Currently, in Finland, the most standard refrigerators are ammonia (R717), carbon dioxide (R744), and various hydrofluorocarbons (HFC), including difluoromethane (R34), pentafluoroethane (R125), and 1,1,1,2-tetrafluoroethane (R134a). Furthermore, ternary and binary mixtures of HFCs are used more extensively, including R404a, R407c, and R410a. In the future, isobutane is recommended to mix with the HFC mixtures as well. (Suomen kylmäyhdistys ry, 2017)

For comparison, Table 1 represents the thermophysical properties of ammonia, carbon dioxide, isobutane, and various HFCs in $263\ K\ (-10°C)$ at saturation pressure. The vapor pressure of carbon dioxide is relatively high compared to HFCs and isobutane and requires high operating pressure. In contrast, the lowest vapor pressure is achieved with isobutane closed to the atmospheric pressure. The enthalpy of vaporization is significantly higher with ammonia compared to HFCs, isobutane, and carbon dioxide. It indicates a reduced mass flow inside the refrigeration pipes because more energy is needed to complete full vaporization from liquid to gas. Moreover, the thermophysical properties of carbon dioxide, HFCs, and isobutane compared to ammonia vary more when the refrigerant is heated. Among the listed refrigerants, carbon dioxide offers reasonable thermophysical properties with low viscosity, average thermal conductivity, low surface tension, and high vapor density.

10

Table 1. Comparison of thermophysical properties of various refrigerants. Data retrieved from NIST Chemistry WebBook (2018).

Property	Unit	CO2	NH3	R32	R125	R134a	Isobutane
Vapor pressure	MPa	2.637	0.289	0.580	0.480	0.199	0.108
Enthalpy of vaporization	kJ/kg	258.989	1297.240	330.466	140.704	206.074	363.670
Surface tension	N/m	6.53E-03	3.64E-02	1.28E-02	8.25E-03	1.30E-02	1.42E-02
Vapor							
Density	kg/m^3	75.485	2.376	15.791	30.122	9.985	2.996
Heat capacity	$J/(kg \cdot K)$	1592	2540	1155	832	854	1556
Viscosity	$Pa \cdot s$	1.42E-05	8.75E-06	1.10E-05	1.14E-05	1.04E-05	6.62E-06
Thermal conductivity	$W/(m \cdot K)$	1.81E-02	2.25E-02	1.09E-02	1.16E-02	1.06E-02	1.33E-02
Liquid							
Density	kg/m^3	945.803	652.260	1089.222	1365.188	1327.620	592.040
Heat capacity	$J/(g \cdot K)$	2.480	4.563	1.697	1.216	1.315	2.230
Viscosity	$Pa \cdot s$	1.01E-04	1.91E-04	1.69E-04	2.36E-04	3.04E-04	2.23E-04
Thermal conductivity	$W/(m \cdot K)$	0.111	0.591	0.153	0.074	0.097	0.103

Interest in utilizing carbon dioxide in refrigerator systems has risen by chemical safety, environmental friendliness, and low cost. Pure ammonia is an excellent refrigerant with unique thermal properties. However, it is easily flammable, poisonous if inhaled, severely corrosive, and poisonous to the environment (Lamberg, Lautkaski and Virolainen, 2015). Furthermore, a global warming potential (GWP) of HFCs is high. Their usage will be restricted, regulated, and limited in the future (European Parliament and Council, 2014; Suomen kylmäyhdistys ry, 2017).

Using carbon dioxide as a refrigerant is not any kind of new solution. Alexander Twining proposed the first reference in 1850 in his British patent. Since then, carbon dioxide became highly commercialized. Until the 1950s, other refrigerants, for example, calcium chloride, glycols, and HFCs with better thermophysical properties replaced carbon dioxide. (William and Bodinus, 1999) As technology progressed, an interest in using carbon dioxide again was initiated by Professor Gustav Lorenzen in the late 1980s. Since the first carbon dioxide-based ice rink was built in Austria in 1999, using carbon dioxide as a refrigerant has become an increasingly popular solution. (Rogstam, 2016)

While most of the new ice rinks are built with indirect circulation, a trend of using carbon dioxide in a direct-controlled system has become a serious alternative. However, the ice rinks are still poorly optimized for carbon dioxide, and dimensioning is under research. Available literature suggests that only a little research has been conducted optimizing ice rinks for carbon dioxide. However, it is assumed that more research is conducted for commercial purposes because optimization offers an advantage over businesses. Currently, the dimensions of the ice rinks rely on the general instructions of IIHF and ASHRAE, which do not take account the type of the coolant (See International Ice Hockey Federation (IIHF), 2016; *ASHRAE Handbook: Refrigeration*. SI Edition, 2018, chap. 44: Ice rinks). However, optimization could reduce overall costs, make the system more efficient in the perspective of heat transfer, improve safety, and offer a market advantage over competitors.

Furthermore, previous studies concerning carbon dioxide in refrigerator units include, for example, the suitability of carbon dioxide as a refrigerant and the energy balance of the ice rink with various indoor temperatures. The experimental setup estimating the overall costs of using carbon dioxide over ammonia, and optimization of refrigeration pipes with an experimental approach are studied as well. (see Shahzad, 2006; Caliskan and Hepbasli, 2010; Nguyen, 2012; Simard, 2012; Rogstam, Abdi and Sawalha, 2014; Bolteau, Rogstam, and Tazi, 2016) Besides, in Finland, outdoor ice rinks using carbon dioxide as a refrigerant have been studied, too. (Väänänen, 2019).

1.4 Scope and structure of the thesis

This thesis presents a comprehensive and accurate heat transfer model for a direct-controlled circulation system when carbon dioxide is used as a refrigerant. The work considers the system from the perspective of heat transfer and does not take into account the economic analysis. Moreover, the subject is restricted to model only the ice rink, and the work does not take account of the other parts of the refrigerator system. This paper does not give direct answers on how to design an ice rink. Instead, it describes the phenomena at a very detailed level and how the systems change if specific variables are modified.

The main goal of this thesis is to construct an efficient tool, which can be used to optimize the dimensions and overall economics of an ice rink with different arrangements and conditions. The thesis is divided into three modules, which are a **heat conduction module,** a **pipe module,** and a **thermophysical property module**. *The heat conduction module* determines a cross-sectional heat balance by thermal resistances networks (TRN) and numerical analysis by the simulation software. Due to the lack of experimental data, it is convenient to validate the results by two theoretical approaches. Moreover, *the pipe module* evaluates the behavior of carbon dioxide and the brine with superior accuracy. The construction of 3D-simulation was excluded because physics with two-phase flow takes significantly more time to solve and provides only a slight enhancement in precision. Finally, *the thermophysical property module* determines the properties of the materials. The property module establishes a construction of *the heat conduction module* and *the pipe module*. It provides a property library for future applications as well.

The tool is built on Microsoft® Excel with the assistance of COMSOL Multiphysics® modeling Software.[3] Both software can interact with each other with COMSOL LiveLink™ simultaneously with a comprehensive list of parameters involved within the tool. The equations presented were programmed inside the Microsoft® EXCEL with Visual Basic for Applications (VBA), which involve over 2,700 lines of code. All modules are available in Microsoft EXCEL®. Besides, *the heat conduction module* uses COMSOL Multiphysics® - Software to certify and visualize the results.

---

[3] The choice of choosing Microsoft® EXCEL as a platform was to make the tool available for everyone inside the company, avoid costs of the simulation software if necessary, and it was requested due to heavy use. Furthermore, COMSOL Multiphysics® is easy to use, convenient to work with, and it can provide reliable results with high theoretical accuracy.

The heat balance is vitally dependent on the heat load, and the aim is not to simulate the heat load on ice rinks. The measurement should be carried out independently with CDF-simulations with external applications, for example, COMSOL Multiphysics® or EQUA IDA ICE® - Software, depending on the shape and purpose of the hall and arrangements of the external heating, lighting, and ventilation systems. Nevertheless, and extensive research on air distribution on ice rinks is obtainable with various arrangements as well (See, for example, Denisikhina, Samoletov, and Brodach, 2017; Taebnia *et al.*, 2019). Moreover, the external total heat load can be estimated by other analyzes (See Bellache, Ouzzane, and Galanis, 2005; Sunyé *et al.*, 2007; Daoud, Galanis, and Bellache, 2008; Karampour, 2011).

The original goal of the study was to model the effect of humid air above the ice by conduction and condensation. However, it was discovered irrelevant in terms of the scope. Therefore, the thermophysical properties of the humid air are not included in Chapter 4.3. However, the calculations are presented in Appendix C because the information is still needed with the concrete in Chapter 4.3.5. As a result, the equations of humid air are coded inside *the thermophysical property module,* which is also assumed to meet future demands and needs.

This thesis proceeds as follows. First, this thesis introduces the theory behind *the heat conduction module* and its explicit solution in Chapter 2. The chapter describes the basics of convection, introduces the concept of thermal resistance networks (TRN), and describes how the network is constructed. Second, Chapter 3 visualizes the fundamentals of convection and evaluates the equations used in unsaturated, subcooled, and saturated regions. Third, Chapter 4 defines the thermophysical properties of the materials by the literature.

After the framework for all three modules are defined, Chapter 5 describes briefly how the modules are constructed in the interphases of Microsoft EXCEL® and COMSOL Multiphysics® - software. In Chapter 6, the results of *the heat conduction module* are carried out by presenting two alternate configurations, based on general instructions IIHF (International Ice Hockey Federation (IIHF), 2016) and arbitrary constraints. Furthermore, the results of *the pipe module* are demonstrated by multivariate analysis for both brine and carbon dioxide. Finally, the deficiencies and advantages of *the thermophysical property module* are described by an in-depth discussion. Nevertheless, the conclusions and future suggestions based on the main findings are carefully described in Chapter 7. The appendices A, B, and C consist of parameters and uncertainties of the thermophysical properties and the calculations of humid air.

2   HEAT CONDUCTION MODULE

This chapter introduces the theory of *the heat conduction module*. It defines the conduction as a heat transfer method and describes the concept of shape factors. Furthermore, the chapter briefly describes how a steady-state heat transfer problems by conduction is usually solved in the industry. Besides, the logic behind *the heat conduction module,* and further definitions of the thermal resistance network of the module will be visualized.

A heat transfer problem can be solved by *analytical method*, *numerical method*, and a *graphical method*. An analytical method is available only for specific and ideal geometries. However, numerical methods are more practical and efficient for complex geometries and transient heat transfer models.[4] The model uses a numerical method by COMSOL Multiphysics® and a partially analytical approach with thermal resistance networks (TRN).[5] The model is constructed with identical materials and the arrangement, presented in Figure 7. The module uses only conduction as a method of heat transfer, and the convection is neglected.

The TRN approach has been widely used in industrial applications as it provides the most straightforward option to obtain reliable results with a cost of accuracy. The disadvantage of TRNs is the assumption of isothermal surfaces, and it does not consider the external temperature fields. Moreover, it considers a unidirectional heat in certain parts of the model. In contrast, the numerical method can evaluate the average temperature of the surfaces, even the fluctuation occurs, and the heat balance should remain the same in both approaches. Furthermore, it is convenient to visualize the differences between these two approaches in Figure 8.

---

[4] The temperature in a transient heat transfer models changes in respect to time, while steady-state models do not take account of the effect of time.
[5] COMSOL Inc. provides a comprehensive documentation of the numerical approach for free, if interested.

Figure 8. Differences in heat transfer between a TRN (left) and numerical simulation (right). Notice that the Figure is just a schematic representation of the difference. Real optimization or calculation has not been made.

2.1   Conduction

Conduction is a heat transfer mechanism in which the heat is moving inside the material by intermolecular interactions in solids, liquids, and gases. A heat transferred by conduction is expressed by Fourier's law.

$$q = -\lambda \nabla T = -\lambda \left(\frac{\partial T}{\partial x} + \frac{\partial T}{\partial y} + \frac{\partial T}{\partial z} \right) \tag{1}$$

where x, y, and z represent a 3-dimensional coordinate system. Many heat transfer systems with complex geometries involve a multidirectional heat transfer. By the approach of thermal resistance networks (TRN), the tool uses *shape factors* to define the thermal resistances between isothermal surfaces. The definition of thermal resistance is

$$Q = \frac{\Delta T}{R} = C \cdot \nabla T \tag{2}$$

where ΔT is the temperature difference between isothermal surfaces, Q is the heat transferred between these surfaces, and C is a thermal conductance. The laws of electrical resistance networks are equal for thermal resistance networks as

$$I = \frac{\Delta V}{R_e} = C_e \cdot \Delta V \tag{3}$$

The shape factor S is defined by the thermal conductance C divided by the averaged thermal conductivity $\bar{\lambda}$ over temperatures of two points T_2 and T_1.
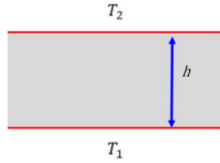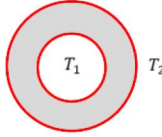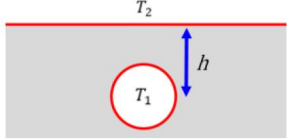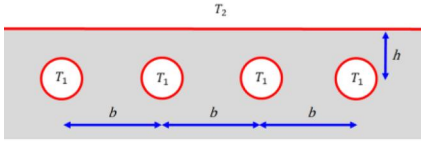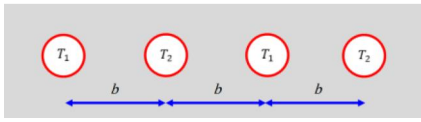
$$Q = C(T_2 - T_1) = S\bar{\lambda}(T_2 - T_1) \tag{4}$$

In steady-state models, the thermal conductivity is an averaged constant between temperature difference.

$$\bar{\lambda} = \frac{1}{T_2 - T_1} \int_{T_1}^{T_2} \lambda \, dT \tag{5}$$

Table 2 presents the shape factors considered in the ice rink. Some of the configurations were excluded due to unsuitability and increased uncertainty but were tested. Additionally, more shape factors can be found in the literature. (VanSant, 1980; Hahne, 1993; Baehr and Stephan, 2011, chap. 2.2.5.1; Çengel and Ghajar, 2011, chap. 3.7; Yi, 2018)

Table 2. Shape factors considered in the heat conduction module.

Configuration	Shape factor	Remarks	Geometry
Plane wall	$S = \dfrac{A}{h}$		
Cylinder	$S = \dfrac{2\pi}{\ln\left(\frac{r_2}{r_1}\right)}$	$r_2 > r_1$	
Buried pipe in a semi-infinite medium	$S = \dfrac{2\pi}{\cosh^{-1}\frac{h}{r}}$	$h > r$	
An array of equally spaced isothermal cylinder model	$S = \dfrac{2\pi}{\ln\left(\frac{2\pi}{\pi D}\sinh\frac{2\pi h}{b}\right)}$	$b > 1.5D$	
Pipes with alternating temperatures in extended medium	$S = \dfrac{2\pi}{\ln\left(\frac{2b}{\pi r}\right)}$	$r < b$	

2.2 Thermal resistance network

Dividing the system into smaller units is necessary to evaluate the heat balance of the ice rink. As the spacing of the heating pipes varies independently with the spacing of the cooling pipes, the overall heat balance of the system is divided into two heat balances (Figure 9 and Figure 10). All the layers and surfaces are in direct contact with each other, only a steady-state condition is considered, and thermal expansion and contraction are neglected.

Understanding Figure 9 and Figure 10 requires a comprehensive explanation of the isothermal average temperatures of each node (Table 3). Moreover, the thermal resistances and their types must be characterized (Table 4). The indexes and temperatures are not only used in this paper but the interface of the tool. The system is constrained with three boundary conditions: the upper surface of the ice (T_1), the surface temperature beneath the insulation layer (T_{13}), and constant heat flux to the ice (Q_1).
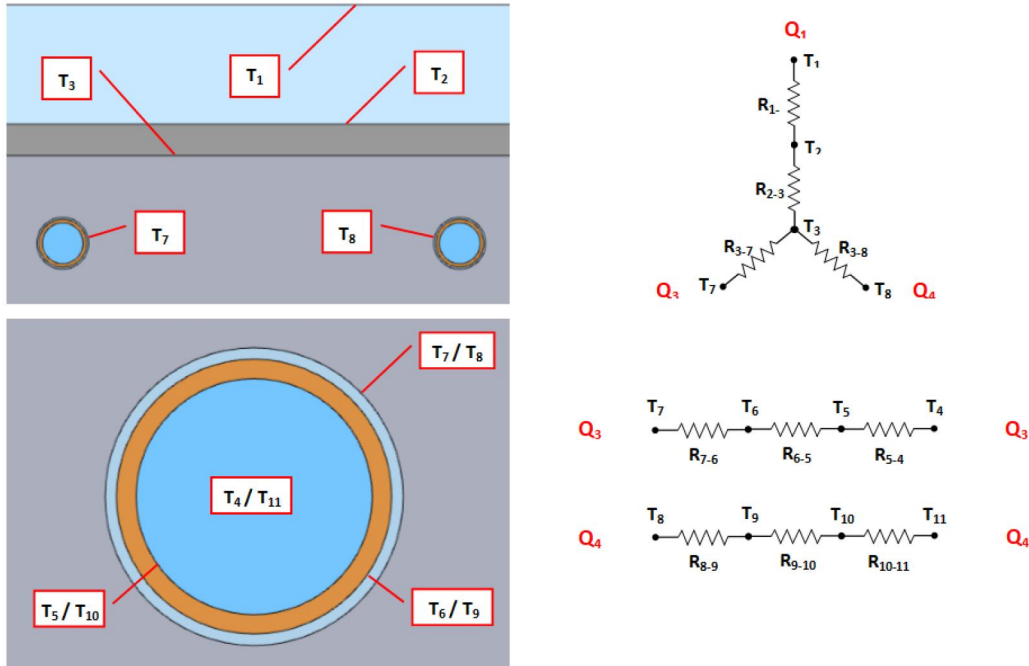

Figure 9. Thermal resistances networks and heat balance of the cooling pipes.
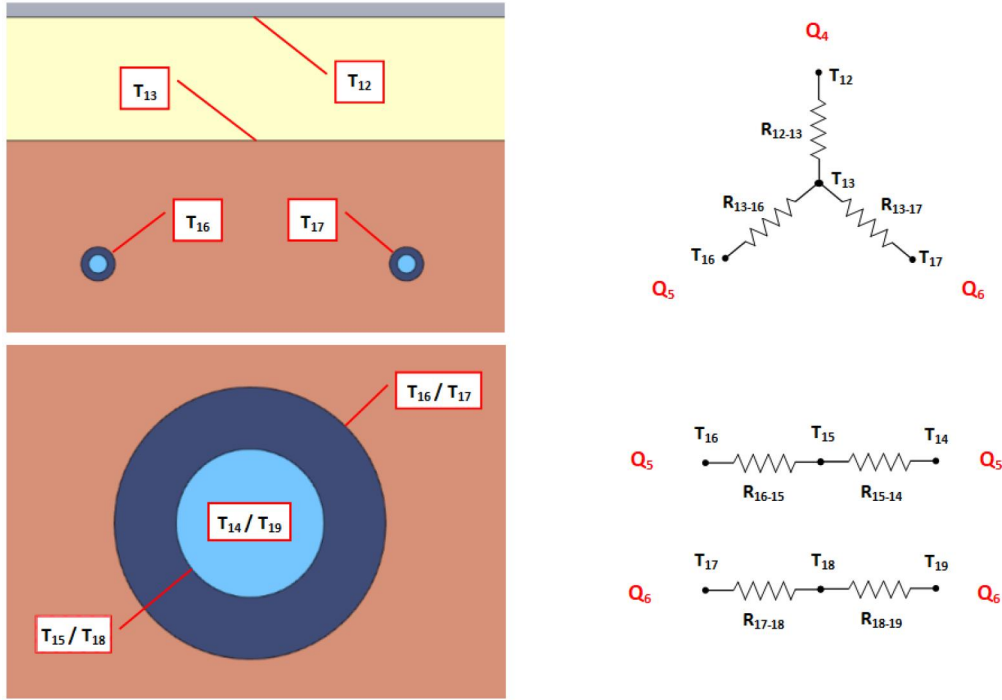
Figure 10. Thermal resistance networks and heat balance of the heating pipes.

*Table 3. Description of isothermal surfaces at average temperatures. *The temperature defines the boundary condition of the system. **The temperature is different in TRN-model and simulation in COMSOL Multiphysics® - software.*

Temperature	Description
T_1	The temperature at the surface of the ice*
T_2	The temperature at the interphase of the reinforcement layer and ice
T_3	The temperature at the interphase of the reinforcement layer and porous concrete**
T_4, T_{11}	The adiabatic bulk temperature of the liquid $\bar{T}_f$ inside the cooling pipe
T_5, T_{10}	The temperature at the pipe wall T_w inside of the cooling pipe
T_6, T_9	The temperature at the interphase between copper and LDPE-layer
T_7, T_8	The temperature at the interphase of the cooling pipe and porous concrete
T_{12}	The temperature on top of the insulation layer
T_{13}^*	The temperature at the interphase of the insulation layer and gravel fill
T_{14}, T_{19}	The adiabatic bulk temperature of the brine $\bar{T}_f$ inside the heating pipe
T_{15}, T_{18}	The temperature at the inside of the heating pipe wall T_w
T_{16}, T_{17}	The temperature at the interphase of the outer surface of the heating pipe and gravel fill

Table 4. Description of thermal resistances between isothermal surfaces. *The effect of the resistance was considered in the construction of thermal resistance networks. However, it was found out that the inclusion of these resistances leads to increased uncertainty between thermal resistance networks and COMSOL simulation. More on the construction is described in more detail in Chapter 6.1.

Temperature	Description
$R_{1-2}, R_{2-3}, R_{12-13}$	1-dimensional conduction by plane wall model
R_{3-7}, R_{3-8}, R_{13-16}, R_{13-16}	2-dimensional conduction by an array of buried pipes
R_{12-7}, R_{12-6}	2-dimensional conduction by an array of buried pipes*
$R_{7-6}, R_{6-5}, R_{8-9}$, $R_{9-10}, R_{16-15}, R_{17-18}$	1-dimensional radial conduction in cylinders
R_{7-8}, R_{16-17}	2-dimensional conduction by an array of pipes with alternating temperatures in extended medium*
R_{6-5}, R_{11-12}, R_{17-18}, R_{22-21}	Internal forced convection
R_{3-7}, R_{3-8}, R_{13-16}, R_{13-16}, R_{12-7}, R_{12-6}	2-dimensional buried pipe model*

The primary goal of the combination of the TRN and numerical simulation is to define in which temperature the carbon dioxide and the brine must flow inside the pipes to overcome the external heat by different arrangements. Nevertheless, the explicit solution of the heat balance of the cooling pipes by the TRN is

$$Q_1 - Q_2 - Q_3 = 0 \qquad\qquad (6)$$

where

$$Q_1 = C_{1-2}(T_1 - T_2) = C_{2-3}(T_2 - T_3)$$

$$Q_2 = C_{5-4}(T_5 - T_4) = C_{6-5}(T_6 - T_5) = C_{7-6}(T_7 - T_6) = C_{3-7}(T_3 - T_7)$$

$$Q_3 = C_{10-11}(T_{10} - T_{11}) = C_{9-10}(T_9 - T_{10}) = C_{8-9}(T_8 - T_9) = C_{3-8}(T_3 - T_8)$$

Additionally, the heat balance for heating pipes is

$$Q_5 + Q_6 - Q_4 = 0 \tag{7}$$

in which

$$Q_4 = C_{12-13}(T_{12} - T_{13})$$

$$Q_5 = C_{14-15}(T_{14} - T_{15}) = C_{15-16}(T_{15} - T_{16}) = C_{16-13}(T_{16} - T_{13})$$

$$Q_6 = C_{19-18}(T_{19} - T_{18}) = C_{18-17}(T_{18} - T_{17}) = C_{17-13}(T_{17} - T_{13})$$

The inlet and outlet temperatures are constrained for temperature differences. To measure the temperature differences between inlet and outlet, a proper heat transfer model for the fluid should be evaluated. As the convection is neglected, the temperature difference is measured at the tube wall.[6]

$$\Delta T_{CP} = T_{10} - T_5 \tag{8}$$

$$\Delta T_{HP} = T_{18} - T_{15}$$

---

[6] Discussion on why tube wall and not the fluid itself is described in RESULTS AND DISCUSSION Chapter.

3 PIPE MODULE

This chapter characterizes the theory of internal forced convection. It introduces the subject by defining the fundamental equations of convection and describes the heat transfer in fluids in general. Furthermore, the chapter dives deep into the theory of internal forced convection in unsaturated, subcooled, and saturated states. Additionally, it critically motivates why the presented equations are selected. By the horizontal arrangement and a low mass flow rate, the system neglects the losses by gravity and minor pressure losses caused by the bends in the loop.

3.1   Convection

Convection is heat transfer by the movement of the fluid. Natural convection occurs by the changes in temperature in different regions. This phenomenon leads to buoyancy forces that move the fluid with no external work. In contrast, the motion of the fluid by forced convection is always determined by external work (Yu *et al.*, 2014). The module considers only forced convection and assumes that the effect of natural convection is negligible. **Newton's cooling law** describes the heat transferred at the interphase of solid and fluid.

$$Q = \alpha A \Delta T \rightarrow q = \alpha \Delta T \tag{9}$$

To describe the motion of the fluid at the fundamental level, we must construct a Cartesian coordinate system (x, y, z) with an infinite amount of small cubical volume units with a depth of dx, a height of dy, and a width of dz. The fluid is treated as an incompressible Newtonian fluid. It states that the density and viscosity of the fluid does do not change in time and temperature. Let $\overline{v}$ be a velocity vector of a particle that enters the volume unit.

$$\overline{v} = \overline{\imath}v + \overline{\jmath}u + \overline{k}w \tag{10}$$

$\overline{v}$ is a three-dimensional vector that acts on the volume unit by all three directions (x, y, z). While further simplicities are made, we continue to show the balances visually acting on the volume unit by only x direction, as in Figure 11.
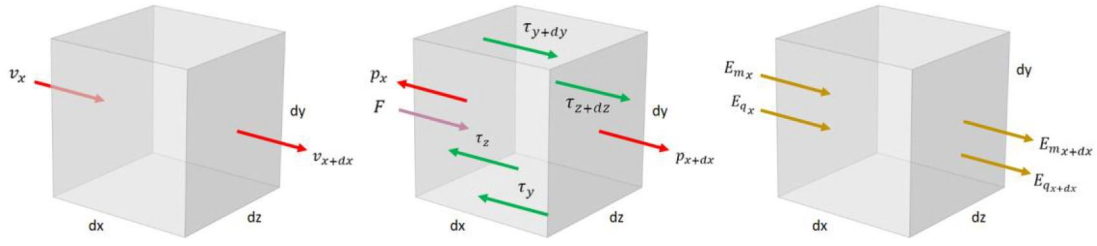
Figure 11. Visualization of Navier-Stokes equations and conservation of energy. The first box illustrates the conservation of mass, the second is Newton's second law, and the third is the conservation of energy.

The first box in Figure 11 shows that the velocity of particle into the volume unit must be equal to velocity out from the volume unit if density remains constant. This **conservation of mass** states that mass cannot be created or removed. In mathematical form, it is expressed as

$$\nabla \overline{v} = 0 \tag{11}$$

$$\Rightarrow \left(\frac{\partial v}{\partial x} + \frac{\partial u}{\partial y} + \frac{\partial w}{\partial z} \right) = 0$$

The second box describes **Newton's second law**. It states that the sum of inertial forces is equal to mass multiplied by acceleration. The inertial forces acting on a fluid consists of pressure p, internal shear stresses τ which is defined as viscosity η, and external forces F which in most cases can be expressed by gravity g. In mathematical form, this is

$$\rho \left(\frac{d\overline{v}}{dt} + \overline{v} \cdot \nabla \overline{v} \right) = -\nabla p + \eta \nabla^2 \overline{v} + \rho F \tag{12}$$

$$\Rightarrow \rho \left(\frac{d\overline{v}}{dt} + v\frac{\partial v}{\partial x} + u\frac{\partial u}{\partial y} + w\frac{\partial w}{\partial z} \right)$$
$$= -\left(\frac{\partial p}{\partial x} + \frac{\partial p}{\partial y} + \frac{\partial p}{\partial z} \right) + \eta \left(\frac{\partial^2 v}{\partial x^2} + \frac{\partial^2 u}{\partial y^2} + \frac{\partial^2 w}{\partial z^2} \right) + \rho F$$

Finally, the third box visualizes that the sum of energy into the volume unit must be equal to the energy from the volume unit. It is known as the **conservation of energy,** which states that the total energy of the system remains constant. To further refine the definition, the energy convected out of the volume unit is equal to the net energy transferred into the volume unit by conduction.

$$\rho c_p(\overline{\boldsymbol{v}} \cdot \nabla T) = \lambda \cdot \nabla^2 T \tag{13}$$

$$\Rightarrow \rho c_p \left(v \frac{\partial T}{\partial x} + u \frac{\partial T}{\partial y} + w \frac{\partial T}{\partial z} \right) = \lambda \left(\frac{\partial^2 T}{\partial x^2} + \frac{\partial^2 T}{\partial y^2} + \frac{\partial^2 T}{\partial z^2} \right) + \eta \phi$$

where ϕ is the viscous dissipation function, which describes the production of heat by internal viscous forces. The first two equations (11) and (12) are known as Navier-Stokes equations, which combined with Equation (13) are used to predict the fluid motion. In all cases, the equations must be solved numerically, as they have no analytical solution.

Some modifications on Equations (11), (12), and (13) must be made. The aim is to define the properties and the state of the fluid from the perspective of heat transfer and not to simulate the behavior of individual particles in all three directions. Most of the equations presented in this chapter are derived from these fundamental equations.[7] Therefore, the motion of the fluid can be applied to the uniaxial approaches. Furthermore, Equations (11), (12), and (13) are valid for an incompressible Newtonian fluid. However, especially in two-phase flow, the thermodynamic properties of the fluid will change as the vapor fraction, as known as a quality, increase. However, further readings on kinematic theory for compressible fluids and non-Newtonian fluids can be found in the literature, if interested (see Kalland, 2008; Baehr and Stephan, 2011, chap. 3.2).

3.2 Internal forced convection

The fluid may flow by the external force with boiling or without boiling. The internal forced convection is divided into an *unsaturated region*, *subcooled region*, and *saturated region*, presented in Figure 12. The graph above the pipe demonstrates the true vapor volume fraction (ε) as a function of equilibrium quality (x_{eq}). The lower graph represents the temperatures of the tube wall (T_w) and the fluid ($\overline{T}_f$).[8]

---

[7] (See, for example, derivation of the Dittus-Boelter equation of Nusselt number at a constant temperature or heat at Baehr and Stephan, 2011, chaps 341, 370–371).
[8] The definitions of ε, x_{eq}, T_W, and $\overline{T}_f$ are described by Figure 14 and Equations (35) and (38).

In a fully unsaturated region ($z < z_{sc}$), there is no boiling, and the heat transfer is defined by forced convection only. At the beginning of the subcooled region ($z_{sc} < z < z_{sat}$) the vapor starts to evaporate at the tube wall at the onset of nucleate boiling point (ONB). However, the vapor does not accumulate before the net vapor generation point (NVG) because the vapor condenses back to liquid due to the lower temperature of the bulk liquid. Nevertheless, all the fluid is saturated in the saturated region ($z > z_{sat}$). (Crowe, 2005, chap. 3; Baehr and Stephan, 2011, p. 516; Çengel and Ghajar, 2011, p. 597)
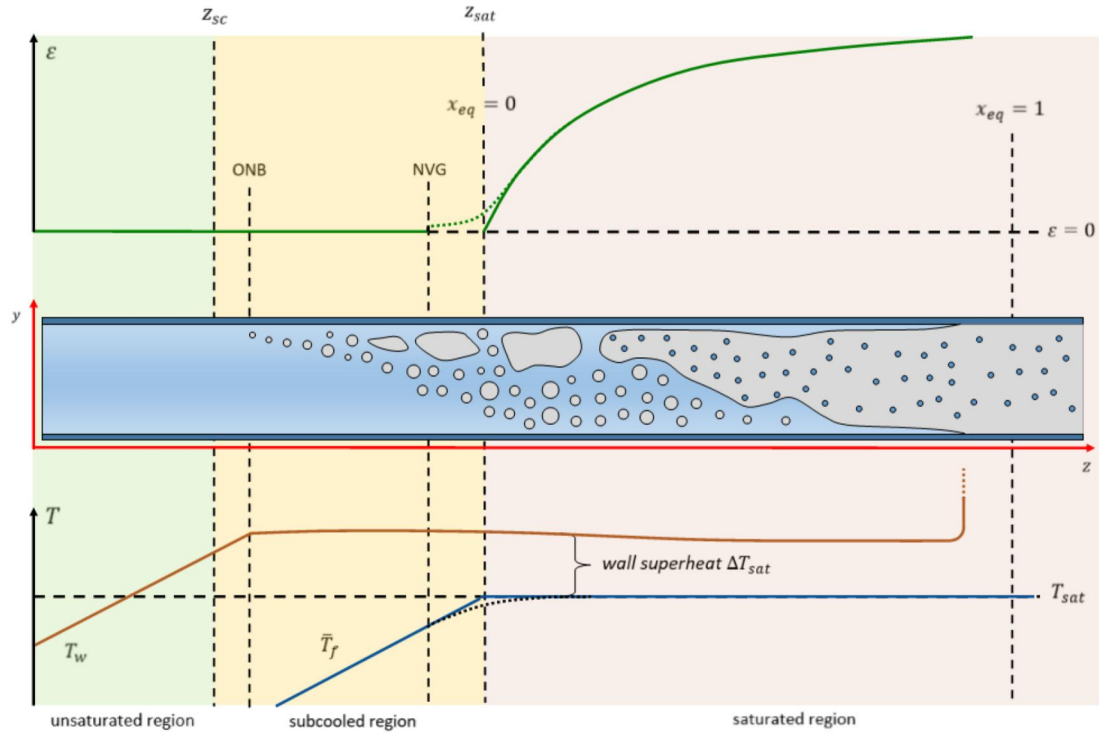

Figure 12. Single- and two-phase flow inside the horizontal tube.

The concept of flow patterns is essential for the analysis to understand the heat transfer in two-phase flow. Defining the flow pattern at the given distance z gives a better understanding of the characteristics of the fluid and how the fluid flows inside the tube. It further leads to a correct estimation of heat transfer in the distance z. Buoyancy forces highly define the flow regime, and the vapor rises at the ceiling of the tube as the carbon dioxide evaporates. As in Figure 12, the subcooled region is primarily controlled by the bubbly flow. The fluid turns into plug flow, slug flow, annular flow, and mist flow as the fluid evaporates and continues through the saturated region. Currently, the most accurate flow map, specially made for carbon dioxide, is presented by Cheng, Ribatski, and Thome (2006). In their study, the boundaries between two flow patterns are presented by mass flux G as a function of vapor quality x, defined in Equations (14) and (15). The different flow patterns are illustrated in Figure 13.
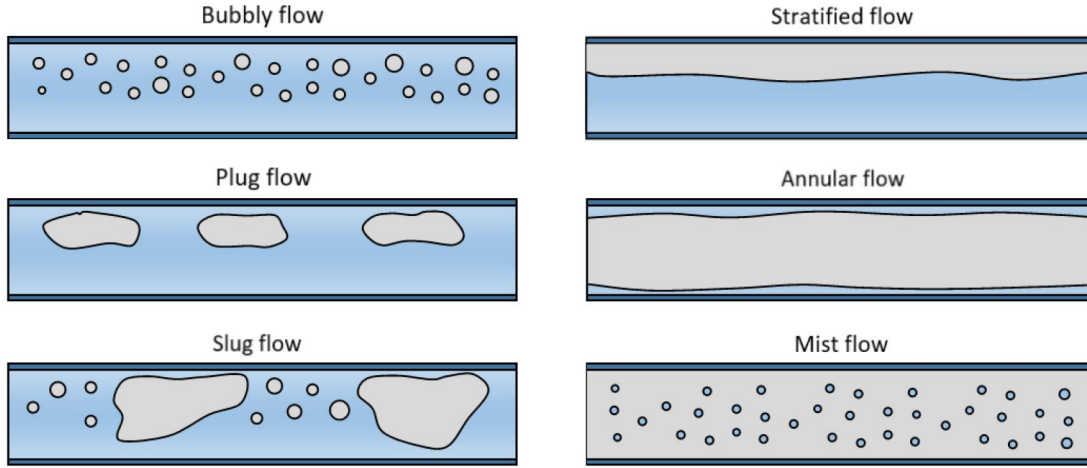
Figure 13. Flow patterns in internal forced horizontal flow. (Crowe, 2005, chap. 3; Baehr and Stephan, 2011, p. 514)

The module assumes a heterogenous flow, which states that the phases move with different velocities due to differences in density. Alternatively, the homogenous model assumes the phases move with the same velocity. The homogenous approach suits best with bubbly or mist flow. However, the heterogeneous approach is more suitable for flow patterns between these two extremes. In other words, whether to choose a homogenous or heterogeneous approach is dependent on the fluid state and the application. Moreover, there are two approaches to calculate the heat balance between the tube wall and the fluid: *constant heat flux* and *constant temperature*. The model assumes a *constant heat flux* in all regions.

Consider a horizontal pipe with a cross-sectional area of A, as in Figure 12. The conservation of mass holds that the total mass flow is equal to the total mass flow out at any section dz.

$$G_{in} = G_{out} \rightarrow \frac{\dot{m}_{in}}{A} = \frac{\dot{m}_{out}}{A} \tag{14}$$

As the fluid evaporates, the vapor mass flow rate $\dot{m}_V$ versus total mass flow rate $\dot{m}$ is defined by the quality of the fluid.

$$x = \frac{\dot{m}_V}{\dot{m}} = \frac{G_V}{G} \tag{15}$$

The quality is 0 when the liquid is subcooled or unsaturated. In contrast, the void fraction ε describes the ratio of vapor surface area A_V to the cross-sectional total surface area of the pipe A at distance z.

$$\varepsilon = \frac{A_V}{A} = \frac{V_V}{V} \tag{16}$$

In consequence, the individual velocities of both phases are defined as

$$v_V = \frac{\dot{m}_V}{\rho_V A_V} = \frac{xG}{\rho_V \varepsilon} \tag{17}$$

$$v_L = \frac{\dot{m}_L}{\rho_L A_L} = \frac{(1-x)G}{\rho_L (1-\varepsilon)} \tag{18}$$

Also, the ratio of velocities is represented by the slip factor, which is 1 in a homogenous approach.

$$s = \frac{v_V}{v_L} \tag{19}$$

It is conventional to use a homogenous approach to estimate the average velocity and temperature of the fluid and the wall. In a fully laminar, developed, and single-phase flow, velocity the temperature profiles $v(r)$ and $T(r)$ are characterized in Figure 14. At the tube wall, the velocity is zero but develops as the distance from the wall increases. In contrast, the maximum temperature of the fluid is on the wall. The minimum temperature is at the middle, at the distance of radius r. However, while the evaporation occurs, the fluid cannot be treated as laminar flow due to extra turbulence, but the average velocity can estimate the velocity and temperature of the fluid $\bar{v}_f$ and average temperature $\bar{T}_f$ at any given distance z. (Baehr and Stephan, 2011, chap. 3.8; Çengel and Ghajar, 2011, chap. 8; Rajendra Karwa, 2017, chap. 7.3) Moreover, the pipes are not heated uniformly, and there will be differentiation in the temperature gradient in the pipe wall due to the placement of heat sources.
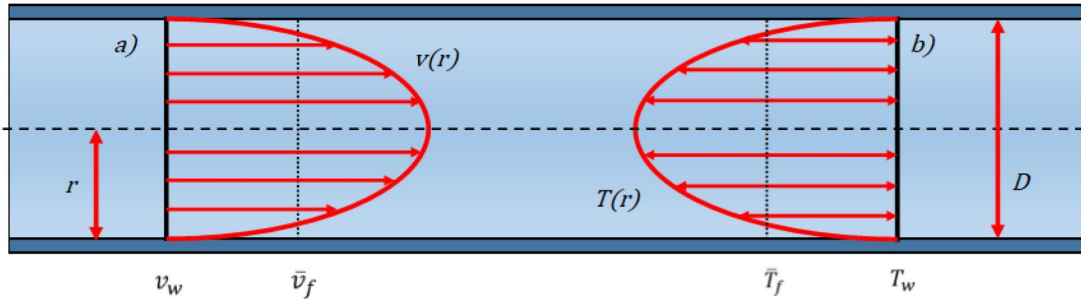
Figure 14. a) Velocity and temperature profiles of a homogenous, laminar, and fully developed flow. At the tube wall, the velocity is 0. In contrast, the temperature is highest at the pipe wall.

Figure 15 represents the changes in thermophysical properties inside the fluid. Between the distances z and $z + dz$, the change in temperature is caused by internal pressure losses and heat flux. Thus, as the fluid moves along the pipe, the averages of fluid quality, void fraction, temperature, pressure, and convective heat transfer coefficient at distance z change. Moreover, a temperature-dependent variables like heat capacity, density, thermal conductivity, surface tension, and enthalpy of vaporization change as well. (Darby and Chhabra, 2017). The change in every thermophysical variable in section dz is defined by a change in temperature dT.

$$\frac{\partial \boldsymbol{U}}{\partial z} = \left(\frac{\partial \boldsymbol{U}}{\partial T}\right) \cdot \left(\frac{\partial T}{\partial z}\right) \tag{20}$$

$$\boldsymbol{U} = [\Delta H_{vap} \quad c_{pV} \quad c_{pL} \quad \rho_V \quad \rho_L \quad \lambda_V \quad \lambda_L \quad \eta_V \quad \eta_L \quad \sigma]$$
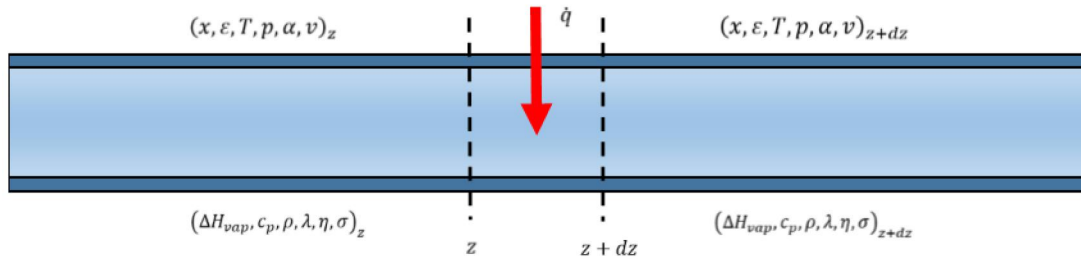

Figure 15. The changes in thermophysical properties at the length dz. The state of the fluid changes, as well as the thermophysical properties of both the vapor and liquid phase. q̇ represent the heat flux to the system.

The pressure loss consists of friction loss, loss by acceleration, and loss by gravity (Baehr and Stephan, 2011, pp. 521–522).

$$\left(\frac{dp}{dz}\right) = \left(\frac{dp}{dz}\right)_{ac} + \left(\frac{dp}{dz}\right)_{fr} + \left(\frac{dp}{dz}\right)_{gr} \tag{21}$$

This subchapter is divided into three sections, which present the appropriate heat transfer model for unsaturated, subcooled, and saturated flow. Thus, a proper heat transfer model is established at any given length z. Only heat transfer equations of the unsaturated region are applied to the brine. In contrast, the heat transfer of CO_2 is defined in all three regions.

3.2.1   Unsaturated region

The heat transfer in the unsaturated region is defined by convection only as in Figure 16 (Çengel and Ghajar, 2011, p. 481).
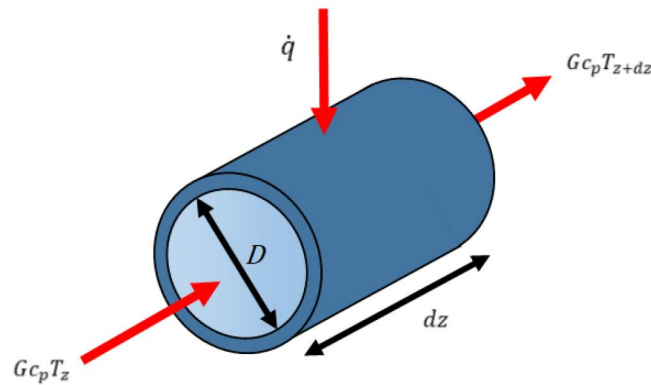
Figure 16. Energy balances of unsaturated fluid.

The energy balance of unsaturated fluid is described by Equation (22).

$$\dot{m}c_pT_z + \dot{Q} = \dot{m}c_pT_{z+dz} \tag{22}[9]$$

---

[9] While $\dot{Q}$ is assumed to be known, the tool uses an iterative method to determine the heat capacity between T_z and T_{z+dz}. The effect is relatively marginal if the heat capacity does not depend on temperature but increases the prediction accuracy with all types of fluid.

The heat flux to the system is purely defined by *Newton's cooling law* between the adiabatic mean temperature of the fluid and the pipe wall.

$$\dot{Q} = \alpha_C A \left(T_w - \bar{T}_f \right) \tag{23}$$

The heat transfer coefficient is defined by Reynolds number (Re), which describes the inertial forces over the viscous forces of the fluid.[10] As the Reynolds number increase, the particle becomes more unpredictable. For clearance, Figure 17 illustrates the particle path in laminar, transition, and turbulent flows. (Gnielinski, 2013; Rajendra Karwa, 2017, chap. 7.3)
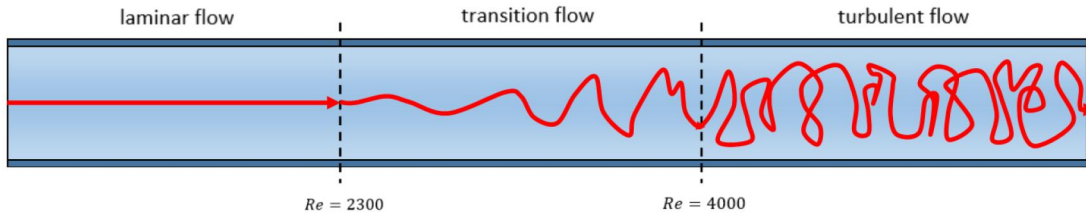
Figure 17. Particle path in laminar flow, transition flow, and turbulent flow. While $Re \leq 2300$, the flow is laminar. Moreover, the transition flow regime occurs when $2300 < Re < 4000$. Finally, the flow becomes turbulent when $Re \geq 4000$.

The convective heat transfer coefficient is usually assumed to be constant in the laminar region. (Baehr and Stephan, 2011, pp. 370–371; Çengel and Ghajar, 2011, p. 482). Unfortunately, this approach does not consider the characteristics of the fluid. Gnielinski (2013) suggests a more advanced model for laminar regions for constant heat flux and constant temperature at the tube wall, which take the characteristics of the fluid into account.

$$Nu = \frac{\alpha_C D}{\lambda_L} = \{N_1^3 + 0.6^3 + [N_2 - 0.6]^3 + N^3\}^{\frac{1}{3}} \tag{24}$$

$$N_1 = 4.354$$

$$N_2 = 1.953 \sqrt[3]{\frac{Re_L Pr_L D}{L}}$$

$$N_3 = 0.924 \sqrt[3]{Pr_L} \sqrt[2]{Re_L \frac{D}{L}}$$

---

[10] The definition of Reynolds number is described in NOMENCLATURE.

In the turbulent region, the convective heat transfer coefficient is obtained by the equation by Gnielinski (2013, 2015).[11] It combines the effect of entry length and viscosity at the pipe wall. The effect of alternate viscosity at the pipe wall is studied by Sieder & Tate (1936) with excellent results.

$$Nu = \frac{\alpha_c D}{\lambda_L} = \frac{\left(\frac{\zeta}{8}\right)(Re_L - 1000)Pr_L}{1 + 12.7\sqrt{\frac{\zeta}{8}}\left(Pr_L^{\frac{2}{3}} - 1\right)}\left[1 + \frac{D^{\frac{2}{3}}}{L}\right]\left[\frac{Pr_f}{Pr_w}\right]^{0.11} \tag{25}$$

It is suggested that the friction factor ζ by Kovanov (1946) is used with Equation (25). Instead, the friction factor is estimated by Equations (27) - (29). In the transition region, the convective heat transfer coefficient is obtained linearly between laminar and turbulent flow by Gnielinski (2013).[12]

$$Nu = (1 - \gamma)Nu_{2300} + \gamma Nu_{4000} \tag{26}$$

$$\gamma = \frac{Re_L - 2300}{4000 - 2300}, \qquad 0 \le \gamma \le 1$$

In the laminar regime, the Darcy friction factor ζ is qualified by Reynold's number.[13]

$$\zeta_L = \frac{64}{Re_L} \tag{27}$$

The Colebrook-White equation is known as an "exact" solution for the friction factor in turbulent and transitional flows. However, the approximation of the equation, provided by Chen (1979), provides excellent accuracy compared to other approximations in the literature.[14]

---

[11] Equation (25) requires an iterative method to solve because it is used to obtain the temperature of the wall if the temperature of the fluid $\bar{T}_f$ is known. The equation is capable to estimate the experimental data with a relative difference of $\pm 6\%$ on average and approximately 90% of all experimental data with a relative difference of $\pm 20\%$. (Fernando *et al.*, 2008; Huber and Walter, 2010; Coetzee, 2015)

[12] The original equation of Gnielinski (1976) is widely used in industrial applications and it is recommended and preferred to use in calculations (Çengel and Ghajar, 2011). In transition region, $5 - 6\%$ uncertainty is present (Pettersen, 2004).

[13] Note that this definition is purely theoretical.

[14] The accuracy of other approximations has been tested and compared, and the uncertainty of using Colebrook-White equation has been questioned (Rohsenow, Hartnett and Cho, 1998, chap. 10; Lira, 2013; Lipovka and Lipovka, 2014; Rajendra Karwa, 2017, chap. 8.5).

$$\frac{1}{\sqrt{\zeta}} = -2 \cdot \log\left(\frac{\epsilon_r}{3.7065 \cdot D} + \frac{5.0452}{Re_L} \cdot \log\left(\frac{\epsilon_r^{1.1098}}{2.8257} + \frac{5.8506}{Re_L^{0.8981}}\right)\right) \qquad (28)$$

$$\epsilon_r = \frac{\epsilon}{D} \qquad (29)$$

Figure 18 represents the overall friction factor in laminar, transient, and turbulent regions with relative roughness between $0.1 - 0.000001$.
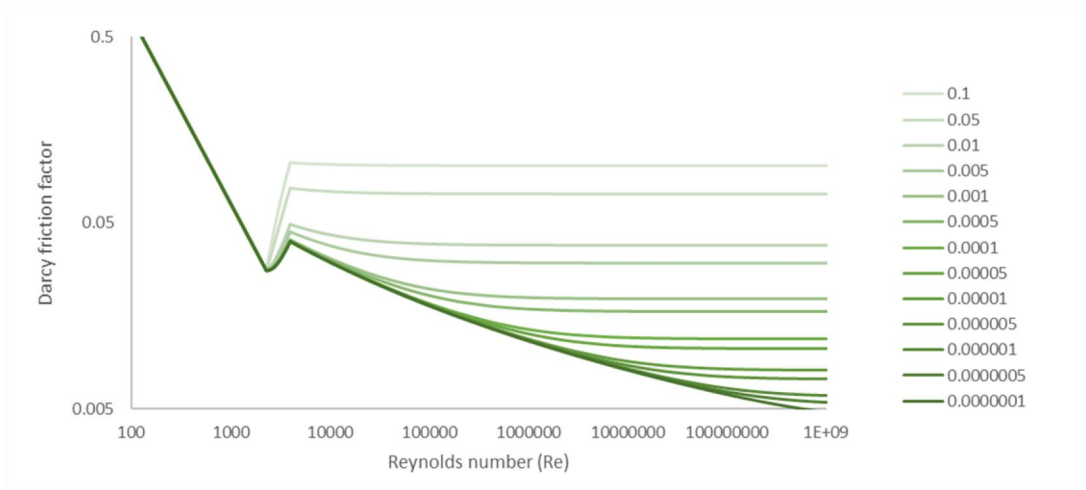
Figure 18. The logarithmic scale of a Darcy friction factor with alternate relative roughness.

The pressure loss does not significantly affect the properties of the fluid in the unsaturated state. However, it contributes to its effect on a total pressure loss. A change in density represents the pressure loss by acceleration.

$$\left(\frac{dp}{dz}\right)_{ac} = G^2 \left(\frac{d}{dz}\right)\left(\frac{1}{\rho_L}\right) \qquad (30)$$

Moreover, pressure loss by friction is qualified by the Darcy-Weisbach equation, presented by Brown (2003).

$$\left(\frac{dp}{dz}\right)_{fr} = -\zeta_L \frac{1}{D} \frac{G^2}{2} \left(\frac{1}{\rho_L}\right) \qquad (31)$$

3.2.2   Subcooled region

The subcooled region begins when the temperature of the wall T_w exceeds the saturation temperature of the fluid. The evaporation occurs when the temperature difference of the wall and the saturation temperature reach a critical value. It is defined as the ONB point, which indicates the minimum temperature difference with given heat flux and pressure. (Sato and Matsumura, 1964; Davis and Anderson, 1966; Crowe, 2005, chap. 3; Baehr and Stephan, 2011, p. 535).

$$(T_w - T_{sat})_{ONB} = \sqrt{\frac{8\sigma\left(\frac{1}{\rho_V} - \frac{1}{\rho_L}\right)T_{sat}q}{\lambda_L \Delta H_{vap}}} \qquad\qquad (32)$$

The wall superheat is defined by Equation (32) in subcooled and saturated regions as the pipe is heated uniformly throughout the tube. However, the decrease in pressure should gradually decrease the wall superheat due to changes in fluid properties if the pressure loss is significant.

Extensive research of saturated flow boiling shows that there is no general correlation to define the heat transfer in flow boiling. Various studies show that heat transfer problems can be approached, for example, by *nucleate boiling, superposition, asymptotic, flow pattern-based, the largest predominant,* and *enhancement factor* approaches (Fang *et al.*, 2019). These approaches are described in Table 5 by mathematical terms.

The *enhancement factor* models enhance the unsaturated equations by a boiling factor. In contrast, the *nucleate boiling* models neglect the effect of forced convection. A great example of a nucleate boiling model is described by Cooper (1984), while most of the superposition models are modifications of Chen (1966).

The *superposition and asymptotic* approaches combine the effect of boiling and internal forced convection by additive and power methods, respectively. Moreover, the *flow pattern-based* approach estimates the heat transfer coefficient by type of a flow pattern, illustrated in Figure 13. Remarkable models made for CO_2 are previously evaluated, for example, by Cheng et al. (2008) and Thome & El Hajal (2004) by the flow pattern approach. Nevertheless, *the largest predominant* approach evaluates the heat transfer coefficient by the most significant value of nucleate boiling and convective boiling. An example of the largest predominant model is a study of Kandlikar (1990). In conclusion, a wide range of correlations can be found in literature, if interested (see, for example, Sun and Mishima, 2009; Fang *et al.*, 2019).

Table 5. Methods of heat transfer coefficient of a two-phase flow.

Method	Expression
Nucleate boiling	$\alpha_{tp} = \alpha_{nb}$
Superposition	$\alpha_{tp} = S \cdot \alpha_{nb} + F \cdot \alpha_{sp}$
Asymptotic	$\alpha_{tp} = \left[(S \cdot \alpha_{nb})^n + \left(F \cdot \alpha_{sp} \right)^n \right]^{\frac{1}{n}}$
Flow pattern based	α_{tp} depend on the flow pattern
Largest predominant	$\alpha_{tp} = \max[\alpha_{tp,nb}, \alpha_{tp,cb}]$
Enhancement factor	$\alpha_{tp} = \psi \alpha_{sp}$

In this thesis, the heat transfer coefficient is estimated by an *enhancement factor* approach by a study of Fang, Wu, and Yuan (2017). It delivers the most accurate values up to date based on experimental data.[15]

$$Nu = \frac{\alpha D}{\lambda_L} \tag{33}$$

$$= 2260 M^{-0.18} Bo^{0.98} Fr_{L0}^{0.48} Bd^{0.72} \left(\frac{\rho_L}{\rho_V} \right)^{0.29} \left[\ln \left(\frac{\bar{\eta}_{Lf}}{\eta_{Lw}} \right) \right]^{-1} Y$$

$$Y = \begin{cases} 1 & p_r \leq 0.43 \\ 1.38 - p_r^{1.15} & p_r > 0.43 \end{cases}$$

where $\bar{\eta}_{Lf}$ is the viscosity of liquid at the mean fluid temperature, η_{Lw} is the viscosity of liquid at the wall temperature, and $p_r = p/p_{cr}$.[16]

---

[15] The model is an enchantment of the previous study by Fang, Zhou & Li (2013) which also determined the heat transfer of boiling CO_2. It delivers the mean absolute relative deviation (MARD) of 4.5 % against the database of 17,778 different data points for all liquids. Furthermore, with 476 datapoints of CO_2, the model is capable to estimate the heat transfer coefficient with MARD of 3.9 %.

[16] The module does not use the equation to define T_w because combined with Newton's cooling law it fails to give an answer even with iterative methods with the current accuracy of thermophysical properties evaluated in Chapter 4.3.1. A significant amount of time was consumed to build an iterative function based on the equation with no success. It was found out that no matter how small or big the temperature difference was, the heat flux never reached $\alpha(T_w - \bar{T}_f)$. However, if the definition of wall superheat by Equation (32) is used to determine the temperature of the wall and the fluid, the equation deviates $1 - 2$ %. Nevertheless, the model is recommended to use when the temperature of the wall and the heat is known.

The NVG point is defined by a critical temperature difference between the average temperature of bulk liquid $\bar{T}_f$ and saturation temperature T_{sat} by Saha and Zuber (1974), which has shown an excellent agreement with alternating operating conditions, fluids, and geometries.

$$\left(\bar{T}_f - T_{sat}\right)_{NVG} = 0.0022 \frac{D\dot{q}_B}{\lambda_L} \qquad\qquad Re_L Pr_L < 70000 \qquad (34)$$

$$\left(\bar{T}_f - T_{sat}\right)_{NVG} = 154 \frac{\dot{q}_B}{c_{pL}G} \qquad\qquad Re_L Pr_L > 70000$$

In the subcooled region, the vapor quality is approximated by Equation (35), which yields negative values in the subcooled region (Saha and Zuber, 1974; Crowe, 2005).

$$x_{eq} = -\frac{\Delta H_{sc}}{\Delta H_{vap}} = -\frac{1}{\Delta H_{vap}} \int_{\bar{T}_f}^{T_{sat}} c_{pL}\, dT \qquad\qquad (35)$$

The equilibrium vapor quality approaches 0 when the average temperature of bulk fluid $\bar{T}_f$ becomes closer to the saturation temperature T_{sat}. The equilibrium vapor in the saturated state is calculated by the accumulation of heat and change in total enthalpy H.

$$x_{eq} = \frac{H - H_V}{\Delta H_{vap}} \qquad\qquad (36)$$

The true vapor quality is estimated by Saha and Zuber (1974) because the vapor quality is negative in the subcooled region. The equation yields positive values in the subcooled region after the NVG point.[17] Nevertheless, the true vapor quality is assumed to be 0 between ONB and NVG,

$$x = \frac{x_{eq} - x_{NVG} \exp\left[\frac{x_{eq}}{x_{NVG}} - 1\right]}{1 - x_{NVG} \exp\left[\frac{x_{eq}}{x_{NVG}} - 1\right]} \qquad\qquad (37)$$

---

[17] Note that the definitions of equilibrium quality and true quality vary due to pressure drop along the pipe, because the enthalpy of vaporization ΔH_{vap} is evaluated in the fluid temperature. Iterative methods are required to solve Equation (34).

Literature suggests an extensive selection of correlations for void fraction ε with horizontal, inclined, and vertical orientations (see Woldesemayat and Ghajar, 2007; Ghajar and Tang, 2012; Ghajar and Bhagwat, 2013). Correlation for especially for horizontal flow presented by Rouhani and Axelsson (1968), is capable of modeling void fraction with high accuracy in horizontal tubes.[18]

$$\varepsilon = \frac{x}{\rho_V} \left\{ C \left[\frac{x}{\rho_V} + \frac{1-x}{\rho_L} \right] + \frac{1.18}{G} \left[\frac{\sigma g(\rho_L - \rho_V)}{\rho_L^2} \right]^{\frac{1}{4}} \right\}^{-1} \tag{38}$$

where $C = 1.12$.[19] The behavior of equations (34) - (38) is illustrated in the upper graph in Figure 12.

The effect of pressure becomes significant as the temperature of the fluid approaches the saturation temperature of the fluid. A pressure drop by friction in the heterogeneous model is studied extensively. However, no model still exists to predict the phenomenon accurately.[20] The module uses the model of Müller-Steinhagen & Heck because it is recommended by several authors (Zhang, Hibiki, and Mishima, 2010; Xu et al., 2012). Additionally, a modification by Xu & Fang (2012) is applied, which enhances the existing uncertainty, especially in microchannels. However, it still proposes a mean absolute relative deviation (MARD) of 25.5 %.[21] The fluid is treated as pure liquid multiplied by a two-phase multiplier Φ_{L0}^2.

$$\left(\frac{dp}{dz} \right)_{fr} = \Phi_{L0}^2 \left(\frac{dp}{dz} \right)_{L0} \tag{39}$$

$$\left(\frac{dp}{dz} \right)_{L0,V0} = \zeta_{L,V} \frac{1}{D} \frac{G^2}{2\rho_{L,V}}$$

$$\Phi_{L0}^2 = \left\{ Y^2 x^3 + (1-x)^{\frac{1}{3}} [1 + 2x(Y-1)] \right\} \cdot A$$

where A is the Xu & Fang correction factor, and Y is defined as

---

[18] As the void fraction increase over 25 %, other models worth considering are presented by Armand & Treschev (1946), Smith (1969), Premoli (1970), Mukherjee (1979), and Minami & Brill (1987), for example.

[19] Also $C = 1.54$ can be used with low velocities.

[20] The most common relations are created by Lockhart & Martinelli (1949), Friedel (1977), Chisholm (1973, 1983), and Müller-Steinhagen & Heck (1986).

[21] In comparison, the model by Lockhart-Martinelli (1949) and Friedel (1977) provide a mean absolute relative error of 49.8 % and 29.3 %, respectively, obtained by 2622 experimental data points of 15 refrigerants, CO_2 included (Xu et al., 2012).

$$A = 1 + 1.54(1 - x)^{0.5}La^{1.47}$$

$$Y = \sqrt{\frac{\left(\frac{dp}{dz}\right)_{V0}}{\left(\frac{dp}{dz}\right)_{L0}}} = \sqrt{\frac{\zeta_V}{\zeta_L}\frac{\rho_L}{\rho_V}}$$

The major pressure loss by acceleration for heterogeneous fluid is defined by Baehr and Stephan (2011) p. 522 by Equation (40).[22]

$$\left(\frac{dp}{dz}\right)_{ac} = G^2\left(\frac{d}{dz}\right)\left[\frac{x^2}{\alpha\rho_G} + \frac{(1-x)^2}{(1-\alpha)\rho_L}\right] \tag{40}$$

3.2.3   Saturated region

In the saturated region, the temperature of the bulk fluid $\bar{T}_f$ has reached the saturation temperature T_{sat} at a given pressure. By Figure 5, it could be observed that the CO_2 operates primarily in this region. Additionally, the temperature does not significantly change along the pipe, which is defined by pressure loss.

$$\left(\frac{dT}{dz}\right) = \frac{\left(\frac{dp}{dz}\right)}{\left(\frac{dp_{sat}}{dT}\right)} \tag{41}$$

Many of the equations in the saturated region are presented in the previous Chapter 3.2.2 Subcooled region. For example, the vapor quality at saturated conditions x is defined by the Equations (36) and (37). The void fraction ε is calculated by Equation (38) and pressure losses by friction and acceleration are measured by equations (39) and (40) as well.

---

[22] Again, the pressure drop by two arbitrary points decrease the value of thermodynamic properties. Therefore, iterative methods are applied to solve the pressure drop. It should be noted that the pressure drop by acceleration compared to friction is relatively very small.

4 THERMOPHYSICAL PROPERTY MODULE

The equations presented in Chapters 2 and 3 require the evaluation of the thermophysical properties of materials. Otherwise, they are useless by themselves. This chapter proposes thermophysical properties and gives a comprehensive overview of the uncertainties. Moreover, the chapter describes how the optimization of the parameters is made and presents how the uncertainties are evaluated.

In general, the properties are evaluated as a function of temperature, while the variation in pressure is negligible. However, the properties of CO_2 are evaluated at saturated conditions, which takes the effect of pressure into account. Consequently, the evaluation of the effect of pressure involves a substantially complex calculation based on Gibbs free energy or Helmholtz free energy with hundreds of parameters (See derivation of the equation of states of water and carbon dioxide by Span and Wagner, 1996; Wagner and Kretzschmar, 2008). The complexity of equations of states (EOS) is directly proportional to the performance of the model. Therefore, the equations presented are relatively simple.

4.1   Optimization of model parameters

A list of parameters for equations is proposed in Appendix A.[23] A minority of models can be obtained from literature, but a majority requires a curve fitting. Consequently, the least-squares method is a traditional way to fit a curve for individual values

$$\min\left[\sum_{1=1}^{n}\left(X_i - X(T_i)\right)^2\right] \tag{42}$$

However, the sum of absolute error suits better with models with low values ($X_i < 1$).

$$\min\left[\sum_{1=1}^{n}|X_i - X(T_i)|\right] \tag{43}$$

---

[23] The optimization requires scaling of each parameter to the magnitude within a range of $0.01 - 100$. The optimization was conducted by using Microsoft EXCEL® add-in Solver with a GRG Nonlinear Method with a converge of 0.00001.

4.2   Uncertainty analysis

A comprehensive list of complete errors is found in Appendix B. The error proposed by literature is a mean absolute relative error (MARD) unless otherwise stated. Furthermore, the uncertainty by curve-fitting is calculated by MARD, while the results are given in percentages.

$$\delta = \frac{1}{n}\sum_{i=1}^{n}\left|\frac{X_i - X(T_i)}{X_i}\right| \tag{44}$$

The overall uncertainty is obtained by adding the uncertainty of curve-fitting δ_{fit} to the uncertainty of literature δ_{lit}.

$$\delta_{tot} \approx \delta_{lit} + \delta_{fit} \tag{45}$$

4.3   Evaluation of thermophysical property models

This thesis uses several databanks to evaluate thermophysical properties. For example, Project 801 from DIPPR *(Design Institute for Physical Property Data, 2019),* which is a part of AIChE *(American Institute of Chemical Engineers),* gives equations for pure substances. Equations are usually fitted to experimental data. The advantage of the database is that the data is critically evaluated. However, it usually lacks the accuracy of some properties, because the models do not take the variation in pressure into account. However, they are usually enough to use in calculations in many industrial applications. Nevertheless, the equations presented by Project DIPPR 801 are listed in Table 6. They are considered in analyzing the validity of thermodynamic property models.

Model	Equation
$$X(T) = \dfrac{a_0 T^{a_1}}{1 + \dfrac{a_2}{T} + \dfrac{a_3}{T}}$$	(46)
$$X(T) = a_0(1 - T_r)^{a_1 + a_2 T_r + a_3 T_r^2 + a_4 T_r^3}, \qquad T_r = \dfrac{T}{T_{cr}}$$	(47)
$$X(T) = a_0 + a_1\left(\dfrac{\frac{a_2}{T}}{\sinh\frac{a_2}{T}}\right)^2 + a_3\left(\dfrac{\frac{a_4}{T}}{\sinh\frac{a_4}{T}}\right)^2$$	(48)
$$X(T) = \exp\left(a_0 + \dfrac{a_1}{T} + a_2 \ln T + a_3 T^{a_4}\right)$$	(49)
$$X(T) = \dfrac{a_0}{a_1^{\,1+\left(1-\frac{T}{a_2}\right)^{a_3}}}$$	(50)
$$X(T) = a_0 + \dfrac{a_1}{T_R} + a_2 T_R + a_3 T_R^2 + a_4 T_R^3, \qquad T_R = 1 - \dfrac{T}{T_{cr}}$$	(51)

Besides, it is common that the data is fitted to experimental data with n-order polynomial function expressed as

$$X(T) = a_n T^n + a_{n-1} T^{n-1} + \cdots + a_2 T^2 + a_1 T + a_0 \tag{52}$$

Moreover, the information by NIST *(National Institute of Standards and Technology)* is widely applied in process technology due to its accuracy and validity. NIST Chemistry WebBook provides data with pressure changes as well, but some of the theoretical equations presented are highly complex. The last major update of the system was made in October 2018, and some of the references became outdated. (Linstrom and Mallard, 2018). This chapter also enhances the accuracy of the NIST Chemistry WebBook with more recent researches on thermodynamic properties for the substances, for example, on viscosity and thermal conductivity of water and steam by 2019 edition of International Steam Tables (Kretzschmar and Wagner, 2019).[24]

---

[24] NIST provides also a software (*REFPROP*, 2019) to obtain the state of the fluid but its license was not available. Fortunately, cost free alternatives have been developed, for example, CoolProp (2017).

Extensive literature research has been performed to evaluate the thermodynamic property models. The resources of NIST Chemistry WebBook and Project DIPPR 801 are extensively used, and information by the Finnish Standards Association is also considered. Some data was found by individual studies as well. The uncertainty analysis was made, and the appropriate models were selected based on minimum uncertainty and validity.

The stationary solids require only the thermal conductivities to be defined. However, COMSOL Multiphysics® needs to address the heat capacities and densities to evaluate the thermal diffusivity, which can be used to construct transient heat transfer models in the future.

4.3.1 Carbon dioxide

The uncertainties and validity of the thermophysical properties of carbon dioxide are evaluated between triple point T_{tr} and critical point T_{cr} at saturated conditions. Moreover, as the pressure changes are low, the unsaturated region uses the saturated properties of carbon dioxide. The properties are displayed visually by figures because some of the equations presented require validity to literature data.[25]

4.3.1.1 Vapor pressure of carbon dioxide

Vapor pressure of carbon dioxide can be presented by Equation (49). However, a 3-order polynomial model, fitted to a study by Span & Wagner (1996), provides a more favorable uncertainty.[26] It was found out that the inverse function was required, and it was achieved by fitting a 6-order polynomial to work by Span & Wagner (1996). Furthermore, Figure 19 illustrates the vapor pressure by Project DIPPR 801 (Equation 49) and Span & Wagner (1996) as a function of temperature. As a result, identical curves can be observed.

---

[25] Equations (55) - (60).

[26] The data was retrieved by Thermophysical Properties and Fluid Systems by NIST Chemistry WebBook. Saturation properties was set with default standard state convection for fluid. The original model by Span & Wagner (1996) is accurate and works as an industrial reference but involves heavy calculations to solve.
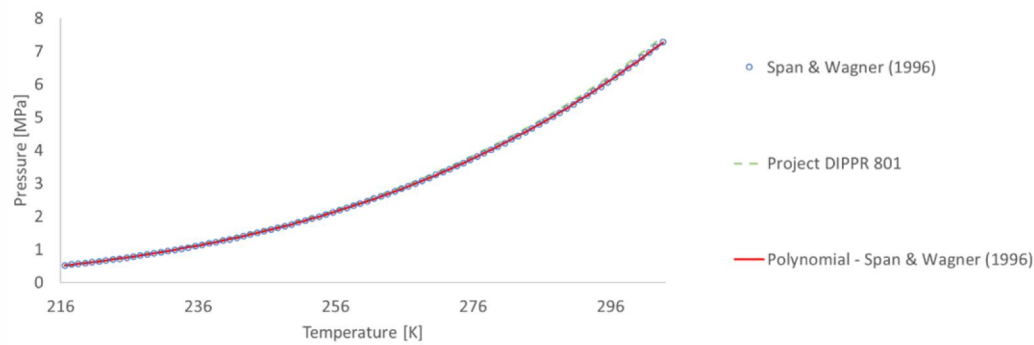
Figure 19. Vapor pressure of CO$_2$.

4.3.1.2 Enthalpy of vaporization of carbon dioxide

By Project DIPPR 801, the enthalpy of vaporization can be modeled by Equation (47). Furthermore, Equation (47) was optimized by using the study of Span & Wagner (1996) as a reference, which produced better uncertainty.[27] A graphical representation illustrates the enthalpy of vaporization with optimized and original parameters by Equation (47). Figure 20 also includes the enthalpies of vapor and liquid separately by the study of Span & Wagner (1996). Nevertheless, it can be observed that the models are congruous, and parameter optimization is not a necessity. The most substantial uncertainties are observed near the critical point.
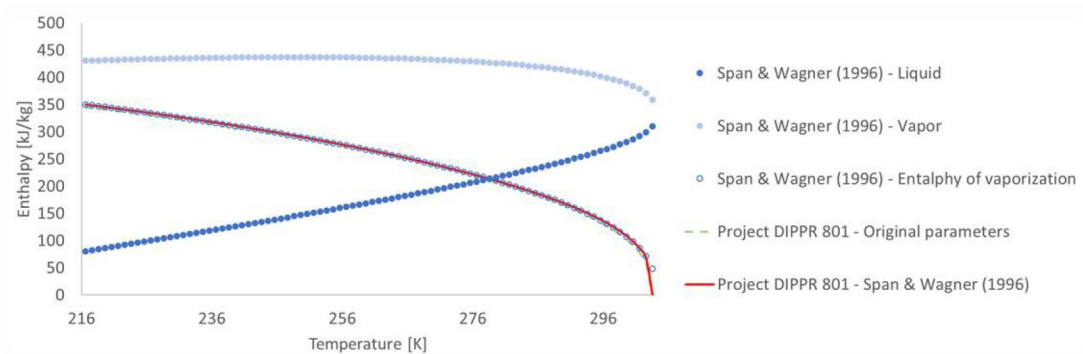
Figure 20. Enthalpy of vaporization of CO$_2$.

---

[27] The data was retrieved by Thermophysical Properties and Fluid Systems by NIST Chemistry WebBook. Saturation properties was set with default standard state convection for fluid.

4.3.1.3 The density of carbon dioxide

The liquid carbon dioxide is an incompressible fluid. The liquid density can be presented by Equation (50) by Project DIPPR 801. Again, the study by Span & Wagner (1996) provides a more accurate representation of the property.

$$\ln \rho_L = \sum_{i=0}^{3} a_i \left(1 - \frac{T}{T_{cr}} \right)^{b_i} \tag{53}$$

In contrast, the density of the vapor phase is strongly dependent on both pressure and temperature. The EOS by Span & Wagner (1996) also provides a model for saturated vapor.

$$\ln \rho_V = \sum_{i=0}^{4} a_i \left(1 - \frac{T}{T_{cr}} \right)^{b_i} \tag{54}$$

In terms of accuracy and consistency of models, equations (53) and (54) are selected to model the density of carbon dioxide. The advantage of these equations is that additional error by curve fitting is not applied. Figure 21 illustrates the densities of vapor and liquid as a function of temperature by Project DIPPR 801 and the equations (53) and (54). For reference, ideal gas law is also represented for vapor, which shows a significant deviation near the critical point. In contrast, the model by Project DIPPR 801 is equal to Equation (53).
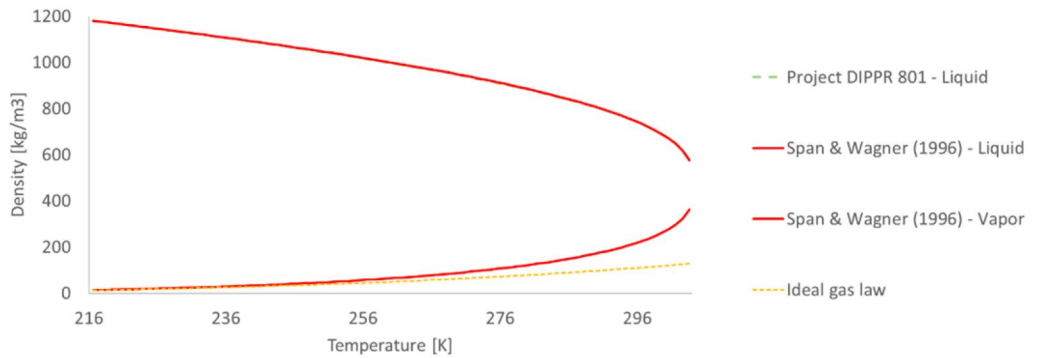
Figure 21. The density of saturated CO_2.

4.3.1.4 Thermal conductivity of carbon dioxide

Project DIPPR 801 delivers a linear 1-order polynomial model for the thermal conductivity of the liquid. In contrast, the model by Vesovic et al. (1990) provides additional value by taking into account the effect of increased pressure.[28] However, it involves a complex calculation based on two-body molecular interactions in the limit of zero-density circumstances, enhancement near the critical point, and experimental residual part. As a result, this thesis proposes an approximation for thermal conductivity for liquid carbon dioxide at saturated conditions, fitted to the model by Vesovic et al. (1990) with an estimated error of 5.12 %.[29]

$$\lambda_L(T) = a_0 + b_0(T - T_{tr})^{b_1} + \sum_{i=0}^{1} c_i b_i^{\frac{T_{cr}-T}{T_{cr}-T_{tr}}} \tag{55}$$

Moreover, the thermal conductivity of vapor is given by Equation (46). Similarly, a more accurate model is achieved by a proposal of approximation, fitted to the study of Vesovic et al. (1990) with a total maximum uncertainty of 5.74 %.

$$\lambda_V(T) = a_0 + b_0(T - T_{tr})^{b_1} + \sum_{i=0}^{2} c_i d_i^{\frac{T_{cr}-T}{T_{cr}-T_{tr}}} \tag{56}$$

The graphical representation shows that that the equations (55) and (56) correlate well with the EOS by Vesovic et al. (1990). Furthermore, Figure 22 also represents the equations Project DIPPR 801 with original parameters for both vapor and liquid. It could be observed that the inaccuracy of Project DIPPR 801 becomes a significant near critical point for both vapor and liquid.

---

[28] The data was retrieved by Thermophysical Properties and Fluid Systems by NIST Chemistry WebBook. Saturation properties was set with default standard state convection for fluid. The study is currently a reference to the NIST Chemistry WebBook.

[29] The equations (55) - (60) were formulated from scratch by trial and error. An estimated uncertainty was created by the uncertainty informed by the study with uncertainty by curve fitting.
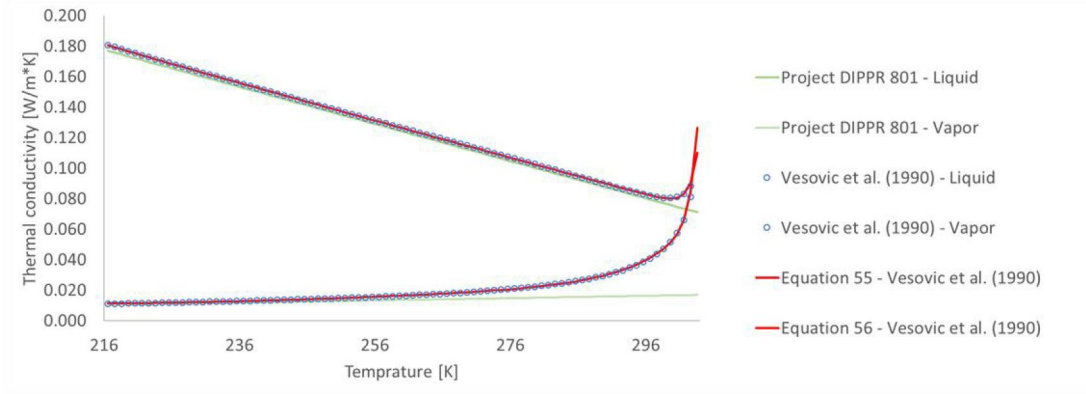
Figure 22. Thermal conductivity of saturated CO₂.

4.3.1.5 Dynamic viscosity of carbon dioxide

The viscosity of liquid carbon dioxide by Project DIPPR 801 can be presented by Equation (49). However, the Equation is inaccurate near the critical point and delivers considerable uncertainty over the whole temperature range. Alternatively, this paper suggests a simplified model with a total error of 2.1 % maximum, fitted to study by Fenghour et al. (1998). The study currently holds as a reference in NIST Chemistry WebBook.

$$\eta_L = a_0 + b_0 c_0^{-\frac{T_{cr}-T}{T_{cr}-T_{tr}}} + \sum_{i=1}^{2} b_i c_i^{\frac{T_{cr}-T}{T_{cr}-T_{tr}}} \tag{57}$$

Moreover, the viscosity of vapor, according to Project DIPPR 801, is presented by Equation (46). Similarly, this paper proposes a more accurate model to model viscosity of vapor at saturated conditions, based on the model by Fenghour et al. (1998) with a total uncertainty of 2.29 %.

$$\eta_V = a_0 + b_0 (T - T_{tr})^{b_1} + \sum_{i=0}^{2} c_i d_i^{\frac{T_{cr}-T}{T_{cr}-T_{tr}}} \tag{58}$$

Figure 23 represents the viscosity of vapor and liquid as a function of temperature. It includes the model of Project DIPPR 801 with original parameters, Equations (57) and (58), and the data by Fenghour et al. (1998). Equations (57) and (58) are almost identical to the study and give a better result compared to the model by Project DIPPR 801.
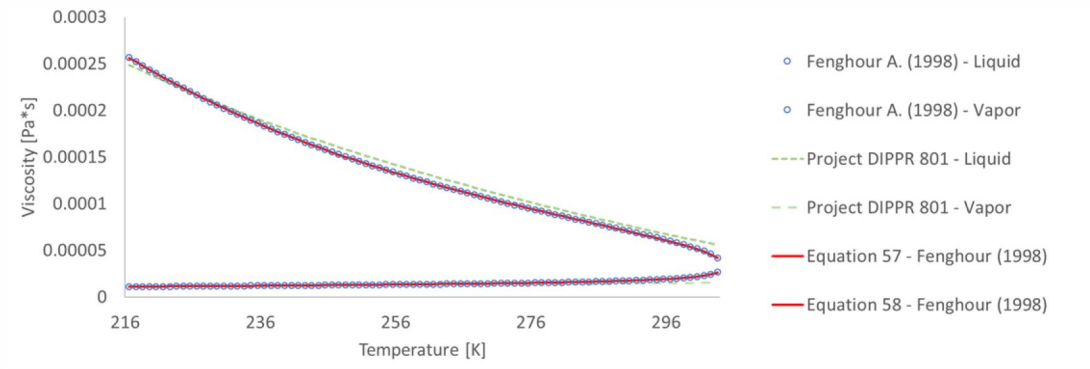
Figure 23. Dynamic viscosity of saturated CO$_2$.

4.3.1.6 Isobaric specific heat capacity of carbon dioxide

By Project DIPPR 801, the isobaric specific heat capacity of liquid can be modeled with 3-order polynomial. In contrast, this paper proposes a simplified model fitted to the study of Span & Wagner (1996) with a total error of 1.53 %.

$$c_{pL} = a_0 + \sum_{i=0}^{3} b_i c_i^{\frac{T-T_{tr}}{T_{cr}-T_{tr}}} \tag{59}$$

Nevertheless, the isobaric heat capacity of vapor by Project DIPPR 801 is interpreted by Equation (48). However, it is only suitable to model ideal gas. Therefore, this paper proposes an approximation for the heat capacity of saturated vapor, fitted to the EOS by Span & Wagner (1996) with a total uncertainty of 0.26 %.

$$c_{pV} = a_o + \sum_{i=0}^{3} b_i c_i^{\frac{T-T_{tr}}{T_{cr}-T_{tr}}} \tag{60}$$

Figure 24 provides a graphical representation of Project DIPPR 801 with the original values and data by Span & Wagner (1996). It shows the consistency of Equations (59) and (60). The model of Project DIPPR 801 is the most inaccurate and especially lacks the accuracy near the critical point. However, the Equations (59) and (60) show a strong correlation with the data by Span & Wagner (1996). Especially scaling the figure enhances the visualization of the accuracy.
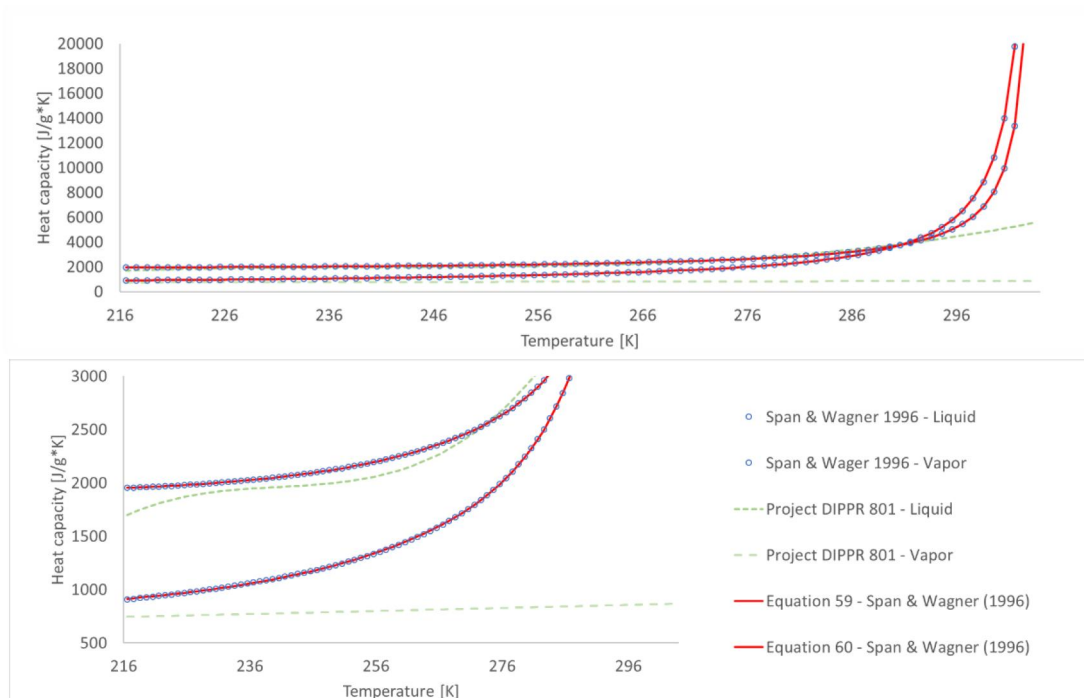
Figure 24. Heat capacity of saturated CO₂. The second figure is scaled.

4.3.1.7 The surface tension of carbon dioxide

The Equation (47) by Project DIPPR 801 and study by Rathjen & Straub (1977) give an equal uncertainty with identical curves, as in Figure 25.[30] Nevertheless, it should be critical towards the values since the effect of pressure is uncertain.
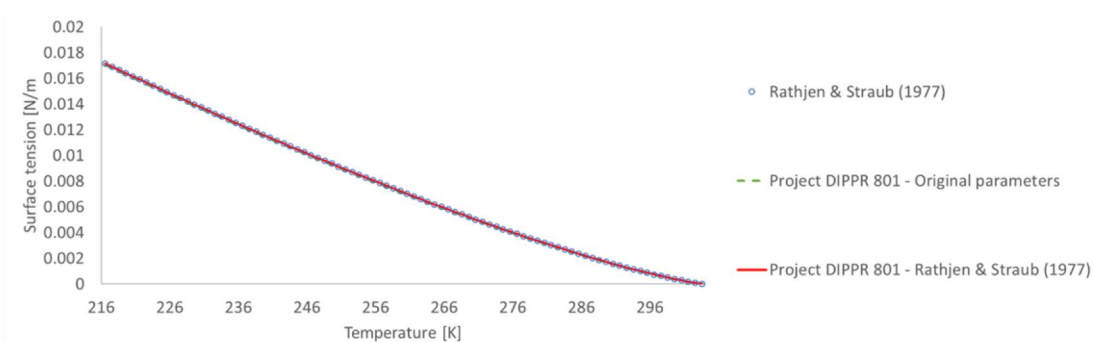
Figure 25. The surface tension of saturated CO₂.

---

[30] The data was retrieved by Thermophysical Properties and Fluid Systems by NIST Chemistry WebBook. Saturation properties was set with default standard state convection for fluid. The study of Rathjen & Straub (1977) stands currently as a reference in NIST Chemistry WebBook.

4.3.2   Ice

The thermophysical properties of the ice are evaluated at atmospheric pressure. The density and the isobaric heat capacity are achieved by a linear representation of Project DIPPR 801. The lines were optimized to match the linearity by Feistel & Wagner (2006) to enhance the total uncertainty.[31] Furthermore, an only relevant reference for the thermal conductivity of ice is presented by the 2-order polynomial of Choi & Okos (1986).[32] Figure 26 visualizes the effect of optimization and compares the result with the model by Project DIPPR 801. As observed, the effect of the optimization is not substantial.
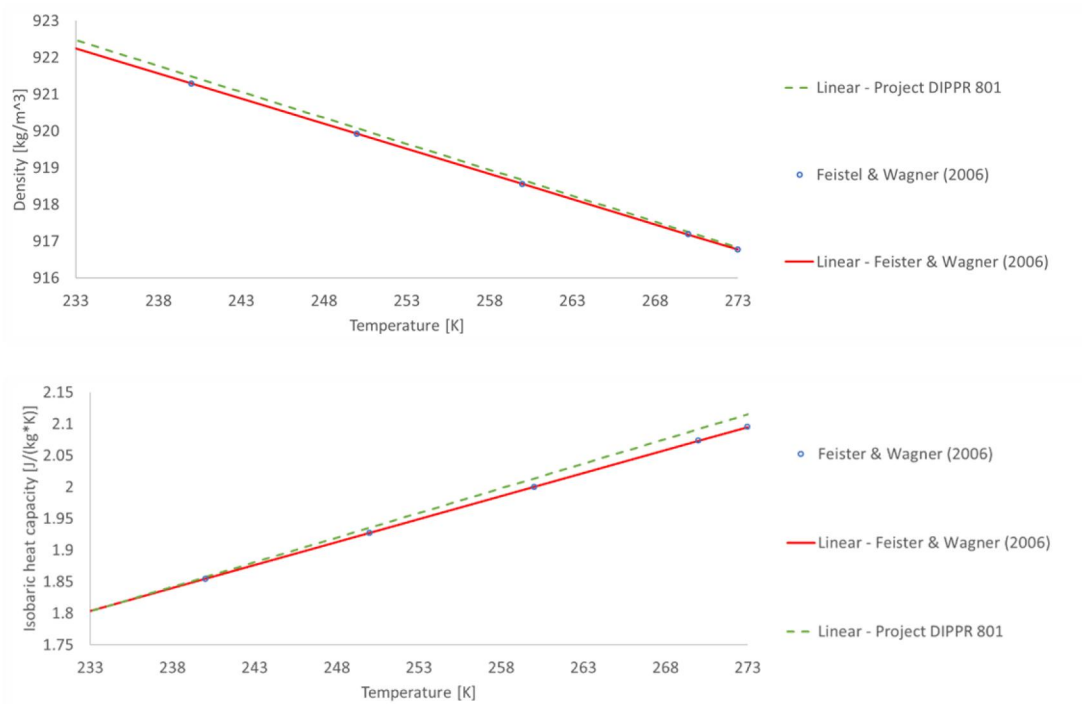
Figure 26. A) The density of ice. B) Specific isobaric heat capacity of ice.

---

[31] Currently, the study holds as a reference by IAPSW (International Association for the Properties of Water and Steam) for ice.

[32] The uncertainty of the model is presented by standard error.

4.3.3   Copper

Finnish Standards Association (SFS) has standardized the properties of copper pipes in Finland.[33] The thermal conductivity of copper depends on the residual resistivity ratio (RRR), which is defined as an electrical purity of a metal. White & Minges (1997) represent a model for thermal conductivity with different RRR-values, as in Figure 27, optimized by 44 references. These 4-order polynomials were fitted to match the values in the temperature range of $150 - 400\ K$. The tool uses the electrical resistivity ratio of 100 as a default value.
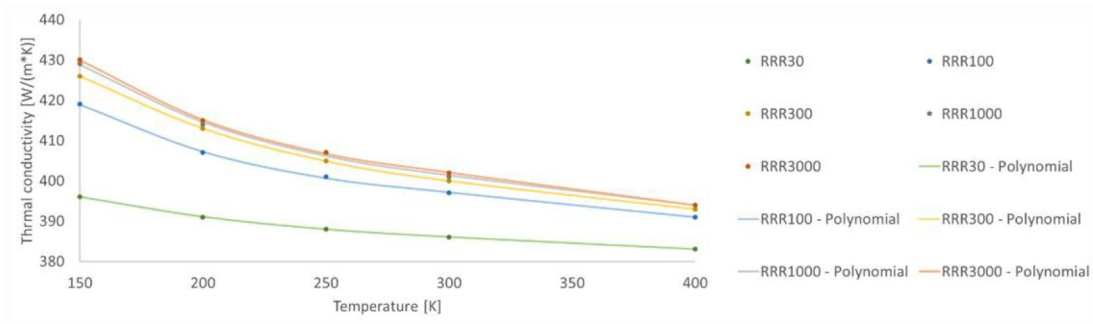
Figure 27. Thermal conductivity of copper with the variable residual resistivity ratio.

The density of copper is assumed to be constant $8960\ kg/m^3$. However, there is a slight expansion and shrinkage in the material when the temperature is increasing or decreasing. However, the effect is assumed to be negligible. In the temperature range of $25 - 300\ K$, the heat capacity is proposed by White & Collocott (1984).

$$c_p = \sum_{n=0}^{8} a_n \left(\frac{T}{100}\right)^n \qquad (61)$$

In the temperature range of $300 - 1300\ K$, the isobaric specific heat capacity is defined by a 4-order polynomial equation by the same study. It was noted that COMSOL Multiphysics® provides a more specific function for heat capacity, but the function equal to the study.

---

[33] See *SFS-EN 13349: Copper and copper alloys. Pre-insulated copper tubes with solid covering*, 2002; *SFS-EN 1057 + A1: Copper and copper alloys. Seamless, round copper tubes for water and gas in sanitary and heating applications*, 2012; *SFS-EN 12735-2:2016: Copper and copper alloys. Seamless, round tubes for air conditioning and refrigeration. Part 2: Tubes for equipment*, 2016.

4.3.4 Polyethylene

The polymers of the system are made by polyethylene. It is cheap to manufacture, durable, and its surface is smooth, which allows the fluid to flow smoothly in the interface. The properties of the polyethylene depend on the type of polymer, crystallinity, linearity, orientation, and morphology. Polyethylene is used on the cooling pipes and as a primary material of the heating pipes. The polymer layer on the copper allows the pipe and concrete to withstand the stresses of thermal expansion and contraction.

Moreover, the polymer used on the cooling pipes is treated as low-density polyethylene (LDPE) due to its requirement for elasticity. Furthermore, the frost protection pipes are made by PEX or PEH polymers, which are abbreviations and trade names for cross-linked polyethylene (XLPE) and high-density polyethylene (HDPE). HDPE makes almost all XLPE pipes, and their thermal properties resemble the HDPE properties as well. The characteristics of HDPE are high linearity, crystallinity, density, and thermal conductivity. In contrast, LDPE is more amorphous, elastic, and lightweight due to its branching. As a result, the model uses a degree of branching θ to measure the thermodynamics properties of polyethylene linearly.

$$X_{PE} = \theta X_{LDPE} + (1 - \theta)X_{HDPE} \qquad (62)$$

where X is either density ρ, thermal conductivity λ, or heat capacity c_p. Extensive research on various types of polyethylene shows that the average density for branched and linear polyethylene are $\rho_{LDPE} = 919 \ kg/m^3$ and $\rho_{HDPE} = 969 \ kg/m^3$, measured in room temperature and pressure (Gaur and Wunderlich, 1983). Moreover, the thermal conductivities of branched and linear polyethylene are $\lambda_{LDPE} = 0.367 \ W/(m \cdot K)$ and $\lambda_{HDPE} = 0.427 \ W/(m \cdot K)$, respectively (Yu *et al.*, 2014). These values are assumed to increase and decrease respectively with increasing temperatures slightly, but the effect is considered negligible. In contrast, the specific heat capacities of both types of polyethylene, c_{pHDPE} and c_{pLDPE}, can be estimated by 6-order polynomials, fitted to the study of Chang (1974).[34]

---

[34] Note that the molar mass of the polyethylene must be determined. The molar masses are extremely high, varying between $10^3 - 10^8 \ g/mol$.
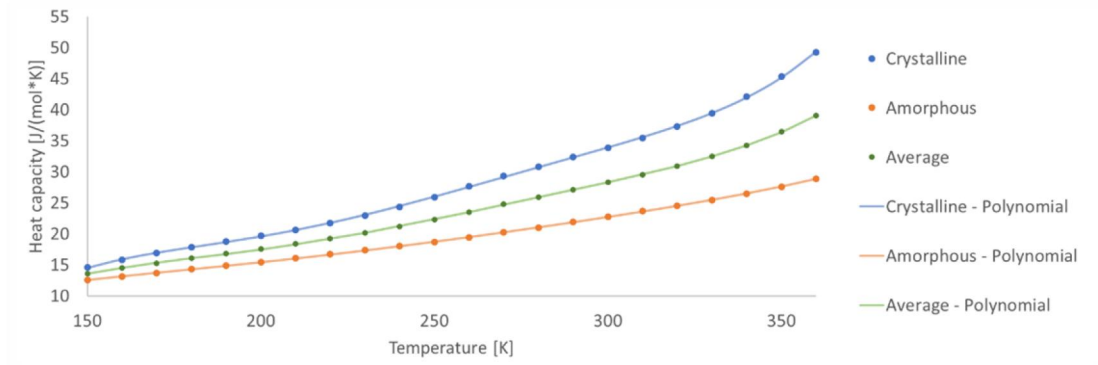
Figure 28. Isobaric heat capacity of polyethylene as a function of temperature.

4.3.5 Concrete element

Figure 29 presents the layered structure of the reinforced porous concrete element. The concrete element consists of concrete, additional air, and reinforcement steel. However, additional air is mixed with the concrete to withstand the internal stresses and overcome the expansion of moisture when the water freezes. The additional air enables the water to expand into the porous structure. It reduces the formation of cracks and structure breakdown. The concrete is treated as a normal-weight concrete (NWC), and the additional air is treated as dry air. The properties of dry and humid air are presented in Appendix D.
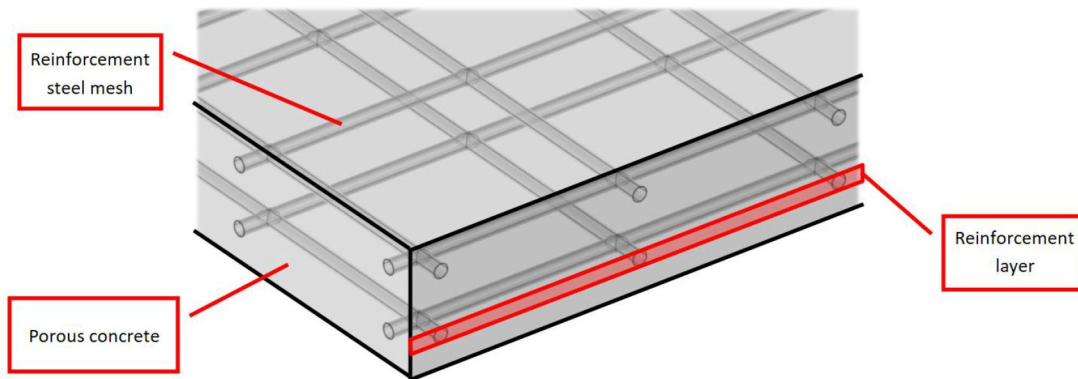
Figure 29. A 3D-view of a reinforced concrete structure.

Thermophysical properties of concrete depend on the content of cement, rough and fine aggregates, porosity, additives, and water (Guo *et al.*, 2011; Chan, 2013; Suomen betoniyhdistys ry, 2019). By the Finnish Standards Association (SFS) the specific isobaric heat capacity and thermal conductivity for normal-weight concrete is defined by 2-order polynomial model as

$$\left(c_p, \lambda_{low}, \lambda_{up}\right)_{NWC} = a_0 + a_1 \left(\frac{T - 273.15}{100}\right) - a_2 \left(\frac{T - 273.15}{100}\right)^2 \qquad (63)$$

where low and up are subscripts for the lower and upper limit of thermal conductivity.[35] A thermal conductivity lies between upper and lower limit values. However, the upper limit is generally used to measure the maximum heat flux through the system. However, the range of validity of Equation (63) is in the range of $293 - 1473\ K$ and the best approximation for assuming the state of concrete in cold environments is to extend the validity range to operating temperature.[36] Moreover, the density is assumed to be averaged constant with a default value of $2380\ kg/m^3$. The marginal shrinkage and contraction in length are considered negligible.

Additionally, the requirement for concrete by stresses in a cold and humid environment is XF3. The expansion of water in the concrete must be taken account by adding extra air into the structure, in an average of 5,5 volume percent ($\phi_V = 0.055$) depending on the grain size and estimated lifespan of the structure. [37] (Suomen betoniyhdistys ry, 2019) Therefore, the properties of porous concrete are treated as a mixture of dry air and normal-weight concrete as

$$\rho_{PC} = \rho_{DA}\phi_V + \rho_{NWC}(1 - \phi_V) \qquad (64)$$

$$c_{pPC} = c_{pDA}\phi_m + c_{pNWC}(1 - \phi_m) \qquad (65)$$

The conversion from volume fraction (ϕ_V) mass fraction (ϕ_m) between the discrete phase and the continuous matrix is calculated by equation (67). In this case, the discrete phase is dry air ($dis = DA$), and continuous matrix is a normal weight concrete ($con = NWC$).

$$\phi_m = \frac{\phi_V \rho_{dis}}{\phi_V \rho_{dis} + (1 - \phi_V)\rho_{con}} \qquad (66)$$

---

[35] See *SFS-EN 1994-1-2 + AC + A1: Eurocode 4. Design of composite steel and concrete structures. Part 1-2: General rules. Structural fire design*, 2014
[36] Operating temperature is near $264\ K$
[37] Expansion is around 9 %

The literature suggests a wide range of theoretical models to estimate the thermal conductivity of porous substances (Progelhof, Throne and Ruetsch, 1976; Pietrak and Wiśniewski, 2015; Zhu, Fan and Zhang, 2016). Additionally, experimental research on porosity and its effect on thermal conductivity of concrete elements is studied extensively (Ganjian, 1990; Tinker and Cabrera, 1992; Asadi *et al.*, 2018; Chen *et al.*, 2019). Supported by Chan (2013) and Zhu (2016), the thermal conductivity of porous concrete is estimated by the lower bound of Hashin-Shtrikman.[38]

$$\lambda_{PC} = \lambda_{NWC} + \frac{\phi_V}{\left(\dfrac{1}{\lambda_{HA} - \lambda_{NWC}} + \dfrac{1 - \phi_V}{3\lambda_{NWC}}\right)} \tag{67}$$

Furthermore, the heat capacity of reinforcement steel inside the concrete is defined by a 4-order polynomial model.[39]

$$c_{pRS} = a_0 + a_1(T - 273.15) + a_2(T - 273.15)^2 + a_3(T - 273.15)^3 \tag{68}$$

However, the validity of the presented model is in the range of $293 - 873\ K$ with unknown uncertainty. Thus, the range of validity must be extended to operation temperature, assuming there are no structural changes in reinforcement steel if the temperature is decreased. By the standard, the thermal conductivity of the reinforcement steel is defined as a linear model with the range of $293 - 1073\ K$. However, it is assumed that it works at the operating temperature.

$$\lambda_{RS} = a_0 - a_1(T - 273.15) \tag{69}$$

---

[38] Hashin-Shtrikman-model is the same as the "exact" solution of original and theoretical model by Maxwell. It assumes a randomly dispersed and non-interacting homogeneous spheres in a homogeneous continuous matrix.
[39] See *SFS-EN 1994-1-2 + AC + A1: Eurocode 4. Design of composite steel and concrete structures. Part 1-2: General rules. Structural fire design*, 2014

The Finnish Standards Association defines the most common type of steel used inside the concrete.[40] The average density of reinforcement steel is $\rho_{RS} = 7850 \ kg/m^3$. As the steel mesh is standardized, the void fraction ω of the reinforced steel mesh inside the reinforcement layer is defined by Equation (70). [41]

$$\omega_m = \left(\frac{m}{DA\rho} \right)_{RS} \tag{70}$$

Thus, the overall thermophysical properties of the reinforcement layer are

$$\rho_{RL} = \rho_{RS}\omega_V + \rho_{PC}(1 - \omega_V) \tag{71}$$

$$c_{pRL} = c_{pRS}\omega_m + c_{pPC}(1 - \omega_m) \tag{72}$$

The conversion between mass fraction and volume fraction is obtained by Equation (66). Moreover, the thermal conductivity of the reinforcement layer is estimated by a geometric mean with a function of void fraction ω which is independent of the direction of heat (Progelhof, Throne and Ruetsch, 1976).

$$\lambda_{RL} = \lambda_{RS}^{\omega_V} + \lambda_{PC}^{(1 - \omega_V)} \tag{73}$$

---

[40] See *SFS 1200: Betonirakenteiden yleiset teräkset. Lajit, nimikkeet ja merkinnät yleisissä tuotteissa*, 1999.
[41] For example, for 8-200 B500K MP, $m = 46.91 \ kg$, $A = 11.75 \ m^2$, and $D = 0.008 \ m$.

4.3.6   Insulation

Extruded polystyrene (XPS) is a common material used in the insulation of buildings. Its most critical thermophysical properties are thermal conductivity and density. The properties depend on the manufacturer and structure. Therefore, the properties cannot be established accurately, and the uncertainty is significant.

Table 7. Thermophysical properties of extruded polystyrene (XPS) and their uncertainties. (*SFS-EN 13164 + A1 Tehdasvalmisteiset lämmöneristystuotteet. Tehdasvalmisteiset suulakepuristetut polystyreenituotteet (XPS). Tuotestandardi*, 2007; Rakennustieto.fi, 2012; Lakatos, 2014)

Property	Unit	Estimated value	Uncertainty
Density	kg/m^3	35	25 … 50
Thermal conductivity	$W/(m \cdot K)$	0.036	0.029 … 0.041
Specific heat capacity	$J/(kg \cdot K)$	1460	–

4.3.7   Gravel fill

The most significant uncertainty becomes with the gravel fill because the type can vary between fine silt and clay to a rough aggregate. Gravel is treated as fine gravel by the international standards.[42] Due to considerable uncertainty, the thermophysical properties are treated as constants, which are defined in Table 8.

Table 8. Thermophysical properties of gravel fill.

Property	Unit	Estimated value	Uncertainty
Density	kg/m^3	1600	–
Thermal conductivity	$W/(m \cdot K)$	0.7	–
Specific heat capacity	$J/(kg \cdot K)$	830	–

---

[42] See *ISO SFS-EN 14688-1:2018: Geotechnical investigation and testing. Identification and classification of soil. Part 1 : Identification and description (ISO 14688-1:2017)*, 2018

4.3.8   Brine

The most common brine is a mixture of (mono)ethylene glycol (MEG) and water. However, due to the toxicity of ethylene glycol for human health, the mixture of 1-2-propylene glycol (PEG) and water is used as well (Gomes, Liteplo, and Meek, 2002). While MEG and PEG are considered in the analysis, thermophysical properties for other brines can be found in the literature with high accuracy (See, for example, Sun and Teja, 2003, 2004). The overall equation for properties of both MEG (λ, $\ln \eta$ and ρ) and PEG ($\ln \eta$ and λ) are described by Equation (74).

$$X_{MIX} = x X_{GL} + (1 - x) X_W - \Psi (X_{GL} - X_W)(1 - x)x \qquad (74)$$

$$\Psi = a_3 + a_4 x + a_5 T + a_6 x^2$$

where X determines a thermodynamic property. However, a few modifications on Equation (74) must be made, especially with propylene glycol. Moreover, the heat capacity of the mixture is calculated by a rule of mixtures.

$$c_{pMIX} = x c_{pW} + (1 - x) c_{pGL} \qquad (75)$$

The thermophysical properties of water were obtained by fitting suitable polynomials to the industrial formulation of water IAPWS-IF97 (Wagner and Kretzschmar, 2008; Huber *et al.*, 2009, 2012; Kretzschmar and Wagner, 2019). Similarly, Project DIPPR 801 represents the properties as polynomials, but the dynamic viscosity is obtained by (49). Due to the increased effect of pressure and a more favorable accuracy of IAPWS-IF97, models by Project DIPPR 801 are not used. However, they show consistency with IAPWS-IF97. The thermophysical properties were evaluated at the averaged operation pressure of 6 bars.

4.3.8.1 Ethylene glycol (MEG)

With relation to Equation (74), the following relations are valid.

$$(\rho, \lambda)_{MEG} = a_0 + a_1 T + a_2 T^2$$

$$\ln \eta_{MEG} = a_0 + \frac{a_1}{T + a_2}$$

Moreover, Project DIPPR 801 gives a relation of heat capacity by Equation (51). Figure 30 visualizes the thermophysical properties of ethylene glycol/water mixtures. In contrast to propylene glycol, an excess volume is observed. The lines represent the mass fraction of ethylene glycol in the brine.

Figure 30. Thermophysical properties of ethylene glycol/water mixtures. The lines present the mass fraction of ethylene glycol in the mixture.

4.3.8.2 Propylene glycol (PEG)

Despite the equation (74), the density of PEG-water mixture is described as

$$\rho_{MIX} = \sum_{i=1}^{3}\sum_{j=1}^{3} A_{i,j}x^{j-1}T^{i-1} \tag{76}$$

In consideration of Equation (74) and case the of viscosity and thermal conductivity, the following relations are valid

$$\ln\eta_{PEG} = a_0 + a_1 T + a_2 T^2$$

$$\lambda_{PEG} = a_0 + \frac{a_1}{T - a_2}$$

By Project DIPPR 801, the isobaric specific heat capacity of propylene glycol is expressed by Equation (51) with the uncertainty of $< 3\,\%$. Figure 31 represents the thermophysical properties of the propylene glycol/water mixtures as a function of temperature. The lines represent the mass fraction of propylene glycol in the brine.
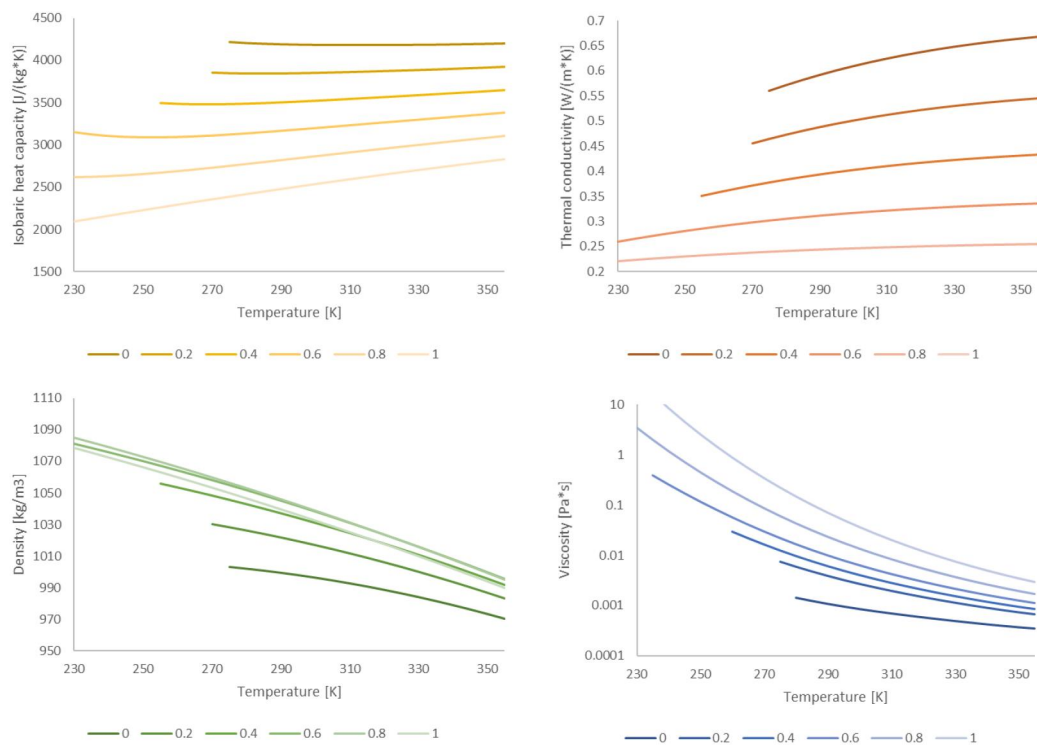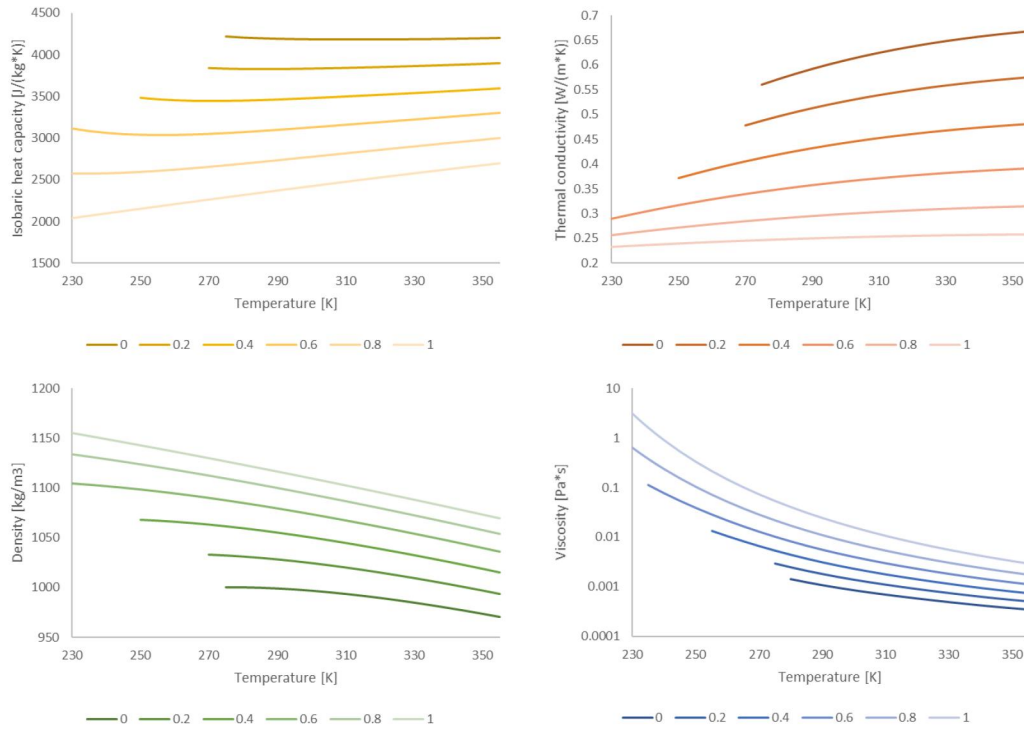

Figure 31. Thermophysical properties of the propylene glycol/water mixture. The lines present the mass fraction of propylene glycol in the mixture.

5 IMPLEMENTATION

The tool was successfully constructed into the interphases of Microsoft EXCEL® and COMSOL Multiphysics® with all assumptions and models described in Chapters 2, 3, and 4. This chapter describes the basic principles, operations, and the current capability of the tool. While the system involves over 2,700 lines of code, the complete in-depth analysis throughout the code is not presented. However, the detailed overview and the basics of the implementation are described.[43] However, the code and the tool will be available in-depth for the designers working in Ramboll Finland Oy.

The list of all adjustable variables is found in Table 9. The table uses "extern_" -prefix for all variables due to consistency and their functionality with COMSOL Multiphysics® software. In general, the parameters in the **green** area are for *the pipe module*, and parameters in the **blue** area are for *the heat conduction module*. Nevertheless, *the thermophysical property module* is equally used by the conduction module and pipe module.

Table 9. Variables of the tool.

Pipe module	Heat conduction module	Parameter	Expressions	Unit	Description	Value	Unit
✓	✗	extern_IceRink_Width	30	m	Width of the ice rink	30	m
✓	✗	extern_CoolingPipe_Length	120	m	Length of an individual cooling pipe	120	m
✓	✗	extern_CoolingPipe_Roughness	0.0015	mm	Absolute roughness fo the cooling pipe	0.0000015	m
✓	✗	extern_HeatingPipe_Length	130	m	Length of the individual heating pipe	130	m
✓	✗	extern_HeatingPipe_Roughness	0.0004	mm	Absolute roughness of the heating pipe	0.0000004	m
✓	✗	extern_CO2_Temperature_Inlet	262.3	K	Defines the inlet temperature into the pipe	262.3	K
✓	✗	extern_CO2_Pressure_Inlet	2.6	Mpa	Defines the inlet pressure of the pipe	2600000	Pa
✓	✗	extern_CO2_Target_Quality	0.5435		Defines the target quality of the refrigerant in pH-diagram	0.5435	
✓	✗	extern_Brine_Pressure_Inlet	0.6	MPa	Defines the inlet pressure of the heating pipe	600000	Mpa
✓	✗	extern_Brine	Ethylene glycol/water		Defines the brine type		
✓	✗	extern_Brine_GlycolContent	0.35		Defines the glycol content in a brine as a mass fraction	0.35	
✓	✗	extern_Brine_Temperature_Inlet	280.5	K	Defines the inlet temperature of the brine	280.5	K
✓	✗	extern_Brine_Temperature_Outlet	275.5	K	Defines the outlet temperature of the brine	275.5	K
✓		extern_Length_Division	120		Defines how many segments the pipe is devided. Works for cooling and heating pipe.		

Pipe module	Heat conduction module	Parameter	Expressions	Unit	Description	Value	Unit
✓	✓	extern_CoolingPipe_Spacing	100	mm	Spacing between cooling pipes.	0.1	m
✓	✓	extern_CoolingPipe_Count	30		Number of cooling pipes.	30	
✓	✓	extern_Cu_Thickness	0.85	mm	Thickness of the copper wall of the cooling pipes.	0.00085	m
✓	✓	extern_CoolingPipe_NOD	12.7	mm	Nominal outer diameter of the cooling pipe.	0.0127	m
✗	✓	extern_LDPE_Thickness	0.5	mm	Thickness of the LDPE layer on the cooling pipe.	0.0005	m
✗	✓	extern_CoolingPipe_Depth	30	mm	Depth of the cooling pipe. Measured from the top of the concrete element.	0.03	m
✓	✓	extern_HeatingPipe_Spacing	500	mm	Spacing between heating pipes i.e. frost protection pipes.	0.5	m
✓	✓	extern_HeatingPipe_NOD	22	mm	Nominal outer diameter of the heating pipe.	0.022	m
✓	✓	extern_HDPE_Thickness	3	mm	Thickness of the heating pipe. PEX or PEH.	0.003	m
✗	✓	extern_HeatingPipe_Depth	80	mm	Heating pipe depth. Measured from the insulation layer.	0.08	m
✗	✓	extern_ConcreteElement_Height	120	mm	Height of the concrete element.	0.12	m
✗	✓	extern_Insulation_Height	100	mm	Height of the insulation layer.	0.1	m
✗	✓	extern_Ice_Height	30	mm	Height of the ice layer.	0.03	m
✗	✓	extern_ReinforcementLayer_Height	8	mm	Height of the reinforcement layer. Consists of reinforcement steel mesh and porus concrete.	0.008	m
✗	✓	extern_Concrete_L2_Height	20	mm	Position of the lower rebar.	0.02	m
✗	✓	extern_GravelFill_Height	274	mm	Height of the gravel fill.	0.274	m
✗	✓	extern_CO2_In_T	264.5338385	K	Temperature of carbon dioxide at inlet	264.5338385	K
✗	✓	extern_CO2_Out_T	263.9344539	K	Temperature of carbon dioxide at outlet	263.9344539	K
✗	✓	extern_MEG_In_T	276.3493321	K	Temperature of heating fluid at inlet	276.3493321	K
✗	✓	extern_MEG_Out_T	274	K	Temperature of heating fluid at outlet	274	K
✓	✓	extern_HeatFlux	112.6760563	W/m^2	Heat flux into the system via ice	112.6760563	W/m^2
✗	✓	extern_GravelFill_ThermalConductivity	0.7	W/(m*K)	Thermal conductivity of gravel fill	0.7	W/(m*K)
✗	✓	extern_Insulation_ThermalConductivity	0.037	W/(m*K)	Thermal conductivity of insulation	0.037	W/(m*K)
✗	✓	extern_Concrete_AirFraction	5.5	%	Extra air inside the concrete element	0.055	1

---

[43] Note that this is a public version of the thesis.

5.1 Heat conduction module

The overview of the interphase in the Microsoft EXCEL® is visualized in Figure 32. The system establishes a COMSOL Multiphysics® - server, loads the COMSOL -simulation into the server, and exchanges the data between the applications in real-time by COMSOL LiveLink® Add-In. Nevertheless, opening the external COMSOL Multiphysics® application is not required, and all the controls are made in Microsoft EXCEL®. The interphase consists of multiple areas that determine the heat balances, temperatures of the isothermal surfaces, and the magnitude of heat transferred between these surfaces.
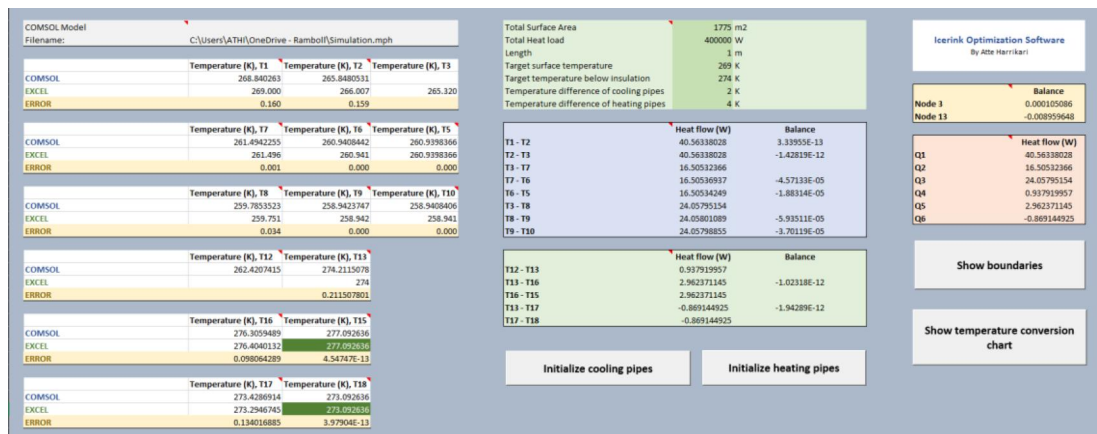
Figure 32. Interphase in Microsoft EXCEL.

In addition to Table 9, the conduction model requires additional variables. They define the total surface area of the ice rink, the total heat load of the ice rink, target surface temperature of the ice, target surface temperature below the insulation layer, and temperature differences between inlets and outlets of both cooling and heating pipes. These variables shown in Figure 32 are fully adjustable. Furthermore, the total heat load is used in *the pipe module* as well.

The operation principle of the conduction module is characterized in Figure 33. Both EXCEL and COMSOL use comparable material properties and geometries defined in the variable list. Moreover, despite the definition of averaged thermal conductivity, the module divides the temperature range between two nodes into 100 subranges, which simulates the accurate integral method with all materials involved in the module. COMSOL uses a "boundary probe" function to determine the average temperature of the surfaces described in Figure 9 and Figure 10, which allows the comparison between the results of the TRN approach and the numerical approach. Besides, the surface of the ice contains a probe that measures the minimum temperature at the surface. From a perspective of performance, the calculation takes roughly 12 seconds to complete.[44]

---

[44] CPU: Intel® Core™ i7-8650U

Set the parameters and the constraints of the ice rink in Microsoft EXCEL®.

Solve the boudary temperatures in Microsoft EXCEL® with Solver Add-In by TRN-approach. Evaluate the temperatures of pipes at the tube wall.

Update the derived temperatures into the COMSOL Multiphysics® Server and update the COMSOL model with current parameters.

Run the COMSOL simulation.

Return the evaluated values of the boundary probes and the 2-dimensional temperature chart into the Microsoft EXCEL®.

Compare the results and the uncertainty of the TRN and COMSOL.

Figure 33. Operation principle of the module.

The heat conduction model outputs the results of both approaches, compares the evaluated temperatures, and creates a cross-sectional temperature field by COMSOL Multiphysics® simulation of the ice rink.

5.2   Pipe module

The purpose of *the pipe module* is to calculate and optimize the pipes, and it currently works with carbon dioxide, ethylene glycol, and propylene glycol. The module includes slightly over 1,400 rows of code. However, the functions coded inside the module are defined as private, which states that the functions are not available by typing into a cell. Consequently, the pipes are optimized by two individual buttons, which run the VBA code. The first button is for the cooling pipes and second for the heating pipes.

The principle of the module is to divide a single pipe into the segments of equal length. The module evaluates and iterates the equilibrium state of the next segment by numerous and powerful iterative functions included in the code. The module assumes constant heat throughout the pipe, and the accuracy of results increases as the pipe is divided into an increased number of segments.

The module creates an array of the state of the fluid. Moreover, it evaluates the required mass flow, the temperature of the fluid and the pipe wall, and pressure, for example. Tables 12 and 13 describe the required variables and outputs of the module for cooling pipes and heating pipes, respectively. The cooling pipes are currently optimized by target quality, and the target outlet temperature optimizes the heating pipes.

Table 10. Variables and outputs of the cooling pipe function.

Required arguments	Unit	Required arguments	Unit
The temperature of the CO_2 in	K	Brine type	
The pressure of the CO_2 in	Pa	The temperature of the brine in	K
Target quality of the CO_2		The temperature of the brine out	K
Heat flux into the ice rink[45]	W/m^2	The pressure of the brine in	Pa
The inner diameter of the cooling pipe[46]	m^2	Required heat flux of the ground [47]	W
The spacing of the cooling pipes	m	The inner diameter of the heating pipe[48]	m
Count of segments		The spacing of the heating pipes	m
The length of the cooling pipe	m	Count of segments	
The absolute roughness of the cooling pipe	m	Length of the heating pipe	m
		The absolute roughness of the heating pipe	m
		The mass fraction of glycol in the brine	

Outputs of module	Unit	Outputs of module	Unit
Number of cooling pipes		Number of heating pipes	
The array of the state of the fluid		The array of the state of the fluid	
The pressure profile	Pa	The pressure profile	Pa
The temperature profile of the fluid	K	The temperature profile of the fluid	K
The temperature profile of the wall	K	The temperature profile of the wall	K
Velocity profile of the fluid	m/s	The velocity profile of the fluid	m/s
Quality/vapor mass fraction profile		The total heat into the single pipe	W
State[49]		Heat flux into the pipe	W/m^2
The total heat into the single pipe	W	The total surface area of the pipe	m^2
Heat flux into the pipe	W/m^2	Required mass flow of a single pipe	kg/h
The total surface area of the pipe	m^2	Required total mass flow	kg/h
Required mass flow of a single pipe	kg/h	Total pressure drop	Pa
Required total mass flow	kg/h		
Total pressure drop	Pa		

As mentioned previously, the code includes numerous iterative functions. The principle of these functions is illustrated in Figure 34. Iteration method is used to evaluate the required mass flow, the temperature of the wall and fluid by Equations (22) and (25), and calculate the pressure drop in subcooled and saturated regions, for example. In general, it tests multiple options and delivers the value which is closest to the target. A `while`-loop inside a `for`-loop makes the construction.

---

[45] Defined by heat load and total surface area

[46] Defined by wall thickness and outer diameter (OD)

[47] Defined by a total requirements and surface area of the ice rink.

[48] Defined by wall thickness and outer diameter (OD)

[49] Unsaturated, subcooled, or saturated state
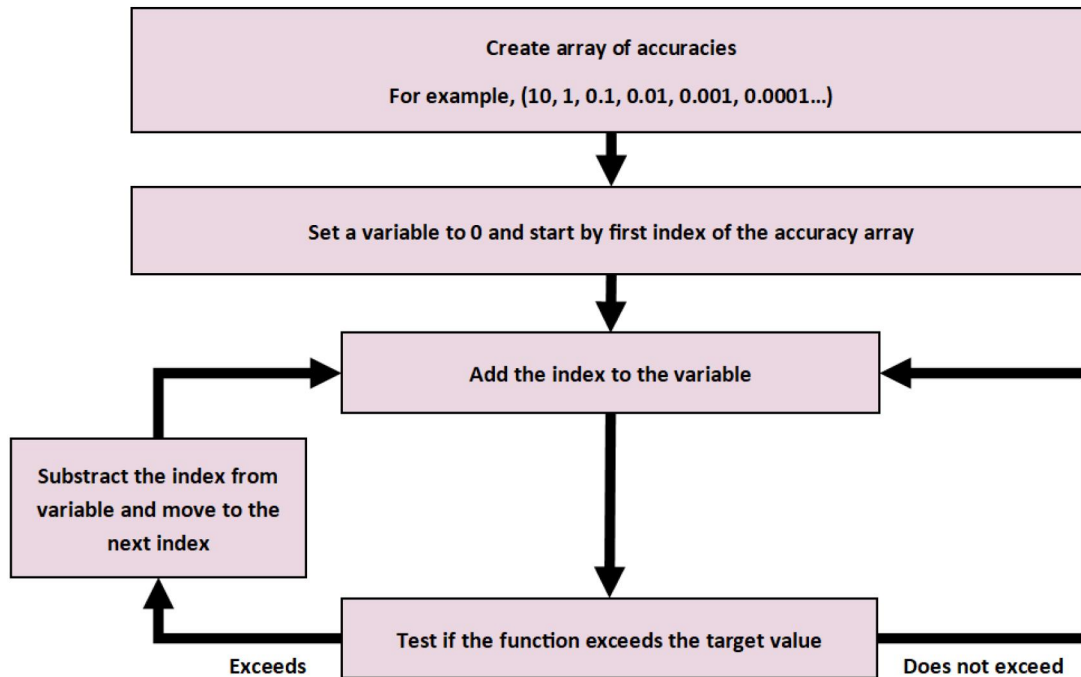
Figure 34. The principle of iterative functions.

5.3   Thermophysical property module

The thermophysical property module involves ten individual files *(.xlsx/.xlsm),* which are linked into the tool and nearly 1,200 lines of code with Visual Basic for Applications (VBA). These individual files determine the model parameters, which are presented in Appendix A. The module retrieves the parameters from the specific thermodynamic property table and uses the parameters to obtain a property with given arguments. Currently, the usage of the module requires the parameter tables to be existent.

Table 11 presents all the functions which will be available for the user. Currently, the functions deliver the property value as a data type of `Single` due to the increased performance in iterative functions within the tool. All the property functions are carefully tested, and they output the values in SI-units. In addition to the thermophysical property functions in Table 11, the module includes the thermophysical properties of saturated steam, dry air, reinforcement steel, and water. Moreover, it contains a high number of constants to determine the critical temperatures, molar masses, and temperatures in triple point, for example.

Table 11. Thermophysical property functions.

Material and property	Description	Arguments[50]
Carbon dioxide[51]		
Tsat_CO2	The saturation temperature of carbon dioxide	Pressure [Pa]
Psat_CO2	The saturation pressure of carbon dioxide	Temperature [K]
Hvap_CO2	Enthalpy of vaporization of carbon dioxide	Temperature [K]
Viscosity_CO2	The viscosity of carbon dioxide	Temperature [K]; Phase [Optional String]
SurfaceTension_CO2	The surface tension of carbon dioxide	Temperature [K]; Phase [Optional String]
Prandlt_CO2	The Prandtl number of carbon dioxide	Temperature [K]; Phase [Optional String]
HeatCapacity_CO2	The heat capacity of carbon dioxide	Temperature [K]; Phase [Optional String]
Density_CO2	The density of carbon dioxide	Temperature [K]; Phase [Optional String]
Conductivity_CO2	The conductivity of carbon dioxide	Temperature [K]; Phase [Optional String]
Humid Air[52]		
Viscosity_HumidAir	The viscosity of humid air	Temperature [K]; Pressure [Pa]; Relative humidity $[0-1]$
HeatCapacity_HumidAir	The heat capacity of humid air	Temperature [K]; Pressure [Pa]; Relative humidity $[0-1]$
Density_HumidAir	The density of humid air	Temperature [K]; Pressure [Pa]; Relative humidity $[0-1]$
Conductivity_HumidAir	The thermal conductivity of humid air	Temperature [K]; Pressure [Pa]; Relative humidity $[0-1]$

---

[50] Take note that the temperatures are generally in Kelvins. To insert temperature in Celsius degrees, take $T\,[°C] = T[K] - 273.15$

[51] Typing "V" or "vapor" delivers the property of vapor. All properties of carbon dioxide are evaluated in saturated temperature and pressure. The function gives error when the temperature is over critical point or lower than triple point.

[52] The properties of humid air evaluated, but they are not involved in the tool. However, they can be used in future applications. The functions of humid air contain the properties of dry air and steam, but these functions are defined private functions and therefore are not available currently for the user. Recommended to use with atmospheric conditions, but no more than 5 bars.

Table 11. Continued.

Propylene glycol[53]

`Viscosity_PEG`	The viscosity of propylene glycol/water mixture	Mass fraction of glycol [0 − 1]; Temperature [K]
`Prandlt_PEG`	The Prandtl number of propylene glycol/water mixture	Mass fraction of glycol [0 − 1]; Temperature [K]
`HeatCapacity_PEG`	The heat capacity of propylene glycol/water mixture	Mass fraction of glycol [0 − 1]; Temperature [K]
`Density_PEG`	The density of propylene glycol/water mixture	Mass fraction of glycol [0 − 1]; Temperature [K]
`Conductivity_PEG`	The thermal conductivity of propylene glycol/water mixture	Mass fraction of glycol [0 − 1]; Temperature [K]

Ethylene glycol[54]

`Viscosity_MEG`	The viscosity of ethylene glycol/water mixture	Mass fraction of glycol [0 − 1]; Temperature [K]
`Prandlt_MEG`	The Prandtl number of ethylene glycol/water mixture	Mass fraction of glycol [0 − 1]; Temperature [K]
`HeatCapacity_MEG`	The heat capacity of ethylene glycol/water mixture	Mass fraction of glycol [0 − 1]; Temperature [K]
`Density_MEG`	The density of ethylene glycol/water mixture	Mass fraction of glycol [0 − 1]; Temperature [K]
`Conductivity_MEG`	The thermal conductivity of ethylene glycol/water mixture	Mass fraction of glycol [0 − 1]; Temperature [K]

Insulation[55]

`HeatCapacity_XPS`	The heat capacity of insulation	Takes no arguments
`Density_XPS`	The density of insulation	Takes no arguments

Polyethylene[56]

`HeatCapacity_PE`	The heat capacity of polyethylene	Degree of branching [0 − 1]; Temperature [K]
`Density_PE`	The density of polyethylene	Degree of branching [0 − 1]; Temperature [K]
`Conductivity_PE`	The thermal conductivity of polyethylene	Degree of branching [0 − 1]; Temperature [K]

---

[53] Includes the thermodynamic properties of water in 6 bars, but these functions are defined as private. Gives errors if the mixture freezes at given temperature.

[54] Includes the thermodynamic properties of water in 6 bars, but these functions are defined as private. Gives errors if the mixture freezes at given temperature.

[55] The thermal conductivity of the insulated was excluded, but it can be adjusted with the interphase of the tool.

[56] It is recommended that the degree of branching is 0.2 for HDPE and 0.8 for LDPE.

Table 11. Continued.

Ice

`HeatCapacity_Ice`	The heat capacity of ice	Temperature [K]
`Density_Ice`	Density of ice	Temperature [K]
`Conductivity_Ice`	Conductivity of ice	Temperature [K]

Gravel Fill[57]

`HeatCapacity_Gravel`	The heat capacity of gravel fill	Takes no arguments
`Density_Gravel`	The density of gravel fill	Takes no arguments

Copper

`HeatCapacity_Copper`	The heat capacity of copper	Temperature [K]
`Density_Copper`	The density of copper	Takes no arguments
`Conductivity_Copper`	The thermal conductivity of copper	Temperature [K]; RRR [Optional String][58]

Porous concrete[59]

`HeatCapacity_PConcrete`	The heat capacity of porous concrete with additional air	Temperature [K]; Air fraction [0 − 1]
`Density_PConcrete`	The density of porous concrete with additional air	Temperature [K]; Air fraction [0 − 1]
`Conductivity_PConcrete`	The thermal conductivity of porous concrete with additional air	Temperature [K]; Air fraction [0 − 1]

Reinforcement layer[60]

`HeatCapacity_RSLayer`	The heat capacity of reinforcement layer with additional air in the concrete	Mass [kg]; Diameter [m]; Depth [m]; Length [m]; Temperature [K]; Air fraction [0 − 1]
`Density_RSLayer`	The density of reinforcement layer with additional air in the concrete	Mass [kg]; Diameter [m]; Depth [m]; Length [m]; Temperature [K]; Air fraction [0 − 1]
`Conductivity_RSLayer`	The thermal conductivity of reinforcement layer with additional air in the concrete	Mass [kg]; Diameter [m]; Depth [m]; Length [m]; Temperature [K]; Air fraction [0 − 1]

---

[57] The thermal conductivity of the gravel fill was excluded, but it can be adjusted with the interphase of the tool.

[58] Typing "30", "100", "300", "1000", or "3000" determines the electrical resistivity ratio. By default, it is "100"

[59] The recommended air fraction is 0.055, but it can vary between 0.04 − 0.066.

[60] The arguments of the reinforced concrete layer functions take the specs of a single reinforcement mesh, its depth, length, rebar diameter, and mass.

6 RESULTS AND DISCUSSION

This chapter describes the results of *the heat conduction module*, *the pipe module*, and *the thermophysical property module* with a discussion. Chapters 2, 3, and 4 act as a complement for the results because they introduce a theoretical framework, continue the discussion on selected and evaluated equations, and provide literature references as a support for the modules.

Nevertheless, the purpose of the chapter is to present the power and deficiencies of the developed tool. Two alternate configurations present the results of *the heat conduction module*. Furthermore, the results of *the pipe module* are presented by multivariate analysis for both brine and carbon dioxide. Finally, the advantages and disadvantages of *the thermophysical property module* are evaluated.

As a disclaimer, these analyses do not recommend the values being used in ice rinks, but rather define in which direction the system change if specific parameters are modified. Moreover, the magnitude in change has not been normalized, which states that a change in a single variable does not correspond to the same magnitude of other variables. Nevertheless, this thesis does not include experimental data. However, the data was requested with no success.

6.1 Heat conduction module

The heat conduction module was created into the interphases of Microsoft EXCEL® and COMSOL Multiphysics®, as in Chapter 5.1, with all assumptions made in Chapter 2. In this chapter, we consider two alternative configurations and measure the differences between thermal resistance network (TRN) and numerical simulation.

A list of variables in both configurations is presented in Table 12. The concrete air fraction and the reinforcement steel mesh are assumed to be equal in both scenarios.[61] The target surface temperature of the ice is set to $269\,K\,(-4\,°C)$, and the target temperature below the insulation layer is set to $274\,K\,(+1\,°C)$. The cross-section is measured near the beginning of the loop. Table 13 and Table 14 show the results of Scenario 1 and 2, and Figure 35 and Figure 36 visualizes the temperature fields of both configurations. [62]

---

[61] Reinforced steel mesh of a type B-200 B500-K MP, and additional air fraction in concrete 0.055 %.
[62] The temperatures are evaluated at the isothermal surfaces presented in Figures 9 and 10.

Table 12. Scenarios of the heat conduction module.

Overall dimensions	Scenario 1	Scenario 2	Unit
Height of the ice	30	25	mm
Height of the concrete element	120	100	mm
Height of the insulation	100	80	mm
Cooling pipes			
Outer diameter	12	16	mm
The thickness of the copper	0.85	1	mm
LDPE thickness	0.5	1	mm
Spacing	100	130	mm
Depth	30	40	mm
Temperature difference	1	2	K
Heating pipes			
Outer diameter	22	15	mm
Wall thickness	3	2.5	mm
Spacing	500	200	mm
Depth	80	110	mm
Thermal conductivity			
Insulation	0.036	0.04	$W/(m \cdot K)$
Gravel fill	0.7	1.5	$W/(m \cdot K)$
Total heat load	200	400	kW
Heat flux	112.68	225.35	W/m^2
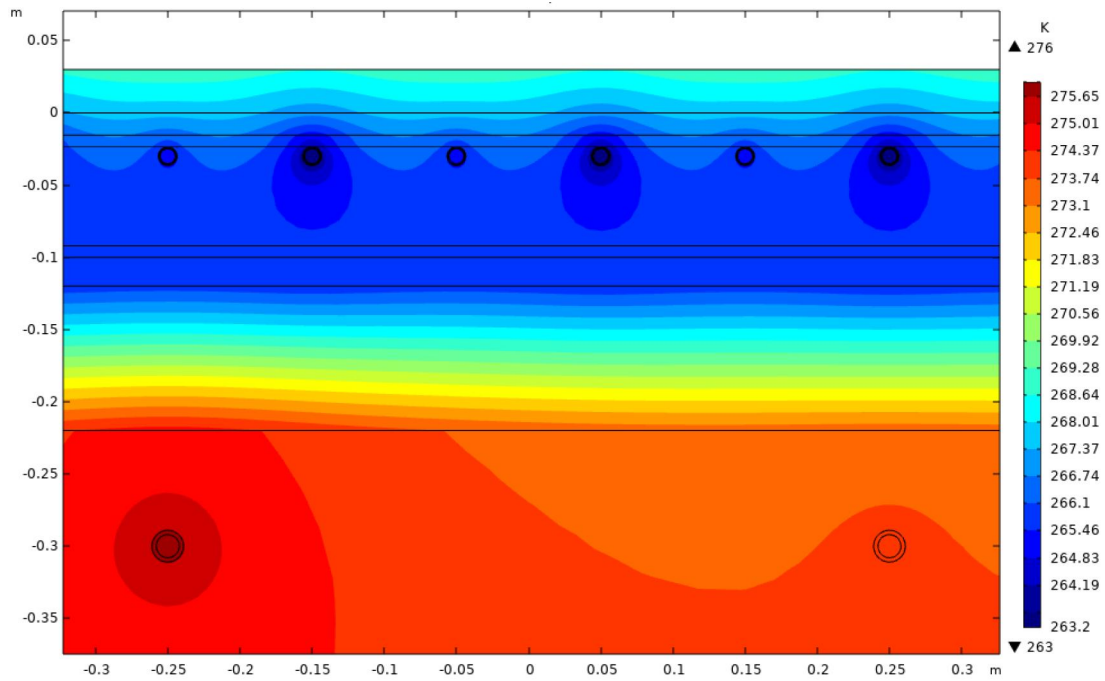
Figure 35. Temperature field of Scenario 1.

Table 13. Results of Scenario 1. Boundary temperatures in Kelvins.

Temperature	COMSOL	TRN	Error
T_1 – Ice surface temperature			
Average	268.932	269	0.068
Minimum	268.821		
T_2	267.432	267.500	0.067
T_5 – Inlet wall of the cooling pipe	264.533	264.533	0
T_6	264.534	264.534	0
T_7	265.882	265.887	0.008
T_8	264.366	264.353	0.013
T_9	263.935	263.935	0
T_{10} – Outlet wall of the cooling pipe	263.934	263.934	0
T_{13} – Temperature below the insulation layer	273.925	274	0.075
T_{15} – Inlet wall of the heating pipe	276.349	276.349	0
T_{16}	276.036	275.975	0.060
T_{17}	273.946	274	0.053
T_{18} – Outlet wall of the heating pipe	274	274	0
Total heat required by ground	5.430 kW		
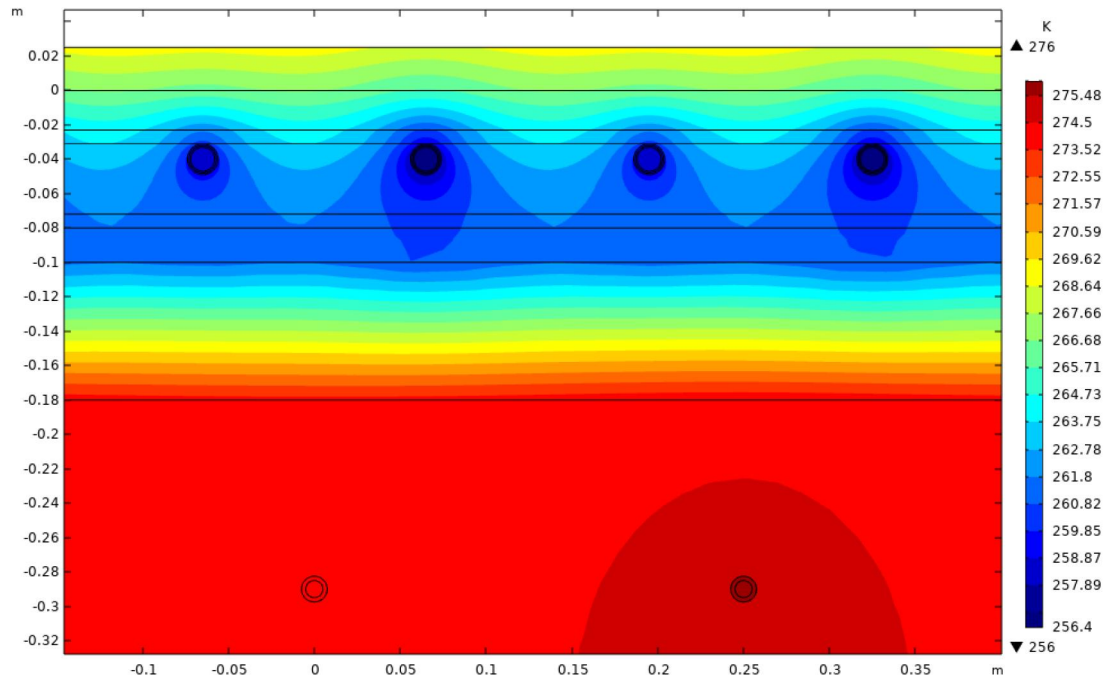
Figure 36. Temperature field of Scenario 2.

Table 14. Results of Scenario 2. Boundary temperatures in Kelvins.

Temperature	COMSOL	TRN	Error
T_1 – Ice surface temperature			
Average	268.878	269	0.122
Minimum	268.364		
T_2	266.382	266.503	0.121
T_5 – Inlet wall of the cooling pipe	258.424	258.424	0
T_6	258.426	258.426	0
T_7	259.732	259.702	0.03
T_8	258.105	258.05	0.055
T_9	256.428	256.428	0
T_{10} – Outlet wall of the cooling pipe	256.426	256.426	0
T_{13} – Temperature below the insulation layer	274.045	274	0.047
T_{15} – Inlet wall of the heating pipe	275.965	275.965	0
T_{16}	275.419	275.476	0.058
T_{17}	274.067	274	0.067
T_{18} – Outlet wall of the heating pipe	274	274	0
Total heat required by ground	11.153	kW	

The significant differences between the configurations are the overall heat load and spacing between the pipes. The deviation between calculation methods is small and does not have a practical significance.

In the TRN, the boundary temperatures are uniform. At the same time, the numerical approach evaluates the average temperature of the boundary, which creates an increased deviation. The reason is the definition of shape factors and a unidirectional heat transfer in certain parts of the system. The TRN does not consider external temperature fields and takes no fluctuation in temperature into account. It was observed that especially the array of equally spaced isothermal cylinders is affected by the external heat load created by the surface. However, the configuration turned out to be most suitable to estimate the heat transfer when compared to alternatives (Table 2). Initially, a heat transfer ($R_{3-7}, R_{3-8}, R_{13-16}$, and R_{13-16}) was measured by a single buried pipe model, but the approach delivered high errors when the pipes became close to each other. Furthermore, the original approach considered the resistances between the array of pipes (R_{7-8} and R_{16-17}) with alternating temperatures, but it was found to create an increased deviation as well.

Initially, both thermal resistance networks were connected by the resistances between the insulation and LDPE (R_{7-12} and R_{8-12}). The connection provided a significant deviation due to the assumption that the cooling pipes absorb all heat. By testing multiple configurations, it was observed that the increased heat load leads to an increased deviation between the calculation methods. The heat penetrates the structure more profoundly and generates more fluctuation in the temperature field. As a result, the connection is not considered within the module. Therefore, the TRN-model is currently unable to measure the temperature field on the top of the insulation layer (T_{12}), and it must be calculated numerically by the simulation software.[63] However, there is an option to calculate the temperature field analytically in the future, and it can be integrated into the tool.

By the TRN approach, the reinforcement layer inside the concrete element is placed directly beneath the ice by the assumption of unidirectional heat transfer in series. In contrast, the numerical simulation places the layer directly above the cooling pipes. This arrangement was found to unify the results of the numerical simulation and TRN model.

The module calculates the temperature differences by wall temperatures within the pipes because the module does not define the local characteristics of the fluid. The state of the fluid may vary significantly depending on the mass flow, the roughness of the tube, and applied heat, for example. It is assumed that the difference is known, and *the pipe module* is recommended to use when evaluating the difference.

The model assumes a steady-state condition with a constant heat load to the ice. The heat into an outlet compared to the inlet was 69 % more intensive in Scenario 1 and 27 % more intensive in Scenario 2, which indicates that the heat load to the ice distributes unevenly throughout the pipe. However, the variation should not affect the total absorbed energy of the refrigerant. The variation by the year, events, day, and night create variation in heat load into the ice. Therefore, the assumption of constant heat with a steady state-conditions

---

[63] Consequently, if the software is not available, the tool is not able to calculate the required heat of the heating pipes.

should be questioned. More importantly, heat flux into the pipe is not constant from all directions. The cooling pipes are heated directly from above, which means that the heat transfer is more intensive at the ceiling of the pipe.

By testing other configurations, the pipe depth and heights of ice and concrete element do not influence the overall conduction, which may be caused by a relatively high thermal conductivity of both materials. Moreover, the increased content of steel in the concrete element slightly increases the total conduction because the thermal conductivity of the steel is nearly 25 times more prominent compared to concrete. Besides, the thickness of the copper has a negligible effect on total energy balance due to extremely high thermal conductivity. In contrast, a minor change in the thickness of the polyethylene may significantly reduce the conduction of heat due to its insulation properties. The increased thickness of the polyethylene, however, will smooth the temperature field if the temperature difference of the inlet and outlet is vast.

The optimal insulation height is a trade-off between the fixed costs of the insulation and variable costs of total energy requirement. It was observed that the thickness of the insulation layer has a critical thickness. The critical thickness states that value beyond the critical value is a waste of material and does not significantly increase the insulation effectiveness. However, a thickness below the critical thickness leads to an increased requirement of heat by the brine. The observation was noticed by debugging the system and changing the dimensions of the structure. Figure 37 demonstrates variable insulation thicknesses of Scenario 1 with a total requirement of heat by heating pipes. It is assumed that all other parameters remain constant. As a result, insulation heights over $150 \ mm$ and under $60 \ mm$ are not recommended.
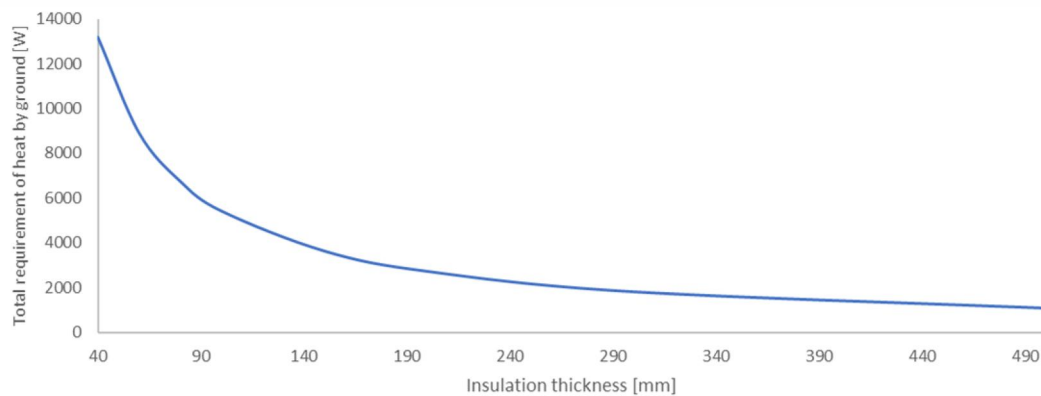
Figure 37. Effect of insulation thickness to the total requirement of heat by heating pipes in Scenario 1.

The thermal conductivity of gravel has a substantial effect on the energy balance of the heating pipes. It was observed that if thermal conductivity is low, the temperature difference between inlet and outlet rises significantly. Moreover, the literature shows that the variation is considerable, depending on the grain size of the gravel and moisture (Dalla Santa *et al.*, 2017).

Testing the module with the configuration by Shahzad (2006) yields a consistent result of the present work.[64] The measured temperature of carbon dioxide by the study is $264.62\ K$. In comparison, the average surface temperature of carbon dioxide by the present work is $263.55\ K$. The deviation may occur by the inclusion of heating pipes beneath the insulation and the difference in thermophysical property values of the materials. Besides, the materials were assumed to be in direct contact with each other, and the assumption neglects the thermal contact resistances at the boundaries. The boundaries may include small spaces of air, for example, and the heat transfer is partially controlled by natural convection. However, the values obtained by the temperature differences across the material layers tend to predict the experimental data more accurately than the study itself. Experimental data supports the study by Shahzad (2006), but the measured heat flux to the ice could deviate from actual heat flux because the measurement technique is not defined.

---

[64] $120\ m$ pipe, heat flux of $136\ \frac{W}{m^2}$, LDPE thickness of $0.45\ m$ with a thermal conductivity of $0.33\ \frac{W}{m^2 K}$, cooling pipe depth $21.15\ mm$, total concrete height of $142.5\ mm$ with a thermal conductivity of constant $1.5\ \frac{W}{m^2 \cdot K}$, assumed temperature difference of $0.6\ K$, and ice surface temperature of $268\ K$.

6.2   Pipe module

The pipe module was created entirely by the information presented in Chapters 3 and 5.2. In this chapter, the results are presented for carbon dioxide and brine with multivariate analysis.

6.2.1   Cooling pipe

Consider a default configuration (Case 0) presented in Table 15. The table considers five other cases, which change one variable at the time assumes that other variables remain constant. For example, Case 3 considers the change in target quality from 0.35 to 0.16. Furthermore, the results are presented in Table 16 and Figure 42. They show the required mass flow rates and delivers the temperature profiles of the wall and the fluid, pressure profile, quality profile, and velocity profile throughout the pipe. It is required to feed the refrigerant in the unsaturated or the subcooled state. If the fluid temperature exceeds the saturation temperature, the fluid should be complete vapor.

Table 15. The default configuration of the cooling pipe.

Property	Unit	Case 0 - Default	Changed value
Case 1 - The absolute roughness of the pipe	mm	0.0015	0.15
Case 2 - The temperature of CO_2 in	K	262	260
Case 3 - Target quality		0.35	0.16
Case 4 - The inner diameter of the pipe	mm	10.3	8
Case 5 - The spacing between the pipes	mm	100	70
The length of the pipe	m	120	
Heat flux to the ice	W/m^2	112.7	
The pressure of CO_2 in	MPa	2.6	

Table 16. Mass flow rates of carbon dioxide in various configurations. Mass flow rates in kg/h.

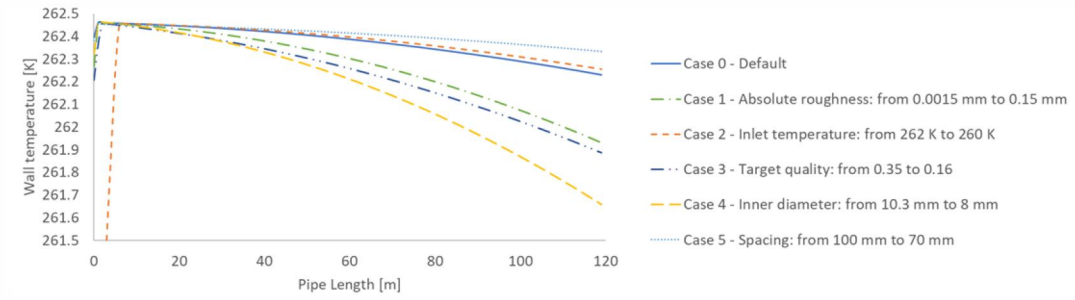| Configuration	Total mass flow rate	Mass flow rate per pipe	Pipe count
Case 0 – Default	7695.0	51.3	150
Case 1 – Absolute roughness: $0.0015\ mm \rightarrow 0.15\ mm$	7689.6	51.3	150
Case 2 – Inlet temperature: $262\ K \rightarrow 260\ K$	7317.0	48.8	150
Case 3 – Target quality: $0.35 \rightarrow 0.16$	16480.8	109.9	150
Case 4 – Inner diameter: $10.3\ mm \rightarrow 8\ mm$	7673.4	51.2	150
Case 5 – Spacing: $100\ mm \rightarrow 70\ mm$	7673.2	35.9	214

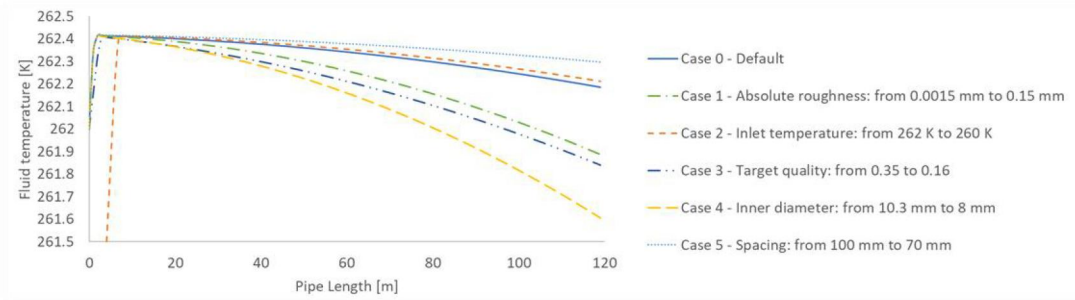*Figure 38. Wall temperature profile of the cooling pipe*

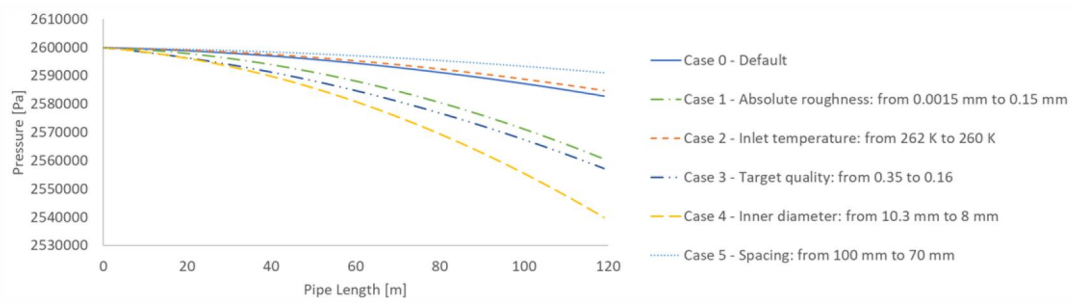*Figure 39. The fluid temperature profile of the cooling pipe.*

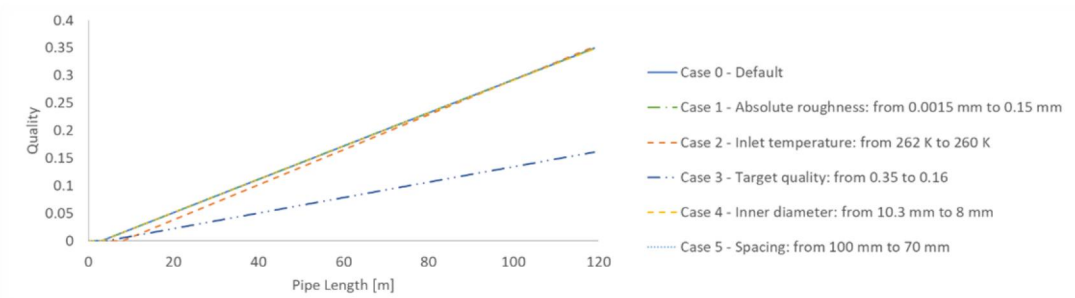*Figure 40. Pressure profile of the cooling pipe.*

Figure 41. Quality profile of the cooling pipe.
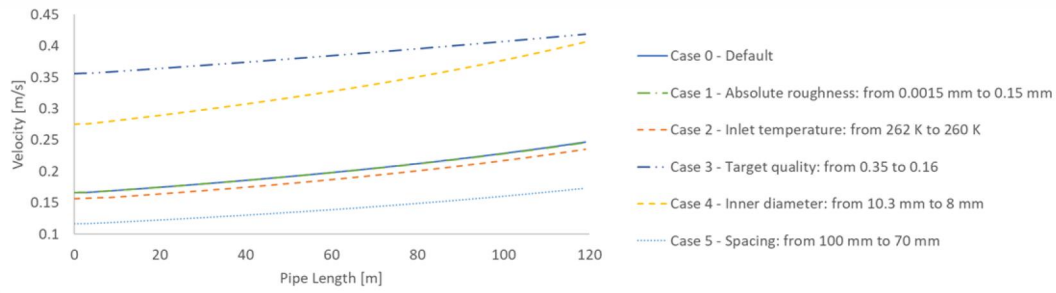
Figure 42. Velocity profile of the cooling pipe.

A smaller diameter, a lowered target quality, and an increased pipe roughness create a more substantial pressure drop. A small diameter requires a fluid to move faster while the mass flow rate is constant. Similarly, while the heat flux is constant, the lowered target quality requires the fluid to move faster to prevent it from absorbing excess energy. Table 16 shows that decreasing the target quality leads to a significant increase in mass flow. Moreover, the increased roughness of the pipe creates increased friction forces, which lead to increased pressure drop.

Interestingly, the default configuration and the change in absolute relative roughness have a similar velocity profile. The similarity is due to the definition of velocity, which is calculated by the mass flux G and homogenous density of the fluid.[65] The increase in velocity is a combination of thermal expansion and increased quality.

The fluid temperature rises sharply at the beginning and reaches the saturated state quickly after the inlet. However, the lowered temperature creates irregular temperature fields and temperature fluctuation on the surface of the ice. The temperature of the fluid continues to follow the profile of the pressure by the vapor pressure curve in a saturated state, presented in Chapter 4.3.1.1.

Nevertheless, the pressure drop in the unsaturated state is linear. It is enhanced by the length and increased quality, which leads to curved profiles in the saturated state. It is estimated that the heat transfer coefficient in unsaturated flow deviates ± 6 % on average.[66] Moreover, the pressure drop in the saturated state could deviate 25.5 % compared to existing correlations based on experimental data.[67] However, the experimental setup of Shahzad (2006) shows that the actual pressure drop could be less than predicted.[68] The deviation may occur due to the uncertainty of the measured heat flux to the ice, lack of information on wall thickness, and uncertainty of the relative roughness pipe, for example. Nevertheless, the heat into the cooling pipe is more significant from above.

The quality profile visualizes the constant heat approach. The quality increases evenly throughout the tube, as in Figure 41. The temperature difference between the wall and the pipe is small. A measured average temperature difference is $0.044\ K$ in all configurations but deviates in those who affect to the heat flux. These include variation in spacing and inner

---

[65] $v = G/\rho$
[66] Gnielinski (2013)
[67] Xu & Fang (2012)
[68] Quality = 0.459, Heat flux to the ice = $138\ W/m^2$,

diameter because a decreased spacing distributes the total heat load into an increased number of pipes, and a smaller diameter decreases the convective surface area. Moreover, the wall superheat by Equation (32) is generally accepted, but it comes with a few disadvantages: The equation is entirely theoretical, and the heat transfer with boiling depends heavily on surface roughness and cavities with alternating shapes. However, the definition of superheat is consistent with the study of Fang (2017), which currently delivers a relative error of ± 3.9 % for the convective heat transfer coefficient for carbon dioxide against the experimental data (Sun and Mishima, 2009; Fang, Wu, and Yuan, 2017).[69]

The effect of subcooling is relatively negligible, and the region is narrow. The fluid turns from the unsaturated state into the saturated state very quickly. The subcooled state cannot be observed in Figure 42, but it is undoubtedly present.

In conclusion, a smaller diameter, a decreased target quality, and increased pipe roughness create a more substantial pressure drop compared to the default configuration. However, the pressure drop could be less than predicted, if compared to experimental data. In the saturated state, the temperature difference between the wall and the fluid is small, and the fluid temperature follows the vapor pressure curve. Finally, the subcooled region is a relatively small segment in all configurations. It could be neglected, assuming the unsaturated fluid turns suddenly into a saturated state.

6.2.2   Heating pipes

Consider ethylene glycol with a default configuration (Case 0) presented in Table 17. The table presents five other cases that change one variable at the time, assuming other parameters unchanged.

Table 17. The default configuration for convective heat transfer of a heating pipe.

Property	Unit	Case 0 - Default	Changed value
Case 1 - Fluid type		Ethylene glycol	Propylene glycol
Case 2 - The inner diameter of the pipe	mm	16	23.2
Case 3 - The temperature of the fluid	K	275.5	280.5
Case 4 - The absolute roughness of the pipe	mm	0.0004	0.04
Case 5 - The mass fraction of glycol		0.35	0.4
The temperature of the wall	K	275	
The length of the tube	m	10	

---

[69] Equation (33)
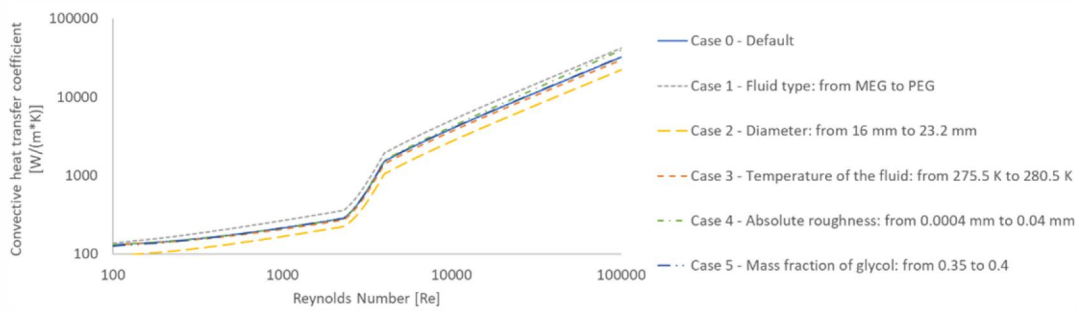
Figure 43. The convective heat transfer coefficient of ethylene glycol (MEG).

Figure 43 shows the changes in the convective heat transfer coefficient as a function of Reynolds number. The pipe diameter and fluid type have the most significant effect on the convective heat transfer coefficient. As the pipe diameter increases, the surface area of the pipe increases as well. The increased surface area should slightly compensate for the reduction in convective heat transfer coefficient. Moreover, Figure 43 shows that propylene glycol slightly increases heat transfer. The result and the figure are consistent with the study by Gnielinski (2013).

Furthermore, the heating pipes are optimized with the assumption of default total requirement of heat derived in Chapter 6.1. Moreover, the outlet and inlet temperatures are fixed, and the temperature difference between the inlet and the outlet is unknown. Table 18 represents a detailed configuration for the optimization. Similarly, by changing the variables while assuming the others remain unchanged, the module derives the required mass flow and the profiles of velocity, temperature, and pressure throughout the tube. The results are delivered in Table 19 and Figures 44 - 47.

*Table 18. The default configuration of the heating pipe. *Inner diameter. **Mass fraction of glycol in the brine.*

Property	Unit	Case 0 - Default	Changed value
Case 1 - Fluid type		Ethylene glycol	Propylene glycol
Case 2 – Temperature in	K	280.5	285.5
Case 3 – Diameter*	mm	16	23.2
Case 4 – Spacing	mm	500	250
Case 5 – Absolute roughness	mm	0.0004	0.04
Case 6 – Mass fraction of glycol**		0.35	0.4
Temperature out	K	275.5	
Pressure in	Pa	600000	
The total requirement of heat by ground	kW	5.430	
The length of the pipe	m	130	

Table 19. Mass flow rates of the brine in different configurations. Mass flow rates in kg/h.

Configuration	Total mass flow rate	Mass flow rate per pipe	Pipe count
Case 0 - Default	1172.6	39.1	30
Case 1 – Fluid type: MEG → PEG	1160.9	38.7	30
Case 2 – Temperature in: $280.5\ K \rightarrow 285.5\ K$	586.1	19.5	30
Case 3 – Diameter: $16\ mm \rightarrow 23.2\ mm$	1172.6	39.1	30
Case 4 – Spacing: $500\ mm \rightarrow 250\ mm$	1172.6	19.5	60
Case 5 - Absolute roughness: $0.004\ mm \rightarrow 0.4\ mm$	1172.6	39.1	30
Case 6 - Mass fraction of glycol: $0.35 \rightarrow 0.4$	1205.0	40.2	30
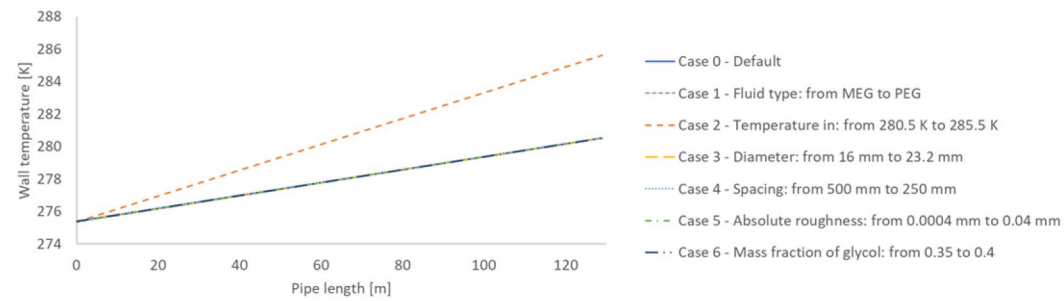
Figure 44. Wall temperature profile of the heating pipe.
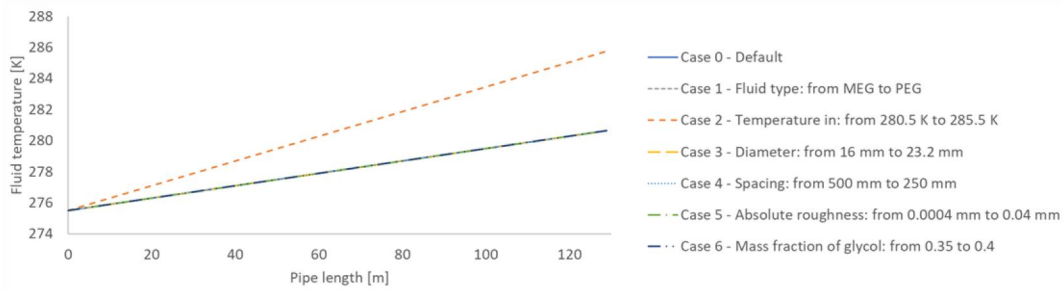
Figure 45. The fluid temperature profile of the heating pipe.
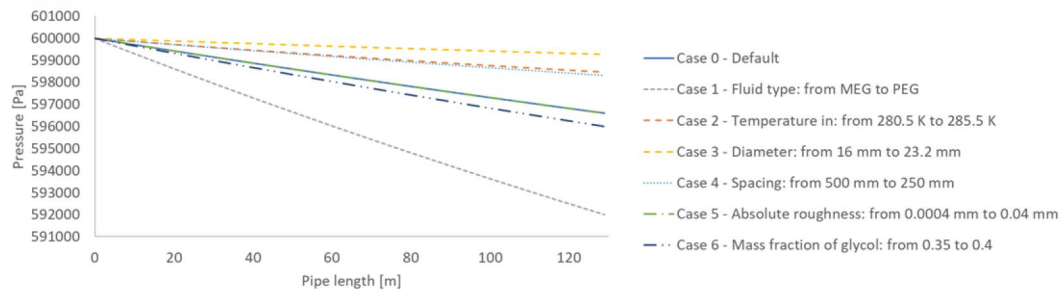
Figure 46. Pressure profile of the heating pipe.
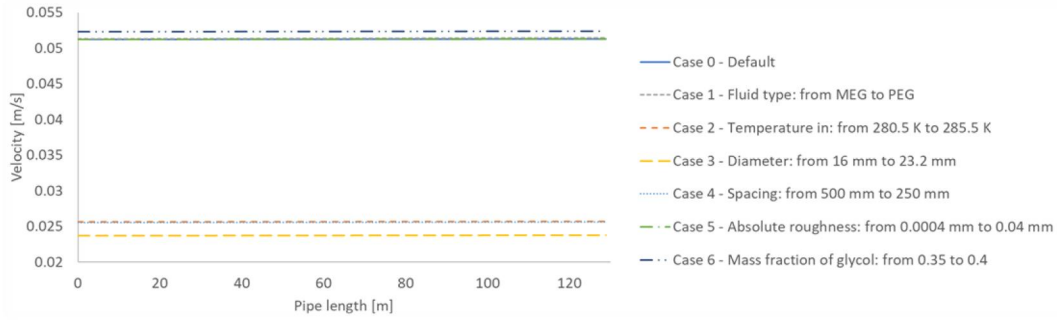
Figure 47. Velocity profile of the heating pipe.

Figure 44 and Figure 45 show that the temperature difference between the wall and the fluid remains constant in all cases, which is $0.118\ K$ with a default configuration. However, the difference should increase in cases 1, 2, 3, and 4 in theory. As a constant heat approach constructs the module, the tightened spacing indicates a diminished heat into the single pipe. Furthermore, as the diameter of the pipe increase, the velocity of the fluid must decrease with the constant mass flow. As a result, a decline in the velocity signifies a decreased heat transfer capacity of the fluid as well. Moreover, the increased temperature of the inlet delivers more heat into the system, and therefore, the required mass flow rate decreases. However, the heat flux into the system is so small that the differences in temperatures can not be observed.

As the mass flow rate is low, the decrease in pressure is minor. Therefore, the decreased spacing, the increased diameter, and the higher inlet temperature lead to a decreased loss in pressure inside the heating pipes. However, changing to propylene glycol may require extra capacity from the pump due to a significant drop in pressure, which is caused by increased viscosity of propylene glycol.

The profiles are linear because of the constant heat approach. As an interference, the thermophysical properties of the brine remain almost unchanged in the temperature range, which can be confirmed by the velocity profile. While propylene glycol may seem a better alternative as a brine in the perspective of heat transfer, the enhancement, compared to ethylene glycol, is relatively negligible. In contrast, changing to propylene glycol decreases the required mass flow rate. Moreover, the uncertainty in the heat transfer coefficient could deviate $\pm 6\ \%$ on average. The pressure drop is assumed to be "exact" with a marginal uncertainty by Chen (1979).

As the fluid temperature decrease, it is expected that the heat transfer capacity of the fluid decreases over the pipe length if compared to experimental data. In other words, the change in temperature could be more significant at the beginning, which leads to curved temperature profiles. Therefore, these results should be validated with experimental setup or data.

In conclusion, the convective heat transfer is vitally dependent on the velocity of the brine. This multivariate analysis has shown that the pipe diameter, the inlet temperature, and the spacing not only contribute to the enhanced heat transfer but a decreased pressure loss as well. Moreover, propylene glycol leads to the increased requirement of power by the pump compared to ethylene glycol. In contrast, propylene glycol slightly decreases the required mass flow and increases the convective heat transfer, but those effects are marginal. Moreover, the results show that the module can estimate the heat transfer in heating pipes successfully with high accuracy. However, the experimental setup is required to validate the data.

6.3　Thermophysical property module

The thermophysical property module was created by using over 1,200 lines of code with Visual Basic for Applications (VBA) with a parameter list introduced in Appendix A. The module correctly uses the information and implementation presented in Chapters 4 and 5.3. The sources included the data by Project DIPPR 801, NIST Chemistry WebBook, Industrial formulation of water IAPWS-IF97, and Finnish Standards Association, for example. This thesis debated between multiple correlations of the same property and evaluated the used model by the least uncertainty of validity.

In general, the data obtained in the literature required a curve fitting, which was made with the least-squares method, presented in Chapter 4.1. Furthermore, the uncertainty of every function presented in Chapter 5.3 was introduced by finding the uncertainty of the literature and adding the uncertainty by curve fitting. The complete list of uncertainties of the property functions are presented in Appendix B. Besides, all the functions were converted into the SI-units.

The heat conduction module and pipe module use the property function to estimate an equilibrium state of the substance. While these functions are evaluated critically, there are some deficiencies included. First, starting with carbon dioxide, the property functions work accurately only between triple point and critical point in the saturated state. Moreover, the unsaturated and subcooled state of the carbon dioxide use the saturated properties, and the uncertainty in these regions may increase. Defining the precise state of carbon dioxide in both regions would have required a correction for pressure, for example, via Gibbs or Helmholtz free energy. However, the correction for pressure is practically useless. Nevertheless, the property functions work well with these regions with the assumption that the variation in pressure is relatively minimal, and the properties are controlled by temperature.

Furthermore, this thesis succeeded in constructing a model for thermal conductivity, dynamic viscosity, and isobaric specific heat capacity of carbon dioxide in the saturated state for both vapor and liquid.[70] The primary sources to obtain the property functions were Span & Wagner (1996), Vesovic (1990), Fenghour (1998), Rathjen & Straub (1977), and Project DIPPR 801.

The properties of the ice were evaluated between the debate of an individual study of thermal conductivity, industrial formulation of water IAPWS-IF97, and Project DIPPR 801. However, the error representation by mean absolute relative deviation (MARD), the uncertainty of thermal conductivity of ice is presented by the standard error.

---

[70] Equations (55) - (60).

The thermodynamic property functions of copper were created by the information of White & Minges (1997), and White & Collocott (1984). The thermal conductivity was found to be dependent on the electrical resistivity ratio (RRR). However, the thermal conductivity is already relatively very high, and changing the resistivity ratio has a marginal effect on the energy balances near the operating temperatures. Furthermore, the density of the copper neglects the thermal expansion and is assumed to be constant. It was concluded that the effect of thermal expansion does not contribute towards the output of system in a perspective of heat transfer.

The polyethylene accounts for LDPE-layer on a cooling pipe and HDPE as a construction material of the heating pipe. The property functions were created by the type of polymer, crystallinity, linearity, orientation, and morphology. It was found out that there is considerable uncertainty between individual studies of density and thermal conductivity of polyethylene. Therefore, these properties were assumed to be an averaged constant with no relation to temperature. Most of these studies were measured at the ambient conditions, and the constants may slightly deviate concerning the average in cold environments. However, the heat capacity was established as a function of temperature with reasonable uncertainty. Furthermore, the thermophysical properties of both types of polyethylene are evaluated by the degree of branching. The degree of branching is assumed to be 0.2 for HDPE and 0.8 for LDPE, by default. The primary resources of data for polyethylene were the studies of Gaur & Wunderlich (1983), Chang (1974), and Yu et al. (2014).

The properties of concrete were evaluated by assuming that additional dry air is mixed with normal-weight concrete (NWC) to overcome the thermal expansion of water in cold and humid environments. The properties of the concrete and reinforcement steel were obtained by the information of the Finnish Standards Association and publications of the Concrete Association of Finland. It was found out that these associations do not represent the uncertainty of their functions, and the definitions of the thermophysical correlations were not evaluated in cold environments.[71] However, this thesis exceeds these boundary conditions and extend the validity of these equations to the operation temperature because there is no better source in the literature to estimate the properties of concrete generally. It was concluded that the required concrete type for the ice rink is XF3, which is defined in the newest publication of the Concrete Association of Finland (2019). As the additional air is mixed with the concrete, the properties of the porous concrete are measured by the rule of mixtures and the Hashin-Shtrikman lower bound method. They were both suitable to evaluate the properties of the continuous matrix with tiny cavities. Nevertheless, it was observed that the content of additional air by volume fraction has a very marginal effect on thermal conductivity and heat capacity, but an increased effect to density.

---

[71] Equations (63) and (68)

The properties of the reinforcement layer consist of reinforcement steel and a porous concrete mass. Similarly, the properties of reinforcement steel are obtained by the information of the Finnish Standards Association with unknown uncertainty. Furthermore, the density is assumed to be a constant with no effect of thermal expansion. Again, the thermal expansion was found to be negligible in terms of heat transfer but might contribute its effect to the internal tension of the materials. Nevertheless, the thermal conductivity is measured by a geometric mean of the reinforcement steel and porous concrete. The definition may be efficient with 2-dimensional heat transfer models like in numerical analysis. However, the thermal resistance network (TRN) uses an approach of parallel conduction.

It was concluded that there is significant uncertainty of the properties of the insulation layer and gravel fill, and the properties are assumed to be constants with no relation to temperature. The deviation may indicate a significant error between isothermal surfaces on each side of the insulation layer and the heat transfer in the ground. Therefore, the possibility to change, especially the thermal conductivity of the insulation and gravel fill, was made possible in the tool interface and was not included in *the thermophysical property module* itself.

Finally, the thermophysical properties of the brine were obtained by the studies of Sun & Teja (2003, 2004). The results of the study are valid outside of the operating temperature of the ice rink. However, this thesis assumes that the studies work at lower temperatures as well.[72] Moreover, further modifications to the model were made; for example, the properties of water were obtained by the industrial formulation of water IAPWS-IF97 at 6 bars. Furthermore, the viscosity of propylene glycol was replaced by the model of Project DIPPR 801 because the equation of the study did not work. Replacing the definitions of the study may result in decreased accuracy due to optimization with the study models. However, the effect is relatively very marginal since the changes indicate an increased accuracy. Moreover, the thermophysical properties of the brine do not consider the effect of the pressure, and the functions will indicate a significant uncertainty when used with high-pressure conditions.[73]

In conclusion, the deficiencies of the property functions were described. However, in general, they propose an accuracy of the level of scientific research. The most substantial uncertainties are found with thermal conductivities and viscosities in all materials compared to other thermophysical properties. The uncertainty may be a result of the method of measurement technique and by the effect of natural convection. In the future, the parameters presented in Appendix A could be coded inside the property functions, which moves the library towards an individual EXCEL Add-In.

---

[72] The thermophysical properties of the studies are evaluated in the range of $290 - 460\,K$, but the heating pipes work generally at $280\,K$.

[73] The high-pressure conditions are estimated to be over 10 bars.

7 CONCLUSIONS AND FUTURE WORK

This thesis presented a comprehensive analysis of a direct-controlled ice rink when carbon dioxide was used as a refrigerant. A refrigeration system introduced the subject with an overview of the heat load to the ice. It was continued by visualizing the structure of ice rink in more detail, and the paper analyzed carbon dioxide as a refrigerant by comparison to its alternatives.

The purpose of this thesis was to construct a tool that could be used to optimize ice rinks in the future. The tool was divided into a **heat conduction module,** a **pipe module,** and a **thermophysical property module.** The modules were constructed into the interphases of COMSOL Multiphysics® and Microsoft EXCEL® with Visual Basic for Applications (VBA).

The heat conduction module determines a cross-sectional heat balance of an ice rink by thermal resistances networks (TRN) and a numerical analysis. The basics of conduction introduced the module with a concept of shape factors in Chapter 2. The theory outlined how the steady-state heat transfer problems are usually solved and revealed the thermal resistance networks used by the module. The implementation was conducted by COMSOL LiveLink® between COMSOL Multiphysics® and Microsoft EXCEL® -software with assumptions of constant heat flux and steady-state conditions. Furthermore, the materials were assumed to be homogenous and in direct contact with each other. The module includes several hundred lines of code to establish a data connection between the software. The results of the module were carried out by presenting two alternate configurations based on general instructions of IIHF (International Ice Hockey Federation (IIHF), 2016) and arbitrary constraints.

The purpose of *the pipe module* is to provide the thermodynamic state of the fluids throughout the pipes. The principles of the module were introduced by the fundamentals of convection in Chapter 3, and the framework of the internal forced convection was carried out by a comprehensive literature review in unsaturated, subcooled, and saturated states. With an assumption of constant heat load, the module was implemented inside Microsoft EXCEL® with over 1600 rows of powerful iterative functions presented in Chapter 5.2. A multivariate analysis explained the results of *the pipe module* for both brine and carbon dioxide.

Finally, *the thermophysical property module* was created to provide an extensive library to the materials involved in ice rinks. Moreover, it serves as a foundation for *the heat conduction module* and *the pipe module*. Over 1,200 lines of code created the library with a parameter list introduced in Appendix A. The references included the data by Project DIPPR 801, NIST Chemistry WebBook, Industrial Formulation of Water IAPWS-IF97, and Finnish Standards Association, for example. The least uncertainty and validity evaluated the models with the complete list of uncertainties presented in Appendix B. It was assumed that the variation in pressure is negligible and controlled by temperature only. However, in general, the property functions were created by a superior accuracy based on scientific research. Nevertheless, all the functions were converted into the SI-units.

The main finding is that there is no significant error between the TRN and numerical solutions by the COMSOL. As a result, the thermal resistance networks and shape factors are suitable to model the conduction in ice rinks. The deviation was caused by the assumption of isothermal surfaces, unidirectional heat transfer, and external temperature fields. The array of isothermal cylinders was found to be the most suitable configuration to measure the heat transfer between a single pipe to its surroundings, compared to its alternatives presented in Table 2. Moreover, the connection between cooling pipes and heating pipes by thermal resistances was tested with no success. It was observed that the increased heat load leads to the increased deviation between the calculation methods because the heat penetrates the structure more profoundly and generates more fluctuation in the temperature field. Moreover, placing the reinforcement layer directly beneath the ice in the TRN approach unifies the results. As a result, the shape factor for an array of buried pipes with alternate temperatures is heavily recommended to evaluate analytically because the configuration was not available in the literature (Figure 48).
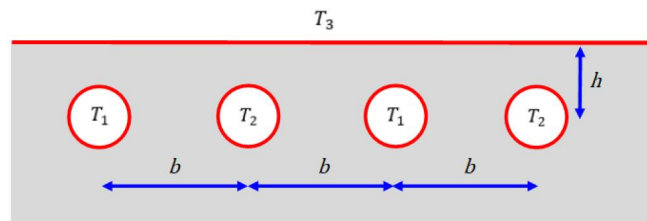
Figure 48. The array of buried pipes with alternate temperatures.

The pipe depth and heights of ice and concrete element do not influence the overall conduction. However, the increased content of steel in the concrete element slightly increases the thermal conductivity. To enhance the heat conduction in the concrete element, an increased number of reinforcement steel meshes should provide uniformity into the temperature field. The properties of concrete were evaluated by assuming that additional dry air is mixed with normal-weight concrete (NWC) to overcome the thermal expansion of water in cold and humid environments. It was noted that the air has a very marginal effect on thermal conductivity and heat capacity but an increased effect on density.

The thickness of the copper does not affect the total energy balance. However, a minor change in the thickness of the polyethylene may significantly reduce the heat transfer in the system. Therefore, it is suggested that the plastic should be replaced by other polymers with higher conductivities or mix the polyethylene with graphene, which is proved to increase the thermal properties of the plastic (Sabet and Soleimani, 2019). The increased conductivity will increase the required temperature of the refrigerant but increase the requirement in pressure as well. Besides, the thickness should be as low as possible. It must protect the pipe from contraction and expansion of concrete caused by changes in temperature.

The optimal insulation height is a trade-off between the fixed costs of the insulation and variable costs of energy requirement. Moreover, there exists considerable uncertainty about the properties of gravel fill. Both materials contribute a massive cross-sectional surface area of the ice rink, and the experimental study, not only for thermal conductivity but density and heat capacity, for both materials, is suggested. Nevertheless, an increased amount of water in the gravel fill could help to achieve better thermal conductivity and energy efficiency (Wang *et al.*, 2013; Dalla Santa *et al.*, 2017).

Testing *the heat conduction module* with the literature delivered a consistent result. The deviation was discussed through the effects of heating pipes beneath the insulation and the difference in thermophysical property values. Furthermore, the theoretical framework assumes materials to be in direct contact with the surrounding materials, which may explain the deviation. The temperature differences across the material layers tend to predict the experimental data more accurately than the literature itself.

In steady-state conditions, the heat into an outlet compared to the inlet was 69% more intensive in Scenario 1 and 27% more intensive in Scenario 2, which indicates that the heat distributes unevenly throughout the cooling pipe. Furthermore, the ice rink should be optimized to overcome the maximum heat load. However, transforming *the heat conduction module* into a transient heat conduction module could lead to more energy-efficient solutions.[74]

It was found that a smaller diameter, lowered target quality, and increased pipe roughness creates a more significant pressure drop inside cooling pipes. Therefore, it is recommended to use pipes with a larger inner diameter and low surface roughness. Furthermore, the ice rinks should be designed for decreased spacing to reduce the mass flow inside the pipe. An option to move into a transverse arrangement of the pipes should be considered because it will reduce the pipe length. A decreased spacing and the transverse arrangement lead to a reduction in total pressure drop and the difference between inlet and outlet temperatures, which create a more uniform temperature field on the surface of the ice. Moreover, the default configuration and the change in absolute relative roughness have a similar velocity profile, which is caused by a definition of velocity.

The temperature of carbon dioxide rises sharply at the beginning and reaches the saturated state quickly after the inlet. However, it is suggested to feed the refrigerant in the subcooled state or slightly under the saturated state into the pipe to avoid large deviations in the temperature field. Furthermore, the temperature of the fluid and the wall continues to follow the profile of the vapor pressure curve in the saturated state with a small temperature difference of $0.044\,K$ on average. Alternatively, it is proposed that the roughness of the pipe could define the definition of superheat because small cavities enhance boiling on the pipe surface. Nevertheless, the study finds that the effect of subcooling is relatively negligible.

---

[74] A transient heat conduction takes time into account.

Currently, the property functions of carbon dioxide work accurately only between triple point and critical point in the saturated state but were used in unsaturated and subcooled states because the effect of pressure is minor. Furthermore, the present work succeeded in constructing a simplified model for thermal conductivity, dynamic viscosity, and isobaric specific heat capacity of carbon dioxide in saturated conditions for both vapor and liquid. The equations should provide additional value to those who seek certain property functions of carbon dioxide.[75] In the future, there is a possibility to extend the validity of the functions in supercritical, vapor, and liquid phases outside the saturated conditions.

By the perspective of heating pipes, the temperature difference between the wall and the fluid increase if the spacing decreases, the inlet temperature of the brine increases, or the inner diameter increases. The predicted temperature difference with a constant heat approach was $0.11\ K$. It was shown that the properties of the brine remain unchanged in the temperature range, which can be confirmed by the velocity profile. In contrast, while propylene glycol may seem a better alternative as brine from the perspective of heat transfer, it may cause a more substantial pressure drop inside the heating pipe. Therefore, the brine should be chosen from the perspective of cost and safety. However, the thermophysical properties of the brine were evaluated by extending the validity of temperature range to cold environments. Moreover, modifications on the properties were made, for example, by increasing the accuracy of water by IAPWS-IF97 and defining the viscosity of propylene glycol by Project DIPPR 801. Replacing the definitions of the study may result in decreased accuracy due to optimization with the study models, but the effect is considered negligible. As a result, the heating pipes should be designed with large diameters, increased spacing, and increased inlet temperature.

Additionally, the convective heat transfer coefficient does not depend on the material of the pipe. Stainless steel and carbon steel, which are significantly cheaper and proved to be corrosion resistant to carbon dioxide, could replace copper as a pipe material (Russick *et al.*, 1996). However, the replacement could lead to higher costs due to installation (Rogstam, Sawalha, and Nilsson, 2005). If the installation costs could be significantly reduced, the arrangement could be tested with *the heat conduction module*. The replacement does not affect *the pipe module* because the convective heat transfer does not depend on the pipe material. Besides, *the pipe module* does not currently support the minor pressure losses caused by fittings.

Due to a lack of experimental data, the functionality of the tool should be evaluated. The experiment by Shahzad (2006) provides data only for a specific configuration. Therefore, the next step is to obtain data from already constructed direct-controlled ice rinks. Alternatively, a pilot ice rink with alternating configurations is recommended to construct. In an ideal experimental setup, two infrared thermometers should measure the minimum and maximum temperature of the surface of the ice, respectively. It is proposed that thermistors are used over thermocouples and resistance temperature detectors (RTD) due to higher accuracy and low cost, if possible. The thermistors should evaluate the temperature of the fluids, pipe wall, and both sides of the insulation layer, at least. The measurement should also include the evaluation of temperature directly above and under the cooling pipe.

---

[75] Equations (55) - (60)

Nevertheless, the pressure transducers should measure the total pressure drop for both pipes. As soon as the experimental data is available, the corrections on the tool should be executed.

The present work has introduced the system with suggestions from the perspective of heat transfer. However, the ideal solutions should consider the economic analysis as well. For example, installation costs, type of materials, and arrangement of the pipes compile towards the total costs. Most importantly, the best arrangement is safe, durable, energy-efficient, and cost-effective, which serves the purpose of use.

In conclusion, *the heat conduction module* provides an excellent platform to design direct-controlled ice rinks with carbon dioxide as a refrigerant. It helps the designers evaluate the heat balance of the ice rink with high prediction accuracy. Moreover, *the pipe module* has shown its potential to evaluate the behavior of the brine and carbon dioxide inside the cooling pipes and heating pipes. Finally, *the thermophysical property module* provides a premise to evaluate the state of the materials in numerous applications. In the future, the integration of ammonia and isobutane into the tool should provide additional value and flexibility towards sustainable design. Construction of a 3D-model could also provide visualization of heat transfer and support the effectiveness of the present work.

REFERENCES

Armand, A. A., and Treschev, G. G. (1946) 'The resistance during the movement of a two-phase system in horizontal pipes', *Izvestiia Vsesoiuznyi Teplotekhnicheskii Institut*. AERE: Atomic Energy Research Establishment Harwell, 1, pp. 16–23.

Asadi, I. *et al.* (2018) 'Thermal conductivity of concrete – A review', *Journal of Building Engineering*, pp. 81–93. doi: https://doi.org/10.1016/j.jobe.2018.07.002.

ASHRAE Handbook: Refrigeration. SI Edition (2018). Atlanta: American Society of Heating, Refrigerating, and Air-Conditioning Engineers.

Baehr, H. D. and Stephan, K. (2011) *Heat and mass transfer : with many worked examples and exercises*. 3., rev. e. Berlin: Springer. Available at: https://aalto.finna.fi/Record/alli.555677.

Bellache, O., Ouzzane, M. and Galanis, N. (2005) 'Numerical prediction of ventilation patterns and thermal processes in ice rinks', *Building and Environment*, 40(3), pp. 417–426. doi: 10.1016/j.buildenv.2004.08.004.

Bolteau, S., Rogstam, J. and Tazi, M. (2016) 'Evaluation of heat recovery performance in a CO2 ice rink', *Refrigeration Science and Technology*, pp. 285–292. doi: 10.18462/iir.gl.2016.1042.

Brown, G. O. (2003) 'The history of the Darcy-Weisbach equation for pipe flow resistance', in *Environmental and Water Resources History*, pp. 34–43.

Caliskan, H. and Hepbasli, A. (2010) 'Energy and exergy analyses of ice rink buildings at varying reference temperatures', *Energy and Buildings*. Elsevier, 42(9), pp. 1418–1425. doi: 10.1016/J.ENBUILD.2010.03.011.

Çengel, Y. A. and Ghajar, A. J. (2011) *Heat and mass transfer : fundamentals & applications*. 4. ed. New York: McGraw-Hill. Available at: https://aalto.finna.fi/Record/alli.529734.

Chan, J. (2013) *Thermal properties of concrete with different Swedish aggregate materials*. Lund University.

Chang, S. S. (1974) 'Heat capacities of polyethylene from 2 to 360 K. II. Two high-density linear polyethylene samples and thermodynamic properties of crystalline linear polyethylene', *J.Res.NBS A Phys.Chem*, 3.

Chen, J. *et al.* (2019) 'Analysis of thermal conductivity of porous concrete using laboratory measurements and microstructure models', *Construction and Building Materials*. Elsevier Ltd, 218, pp. 90–98. doi: 10.1016/j.conbuildmat.2019.05.120.

Chen, J. C. (1966) 'A correlation for boiling heat transfer to saturated fluids in convective flow', *Industrial and engineering chemistry process design and development*, 5(3), pp. 322–329.

Chen, N. H. (1979) 'An Explicit Equation for Friction Factor in Pipe', *Industrial & Engineering Chemistry Fundamentals*. American Chemical Society, 18(3), pp. 296–297. doi: 10.1021/i160071a019.

Cheng, L. *et al.* (2006) 'New flow boiling heat transfer model and flow pattern map for

carbon dioxide evaporating inside horizontal tubes', *International Journal of Heat and Mass Transfer*, 49(21–22), pp. 4082–4094. doi: 10.1016/j.ijheatmasstransfer.2006.04.003.

Cheng, L., Ribatski, G., and Thome, J. R. (2008) 'New prediction methods for CO2 evaporation inside tubes: Part II—An updated general flow boiling heat transfer model based on flow patterns', *International Journal of Heat and Mass Transfer*, 51(1), pp. 125–135. doi: https://doi.org/10.1016/j.ijheatmasstransfer.2007.04.001.

Chisholm, D. (1973) 'Pressure gradients due to friction during the flow of evaporating two-phase mixtures in smooth tubes and channels', *International Journal of Heat and Mass Transfer*, pp. 347–358. doi: https://doi.org/10.1016/0017-9310(73)90063-X.

Chisholm, D. (1983) *Two-phase flow in pipelines and heat exchangers*. G. Godwin in association with Institution of Chemical Engineers.

Choi, Y.-H. (1986) 'Effects of temperature and composition on the thermal conductivity and thermal diffusivity of some food components', *Korean Journal of Food Science and Technology*. Korean Society of Food Science and Technology, 18(5), pp. 357–363.

Coetzee, N. (2015) 'Heat Transfer Coefficients of Smooth Tubes in the Turbulent Flow Regime By', (May).

Cooper, M. G. (1984) 'Heat Flow Rates in Saturated Nucleate Pool Boiling-A Wide-Ranging Examination Using Reduced Properties', in Hartnett, J. P. and Irvine, T. F. B. T.-A. in H. T. (eds). Elsevier, pp. 157–239. doi: https://doi.org/10.1016/S0065-2717(08)70205-3.

Crowe, C. T. (2005) *Multiphase Flow Handbook*. CRC Press.

Dalla Santa, G. *et al.* (2017) 'Laboratory Measurements of Gravel Thermal Conductivity: An Update Methodological Approach', *Energy Procedia*. Elsevier B.V., 125, pp. 671–677. doi: 10.1016/j.egypro.2017.08.287.

Daoud, A., Galanis, N., and Bellache, O. (2008) 'Calculation of refrigeration loads by convection, radiation, and condensation in ice rinks using a transient 3D zonal model', *Applied Thermal Engineering*, 28(14–15), pp. 1782–1790. doi: 10.1016/j.applthermaleng.2007.11.011.

Darby, R. and Chhabra, R. P. (2017) *Chemical Engineering Fluid Mechanics: Third Edition*. CRC Press, Taylor & Francis Group LCC.

Davis, E. J., and Anderson, G. H. (1966) 'The incipience of nucleate boiling in forced convection flow', *AIChE Journal*. Wiley Online Library, 12(4), pp. 774–780.

Denisikhina, D., Samoletov, M. and Brodach, M. (2017) 'Air distribution in indoor ice skating rinks', *REHVA Journal*, (August), pp. 46–51. Available at: https://www.rehva.eu/fileadmin/REHVA_Journal/REHVA_Journal_2017/RJ4/p.46/46-51_RJ1704_WEB.pdf.

Design Institute for Physical Property Data, (U. S) (2019) *DIPPR Project 801, full version : evaluated standard thermophysical property values*. Provo, Utah: BYU DIPPR, Thermophysical Properties Laboratory. Available at: https://aalto.finna.fi/Record/alli.905955.

European Parliament and Council (2014) 'Regulation (EU) No 517/2014 of the European Parliament and of the Council of 16 April 2014 on fluorinated greenhouse gases and

repealing Regulation (EC) No 842/2006', *Official Journal of the European Union*, 2014(517), p. L150/195-230. Available at: http://eur-lex.europa.eu/eli/reg/2014/517/oj.

Fang, X. *et al.* (2019) 'Saturated flow boiling heat transfer: review and assessment of prediction methods', *Heat and Mass Transfer/Waerme- und Stoffuebertragung*, 55(1), pp. 197–222. doi: 10.1007/s00231-018-2432-1.

Fang, X., Wu, Q. and Yuan, Y. (2017) 'A general correlation for saturated flow boiling heat transfer in channels of various sizes and flow directions', *International Journal of Heat and Mass Transfer*, 107, pp. 972–981. doi: https://doi.org/10.1016/j.ijheatmasstransfer.2016.10.125.

Fang, X., Zhou, Z. and Li, D. (2013) 'Review of correlations of flow boiling heat transfer coefficients for carbon dioxide', *International Journal of Refrigeration*. Elsevier Ltd and IIR, 36(8), pp. 2017–2039. doi: 10.1016/j.ijrefrig.2013.05.015.

Feistel, R. and Wagner, W. (2006) 'A New Equation of State for H2O Ice Ih', *Journal of Physical and Chemical Reference Data*. American Institute of Physics, 35(2), pp. 1021–1047. doi: 10.1063/1.2183324.

Fenghour, A., Wakeham, W. A. and Vesovic, V. (1998) 'The Viscosity of Carbon Dioxide', *Journal of Physical and Chemical Reference Data*. American Institute of Physics, 27(1), pp. 31–44. doi: 10.1063/1.556013.

Fernando, P. *et al.* (2008) 'A minichannel aluminium tube heat exchanger - Part I: Evaluation of single-phase heat transfer coefficients by the Wilson plot method', *International Journal of Refrigeration*, 31(4), pp. 669–680. doi: 10.1016/j.ijrefrig.2008.02.011.

Ferrantelli, A., Viljanen, K. and Kurnitski, J. (2019) 'Energy analysis in ice hockey arenas and analytical formula for the temperature profile in the ice pad with transient boundary conditions', *Advances in Building Energy Research*, (May). doi: 10.1080/17512549.2019.1615549.

Friedel, L. (1977) 'Momentum exchange and pressure drop in two-phase flow', in *Two-phase flows and heat transfer, Vol. 1*.

Ganjian, E. (1990) 'The Relationship between Porosity and Thermal Conductivity of Concrete', pp. 1–286. Available at: http://etheses.whiterose.ac.uk/2044/.

Gaur, U. and Wunderlich, B. (1983) 'Heat capacity and other thermodynamic properties of linear macromolecules. VII. Other carbon backbone polymers', *Journal of Physical and Chemical Reference Data*. American Institute of Physics for the National Institute of Standards and …, 12(1), pp. 29–63.

Ghajar, A. J. and Bhagwat, S. M. (2013) 'Effect of void fraction and two-phase dynamic viscosity models on prediction of hydrostatic and frictional pressure drop in vertical upward gas-liquid two-phase flow', *Heat Transfer Engineering*, 34(13), pp. 1044–1059. doi: 10.1080/01457632.2013.763541.

Ghajar, A. J. and Tang, C. C. (2012) 'Void Fraction and Flow Patterns of Two-Phase Flow in Upward and Downward Vertical and Horizontal Pipes - Advances in Multiphase Flow and Heat Transfer V.4', 4, pp. 175–201. doi: DOI: 10.2174/97816080522951120101.

Gnielinski, V. (1976) 'New equations for heat and mass transfer in turbulent pipe and

channel flow', *Int.Chem.Eng.*, 16(2), pp. 359–368.

Gnielinski, V. (2013) 'On heat transfer in tubes', *International Journal of Heat and Mass Transfer*, 63, pp. 134–140. doi: https://doi.org/10.1016/j.ijheatmasstransfer.2013.04.015.

Gnielinski, V. (2015) 'Turbulent Heat Transfer in Annular Spaces—A New Comprehensive Correlation', *Heat Transfer Engineering*. Taylor & Francis, 36(9), pp. 787–789. doi: 10.1080/01457632.2015.962953.

Gomes, R., Liteplo, R., and Meek, M. E. (2002) *Ethylene glycol: human health aspects*.

Guo, Lixia *et al.* (2011) 'Thermal conductivity and heat transfer coefficient of concrete', *Journal of Wuhan University of Technology-Mater.Sci.Ed.*, 26(4), pp. 791–796. doi: 10.1007/s11595-011-0312-3.

Hahne, E. (1993) 'E1 Steady-State Heat Conduction', in *VDI Heat Atlas*.

Hakala, P. and Kaappola, E. (2007) *Kylmälaitoksen suunnittelu*. 2. tark. p. Helsinki: Opetushallitus.

Huber, D. and Walter, H. (2010) 'Forced convection heat transfer in the transition region between laminar and turbulent flow for a vertical circular tube', *International Conference on Theoretical and Applied Mechanics, International Conference on Fluid Mechanics and Heat and Mass Transfer - Proceedings*, pp. 132–136.

Huber, M. L. *et al.* (2009) 'New International Formulation for the Viscosity of H2O', *Journal of Physical and Chemical Reference Data*. American Institute of Physics, 38(2), pp. 101–125. doi: 10.1063/1.3088050.

Huber, M. L. *et al.* (2012) 'New International Formulation for the Thermal Conductivity of H2O', *Journal of Physical and Chemical Reference Data*. American Institute of Physics, 41(3), p. 33102. doi: 10.1063/1.4738955.

Ian H. Bell and the CoolProp Team. (2017) *CoolProp*. Available at: www.coolprop.org (Accessed: 17 June 2020).

International Ice Hockey Federation (IIHF) (2016) *IIHF Ice Rink Guide*. Available at: https://www.iihf.com/en/static/5890/iihf-ice-rink-guide.

ISO SFS-EN 14688-1:2018: Geotechnical investigation and testing. Identification and classification of soil. Part 1 : Identification and description (ISO 14688-1:2017) (2018).

Kalland, K. M. (2008) *A Navier-Stokes Solver for Single- and Two-Phase Flow*. University of Oslo.

Kandlikar, S. G. (1990) 'A general correlation for saturated two-phase flow boiling heat transfer inside horizontal and vertical tubes', *Journal of Heat Transfer*, 112(1), pp. 219–228. doi: 10.1115/1.2910348.

Karampour, M. (2011) *Measurement and modelling of ice rink heat loads*. KTH School of Industrial Engineering and Management.

Konakov, P. K. (1946) 'A new correlation for the friction coefficient in smooth tubes', *Berichte der Akademie der Wissenschaften der UDSSR*, 51.

Kretzschmar, H.-J. and Wagner, W. (2019) *International Steam Tables: Properties of Water*

and Steam Based on the Industrial Formulation IAPWS-IF97. Springer.

Lakatos, Á. (2014) 'Comparison of the thermal properties of different insulating materials', *Advanced Materials Research*, 899(February), pp. 381–386. doi: 10.4028/www.scientific.net/AMR.899.381.

Lamberg, S., Lautkaski, R. and Virolainen, K. (2015) 'Safety Guide of Ammonia Refrigerating Systems', (April).

Linstrom, P. J., and Mallard, W. G. (eds) (2018) *NIST Chemistry WebBook*. 69th edn. Gaithersburg MD, 20899: National Institute of Standards and Technology. doi: https://doi.org/10.18434/T4D303.

Lipovka, A. Y. and Lipovka, Y. L. (2014) 'Determining Hydraulic Friction Factor for Pipeline Systems', *Журнал Сибирского Федерального Университета. Техника И Технологии*, 7(1), pp. 62–82.

Lira, I. (2013) 'On the uncertainties stemming from use of the colebrook-white equation', *Industrial and Engineering Chemistry Research*, 52(22), pp. 7550–7555. doi: 10.1021/ie4001053.

Lockhart, R. W., and Martinelli, R. C. (1949) 'Proposed correlation of data for isothermal two-phase, two-component flow in pipes', *Chem.Eng.Prog*, 45(1), pp. 39–48.

Minami, K. and Brill, J. P. (1987) 'Liquid Holdup in Wet-Gas Pipelines', *SPE Production Engineering*. Society of Petroleum Engineers, 2(01), pp. 36–44. doi: 10.2118/14535-PA.

Mukherjee, H. (1979) 'An Experimental Study of Inclined Two-Phase Flow Ph. D', *University of Tulsa, Tulsa, Oklahoma*.

Müller-Steinhagen, H. and Heck, K. (1986) 'A simple friction pressure drop correlation for two-phase flow in pipes', *Chemical Engineering and Processing: Process Intensification*. Elsevier, 20(6), pp. 297–308.

Nguyen, T. (2012) *Carbon dioxide in ice rink refrigeration*. Royal Institute of Technology (KTH), Stockholm.

Pettersen, J. (2004) 'Flow vaporization of CO2 in microchannel tubes', *Experimental Thermal and Fluid Science*, 28(2–3), pp. 111–121. doi: 10.1016/S0894-1777(03)00029-3.

Pietrak, K. and Wiśniewski, T. (2015) 'A review of models for effective thermal conductivity of composite materials', *Journal of Power of Technologies*, 95(1), pp. 14–24.

Premoli, A. (1970) 'An empirical correlation for evaluating two-phase mixture density under adiabatic conditions', in *European Two-Phase Flow Group Meeting, 1970*.

Progelhof, R. C., Throne, J. L. and Ruetsch, R. R. (1976) 'Methods for predicting the thermal conductivity of composite systems: A review', *Polymer Engineering & Science*, 16(9), pp. 615–625. doi: 10.1002/pen.760160905.

Rajendra Karwa (2017) *Heat and mass transfer*. Jodhpur, Rajasthan: Springer Nature. doi: 10.4324/9781315119717.

Rakennustieto.fi (2012) *XPS-ERISTEET Lämmöneristystarvikkeet*.

Rathjen, W. and Straub, J. (1977) 'Temperature dependence of surface tension, coexistence

curve, and vapor pressure of CO2, CClF3, CBrF3, and SF6', *Heat transfer in boiling, New York: Academic Press.*

REFPROP (2019) *Version 10*. Available at: https://www.nist.gov/srd/refprop (Accessed: 22 May 2020).

Rogstam, J. (2016) 'Evolution of CO2 as refrigerant in ice rink applications', *12TH IIR Gustav Lorentzen Natural Working Fluids Conference*, pp. 1–8. doi: 10.18462/iir.gl.2016.1043.

Rogstam, J., Abdi, A. and Sawalha, S. (2014) 'Carbon dioxide in ice rink refrigeration', *11th IIR Gustav Lorentzen Conference on Natural Refrigerants: Natural Refrigerants and Environmental Protection, GL 2014*, (November 2017), pp. 585–592.

Rogstam, J., Sawalha, S., and Nilsson, P. . (2005) 'Ice Rink Refrigeration System With CO2 As Secondary Fluid', *Environmental Science*, pp. 1–8.

Rohsenow, W. M., Hartnett, J. P., and Cho, Y. I. (1998) *Handbook of heat transfer*. McGraw-Hill New York.

Rouhani, S. Z. and Axelsson, E. (1968) 'Calculation of void volume fraction in the subcooled and quality boiling regions'. AB Atomenergi.

Russick, E. M. *et al.* (1996) 'Corrosive effects of supercritical carbon dioxide and cosolvents on metals', *The Journal of Supercritical Fluids*, 9(1), pp. 43–50.

Sabet, M. and Soleimani, H. (2019) 'Inclusion of graphene on LDPE properties', *Heliyon*. Elsevier Ltd, 5(7), p. e02053. doi: 10.1016/j.heliyon.2019.e02053.

Saha, P. and Zuber, N. (1974) 'Point of net vapor generation and vapor void fraction in subcooled boiling', in *International Heat Transfer Conference Digital Library*. Begel House Inc.

Sato, T., and Matsumura, H. (1964) 'On the conditions of incipient subcooled boiling with forced convection', *Bulletin of JSME*, 7, pp. 392–398. Available at: http://www.mendeley.com/research/geology-volcanic-history-eruptive-style-yakedake-volcano-group-central-japan/.

Seghouani, L., Daoud, A. and Galanis, N. (2009) 'Prediction of yearly energy requirements of indoor ice rinks', *Energy and Buildings*. Elsevier, 41(5), pp. 500–511. doi: 10.1016/J.ENBUILD.2008.11.014.

SFS-EN 1057 + A1: Copper and copper alloys. Seamless, round copper tubes for water and gas in sanitary and heating applications (2012).

SFS-EN 12735-2:2016: Copper and copper alloys. Seamless, round tubes for air conditioning and refrigeration. Part 2: Tubes for equipment (2016).

SFS-EN 13164 + A1 Tehdasvalmisteiset lämmöneristystuotteet. Tehdasvalmisteiset suulakepuristetut polystyreenituotteet (XPS). Tuotestandardi (2007).

SFS-EN 13349: Copper and copper alloys. Pre-insulated copper tubes with solid covering (2002).

SFS-EN 1994-1-2 + AC + A1: Eurocode 4. Design of composite steel and concrete structures. Part 1-2: General rules. Structural fire design (2014).

SFS 1200: Betonirakenteiden yleiset teräkset. Lajit, nimikkeet ja merkinnät yleisissä tuotteissa (1999).

Shahzad, K. (2006) *An ice rink refrigeration system based on CO2 as secondary fluid in copper tubes*. Royal Institute of Technology (KTH), Stockholm.

Sieder, E. N. and Tate, G. E. (1936) 'Heat Transfer and Pressure Drop of Liquids in Tubes', *Industrial and Engineering Chemistry*, 28(12), pp. 1429–1435. doi: 10.1021/ie50324a027.

Simard, L. (2012) 'Ice rink uses CO2 system', *ASHRAE Journal*, 54(3), p. 38.

Smith, S. L. (1969) 'Void fractions in two-phase flow: a correlation based upon an equal velocity head model', *Proceedings of the Institution of Mechanical Engineers*. SAGE Publications Sage UK: London, England, 184(1), pp. 647–664.

Span, R. and Wagner, W. (1996) 'A New Equation of State for Carbon Dioxide Covering the Fluid Region from the Triple-Point Temperature to 1100 K at Pressures up to 800 MPa', *Journal of Physical and Chemical Reference Data*. American Institute of Physics, 25(6), pp. 1509–1596. doi: 10.1063/1.555991.

Sun, L. and Mishima, K. (2009) 'An evaluation of prediction methods for saturated flow boiling heat transfer in mini-channels', *International Journal of Heat and Mass Transfer*. Elsevier Ltd, 52(23–24), pp. 5323–5329. doi: 10.1016/j.ijheatmasstransfer.2009.06.041.

Sun, T., and Teja, A. S. (2003) 'Density, viscosity, and thermal conductivity of aqueous ethylene, diethylene, and triethylene glycol mixtures between 290 K and 450 K', *Journal of Chemical and Engineering Data*, 48(1), pp. 198–202. doi: 10.1021/je025610o.

Sun, T., and Teja, A. S. (2004) 'Density, viscosity and thermal conductivity of aqueous solutions of propylene glycol, dipropylene glycol, and tripropylene glycol between 290 K and 460 K', *Journal of Chemical and Engineering Data*, 49(5), pp. 1311–1317. doi: 10.1021/je049960h.

Sunyé, R. *et al.* (2007) *Develop and verify methods for determining ice sheet cooling loads*, *ASHRAE Research Project RP 1289*. Canada.

Suomen betoniyhdistys ry (2019) *by 47 Betonirakentamisen laatuohjeet 2019*. By-koulutus (by Tekniset ohjeet).

Suomen kylmäyhdistys ry (2017) *Kylmäainetilanne 2017*. Available at: http://www.skll.fi/www/att.php?type=2&id=305.

Taebnia, M. *et al.* (2019) 'Air distribution and air handling unit configuration effects on energy performance in an air-heated ice rink arena', *Energies*, 12(4). doi: 10.3390/en12040693.

Thome, J. R., and El Hajal, J. (2004) 'Flow boiling heat transfer to carbon dioxide: General prediction method', *International Journal of Refrigeration*, 27(3), pp. 294–301. doi: 10.1016/j.ijrefrig.2003.08.003.

Tinker, J. a. and Cabrera, J. G. (1992) 'Modeling the Thermal Conductivity of Concrete Based on Its Measured Density and Porosity', *Thermal Performance of the Exterior Envelopes of Buildings V*, pp. 91–95.

Väänänen, O. (2019) *Ulkotekojään energiajärjestelmä: Lämmönkeruujärjestelmän mitoitus*. Tampereen ammattikorkeakoulu.

VanSant, J. H. (1980) *Conduction heat transfer solutions*. Livermore, CA (United States). doi: 10.2172/7035199.

Vesovic, V. *et al.* (1990) 'The Transport Properties of Carbon Dioxide', *Journal of Physical and Chemical Reference Data*. American Institute of Physics, 19(3), pp. 763–808. doi: 10.1063/1.555875.

Wagner, W., and Kretzschmar, H.-J. (eds) (2008) 'IAPWS Industrial Formulation 1997 for the Thermodynamic Properties of Water and Steam', in *International Steam Tables: Properties of Water and Steam Based on the Industrial Formulation IAPWS-IF97*. Berlin, Heidelberg: Springer Berlin Heidelberg, pp. 7–150. doi: 10.1007/978-3-540-74234-0_3.

Wang, H. *et al.* (2013) 'Modeling the Soil Water Retention Curves of Soil-Gravel Mixtures with Regression Method on the Loess Plateau of China', *PLoS ONE*, 8(3). doi: 10.1371/journal.pone.0059475.

White, G. K. and Collocott, S. J. (1984) 'Heat Capacity of Reference Materials: Cu and W', *Journal of Physical and Chemical Reference Data*. American Institute of Physics, 13(4), pp. 1251–1257. doi: 10.1063/1.555728.

White, G. K., and Minges, M. L. (1997) 'Thermophysical properties of some key solids: an update', *International Journal of Thermophysics*. Springer, 18(5), pp. 1269–1327.

William, S. and Bodinus, P. E. (1999) 'The Rise and Fall of Carbon Dioxide Systems', *ASHRAE Journal*, (April), pp. 37–42.

Woldesemayat, M. and Ghajar, A. (2007) 'Comparison of void fraction correlations for different flow patterns in horizontal and upward inclined pipes', *International Journal of Multiphase Flow*, 33, pp. 347–370. doi: 10.1016/j.ijmultiphaseflow.2006.09.004.

Xu, Y. *et al.* (2012) 'Evaluation of frictional pressure drop correlations for two-phase flow in pipes', *Nuclear Engineering and Design*, 253, pp. 86–97. doi: 10.1016/j.nucengdes.2012.08.007.

Xu, Y. and Fang, X. (2012) 'A new correlation of two-phase frictional pressure drop for evaporating flow in pipes', *International Journal of Refrigeration*, 35(7), pp. 2039–2050. doi: 10.1016/j.ijrefrig.2012.06.011.

Yi, J. (2018) 'Methods of Heat Transfer Analysis of Buried Pipes in District Heating and Cooling Systems 2. Method and Influence Factors of Heat Transmission and Distribution Pipeline', *Applied Engineering*, 2(2), pp. 33–38. doi: 10.11648/j.ae.20180202.12.

Yu, J. *et al.* (2014) 'Thermal conductivity of highly crystallized polyethylene', *Polymer*, pp. 195–200. doi: https://doi.org/10.1016/j.polymer.2013.12.001.

Zhang, W., Hibiki, T. and Mishima, K. (2010) 'Correlations of two-phase frictional pressure drop and void fraction in mini-channel', *International Journal of Heat and Mass Transfer*. Elsevier Ltd, 53(1–3), pp. 453–465. doi: 10.1016/j.ijheatmasstransfer.2009.09.011.

Zhu, H., Fan, T. and Zhang, D. (2016) 'Composite Materials with Enhanced Conductivities', *Advanced Engineering Materials*, 18(7), pp. 1174–1180. doi: 10.1002/adem.201500482.

APPENDICES

Appendix A – Parameters for thermophysical properties

Appendix B – Uncertainty of thermophysical properties

Appendix C – Thermophysical properties of humid air

Appendix A - Parameters for thermophysical properties.

Table 1. Parameters of carbon dioxide. General properties.

Property	Model	Equation	Unit	Parameter/index	0	1	2	3	4	5	6
Vapor pressure	Project DIPPR 801	49	Pa	a	47.0169	-2839	-3.86	2.81115E-16	6		
	3-order polynomial - Span & Wagner (1996) - Pressure	52	Pa	a	-2938419.33	433847.9386	-2172.277426	3.777778902			
	6-order polynomial - Span & Wagner (1996) - Temperature	52	Pa	a	190.894218	6.21564E-05	-2.69813E-11	8.20897E-18	-1.4551E-24	1.35336E-31	-5.11624E-39
Enthalpy of vaporization	Project DIPPR 801 - Original parameters	47	J/kmol	a	21730000	0.382	-0.4339	0.42213			
	Project DIPPR 801 - Span & Wagner (1996)	47	J/kmol	a	18118753.98	-0.334592066	0.631368011	0.054064566	-0.034237421		
Surface Tension	Project DIPPR 801 - Original parameters	47	N/m	a	0.08414	1.284					
	Project DIPPR 801 - Rathjen & Straub (1977)	47	N/m	a	0.084652993	1.282080316					

Table 2. Parameters of carbon dioxide. Saturated liquid.

Property	Model	Equation	Unit	Parameter/index	0	1	2	3	4
Density	Project DIPPR 801 - Liquid	50	kmol/m:	a	2.768	0.26212	304.21	0.2908	
	Span & Wagner (1996) - Liquid	53	kg/m3	a	1.9245108	-0.62385555	-0.32731127	0.39245142	
				b	0.34	0.5	1.666666667	1.833333333	
Thermal Conductivity	Project DIPPR 801	52	W/(m*K)	a	0.4406	-0.0012175			
	Equation 58 - Vesovic et al. (1990)	55	W/(m*K)	a	0.180573879	0.976941346			
				b	-0.001364256	0.003976015			
				c	0.032558188	3.18075E-17			
				d	9.88116E-35				
Viscosity	Project DIPPR 801	49	Pa*s	a	18.775	-402.92	-4.6854	-6.9171E-26	10
	Equation 60 - Fenghour (1998)	57	Pa*s	a	2.05243E-05				
				b	4.7316E-05	-2.18716E-05	-4.5E-06		
				c	0.200510058	0.008337561	1E-25		
Heat capacity	Project DIPPR 801	52	J/(kmol*	a	-8304300	104370	-433.33	0.60052	
	Equation 62 - Span & Wagner (1996)	59	J/(kg*K)	a	1894.858555	5473.563047	14274.75994	27634.02661	
				b	2207.995268				
				c	0.026474986	2.97313E-07	6.02005E-22	8.65099E-65	

Table 3. Parameters of carbon dioxide. Saturated vapor.

Property	Model	Equation	Unit	Parameter/index	0	1	2	3	4
Density	Span & Wagner (1996) - Vapor	69	kg/m3	a	-1.7074879	-0.8227467	-4.6008549	-10.111178	-29.742252
				b	0.34	0.5	1	2.333333333	4.666666667
Thermal Conductivity	Project DIPPR 801	46	W/(m*K)	a	3.69	-0.3838	964	1860000	
	Equation 59 - Vesovic et al. (1990)	56	W/(m*K)	a	0.011430679				
				b	1.01926E-05	1.634213647			
				c	0.058490048	0.041418201	5.01051E-05		
				d	6.5294E-38	1.15667E-05	8.73925E-16		
Viscosity	Project DIPPR 801	46	Pa*s	a	0.000002148	0.46	290		
	Equation 61 - Fenghour (1998)	58	Pa*s	a	1.11835E-05				
				b	1.50839E-08	1.346651002			
				c	6.48138E-06	8.84983E-07	1.49996E-06		
				d	2.24827E-05	3.83213E-20	9.99994E-31		
Heat Capacity	Project DIPPR 801	48	J/(kmol*	a	29370	34540	1428	26400	588
	Equation 63 - Span & Wagner (1996)	60	J/(kg*K)	a	759.5776062				

	a2	a3	a4	a5
b	2845.846499	8429.525497	21605.79317	46095.42463
c	0.054623874	1.41742E-06	1.58274E-19	1.60637E-58

Table 4. Parameters of ice in atmospheric pressure.

Property	Model	Equation	Unit	a0	a1	a2
Density	Linear - Feister & Wagner (2006)	52	kmol/m³	52.96187503	-0.00760253	
	Linear - Project DIPPR 801	52	kmol/m³	53.03	-0.0078409	
Thermal conductivity	2-order polynomial - Choi & Okos (1986)	52	W/(m*K)	2.2199	-0.006248	0.00010154
Heat capacity	Linear - Feister & Wagner (2006)	52	J/(kmol)*	1889.193819	131.321946	
	Linear - Project DIPPR 801	52	J/(kmol)*	-262.49	140.52	

Table 5. Parameters of water in atmospheric pressure.

Property	Model	Equation	Unit	a0	a1	a2	a3	a4	a5
Density	4-order polynomial - Wagner et al. (2008)	52	kg/m3	-1164.986226	24.3170742	-0.101075962	0.000186529	-1.3247E-07	
	3-order polynomial - Project DIPPR 801	52	kmol/m³	-13.851	0.64038	-0.0019124	1.8211E-06		
Thermal conductivity	3-order polynomial - Huber et al. (2011)	52	W/(m*K)	-2.112170949	0.020239568	-4.96094E-05	4.1285E-08		
	3-order polynomial - Project DIPPR 801	52	W/(m*K)	-0.432	0.0057255	-0.000008078	1.861E-09		
Viscosity	5-order polynomial - Huber et al. (2009)	52	Pa*s	1890608.064	-27737.79704	163.265813	-0.48135913	0.000710348	-4.19533E-07
	Project DIPPR 801 - Original Parameters	49	Pa*s	-52.843	3703.6	5.866	-5.879E-29	10	0
Heat capacity	5-order polynomial - Wagner et al. (2000)	52	kJ/(kg*K)	193.9111909	-2.851853644	0.017146211	-5.1524E-05	7.73459E-08	-4.63731E-11
	4-order polynomial - Project DIPPR 801	52	J/(kmol)*	276370	-2090.1	8.125	-0.014116	9.3701E-06	-

Table 6. Parameters of dry air in atmospheric pressure.

Property	Model	Equation	Unit	a0	a1	a2	a3	a4
Thermal conductivity	Project DIPPR 801 - Stephan & Laeseke (1985)	46	W/(m*K)	0.00020467	0.850411382	-0.212999135	101.2043444	
	Project DIPPR 801 - Original parameters	46	W/(m*K)	0.00031417	0.7786	-0.7116	2121.7	
Viscosity	Project DIPPR 801 - Kadoya et al. (1985)	46	Pa*s	1.04309E-06	0.550836014	89.5661496	-0.00032	
	Project DIPPR 801	46	Pa*s	0.000001425	0.5039	108.3	0	
Heat capacity	3-order polynomial - Toulokian & Makita (1970)	52	kcal/(kg)'	0.249679	-7.55179E-05	1.69194E-07	-6.46128E-11	
	Project DIPPR 801	48	J/(kmol)*	28958	9390	3012	7580	1484
	2-order polynomial - Lemmon et al. (1999)	52	J/(kg*K)	1034.971991	-0.224813855	0.000043443		

Table 7. Properties of steam in atmospheric pressure.

Property	Model	Equation	Unit	a0	a1	a2	a3	a4
Vapor pressure	Buck (2012) - Water		Pa	0.61121	18.678	234.5	257.14	
	Buck (1981) - Ice		Pa	0.61115	23.036	279.82	333.7	
Thermal conductivity	Project DIPPR 801	46	W/(m*K)	6.2041E-06	1.3973			
	2-order polynomial - Huber et al. (2011)	52	W/(m*K)	11.92646898	-0.025973459	0.000160173		
Viscosity	Project DIPPR 801	46	Pa*s	1.7096E-09	1.1146			
	3-order polynomial - Huber et al. (2009)	52	Pa*s	10.71911728	-0.059528233	0.000259047	-2.37595E-07	
Heat capacity	Project DIPPR 801	48	J/(kmol)*	33363	26790	2610.5	8896	1169
	4-order polynomial - Wagner et al. (2000)	52	kJ/(kg*K)	14.02714649	-0.155767494	0.000746951	-1.59603E-06	1.29436E-09

Table 8. Properties of concrete in atmospheric pressure.

Property	Model	Equation	Unit	a0	a1	a2

Property	Model	Equation	Unit	a0	a1	a2	a3
Heat capacity	2-order polynomial	63	J/(kg*K)	890	56.2	-3.4	
Thermal conductivity	2-order polynomial, Upper Limit	63	W/m*K	2	-0.2451	0.0107	
	2-order polynomial, Lower Limit	63	W/m*K	1.36	-0.136	0.0057	

Table 9. Properties of reinforcement steel

Property	Model	Equation	Unit	a0	a1	a2	a3
Heat capacity	3-order polynomial	68	J/(kg*K)	425	0.773	-0.00169	0.00000222
Thermal conductivity	Linear	69	W/m*K	54	-0.0333		

Table 10. Properties of copper in atmospheric pressure.

Property	Model	Equation	Unit	a0	a1	a2	a3	a4	a5	a6	a7	a8
Thermal conductivity	3-order polynomial - RRR = 30	52	W/m*K	428.754717	-0.335202156	0.000914286	-9.0566E-07					
	3-order polynomial - RRR = 100	52	W/m*K	505.5283019	-0.917879605	0.002685714	-2.7673E-06					
	3-order polynomial - RRR = 300	52	W/m*K	510.754717	-0.861868823	0.002314286	-2.23899E-06					
	3-order polynomial - RRR = 1000	52	W/m*K	528.3207547	-1.034699012	0.002914286	-2.91824E-06					
	3-order polynomial - RRR = 3000	52	W/m*K	537.8962264	-1.14007637	0.003314286	-3.40881E-06					
Heat capacity	White & Collocott 1984 (25 - 300 K)	61	J/(mol)*†	4.89287	-57.51701	238.2039	-345.4283	275.8975	-132.5425	38.17399	-6.07962	0.4118687
	White & Collocott 1984 (300 - 1300 K)	52	J/(mol)*†	351.6652889	0.122834808	-2.4899E-05						

Table 11. Properties of polyethylene.

Property	Model	Equation	Unit	a0	a1	a2	a3	a4	a5
Heat capacity	5-order polynomial - Amorphous - Chang (1974)	67	kJ/(kmol	-413.6444462	9.265007535	-0.079337882	0.000335235	-6.9261E-07	5.62677E-10
	5-order polynomial - Crystalline - Chang (1974)	67	kJ/(kmol	-38.49337019	0.997724569	-0.008065256	3.34897E-05	-6.763E-08	5.40555E-11
	5-order polynomial - Average - Chang (1974)	67	kJ/(kmol	-226.0689082	5.131366052	-0.043701569	0.000184362	-3.8012E-07	3.08366E-10

Table 12. Properties of ethylene glycol

Property	Model	Equation	Unit	a0	a1	a2	a3	a4	a5
Density	Sun & Teja (2003)	74	kg/m3	1127.68	-0.65816	-0.00061765	0.3059	0.13781	-0.0018961
Viscosity	Sun & Teja (2003)	74	Pa*s	-3.61359	986.519	127.861	-0.165301	-0.287325	0.00110978
Thermal conductivity	Sun & Teja (2003)	74	W/m*K	0.24658	0.00025372	-1.3186E-06	0.14219	0.38715	-0.00066551
Heat capacity	Project DIPPR 801	51	J/(kmol*	110130	8246	453090	-960820	446760	

Table 13. Properties of propylene glycol

Property	Model	Equation	Unit	Parameter/index	0	1	2	3	4	5	6
Density	Sun & Teja (2004)	76	kg/m3	A1		1003.7	-0.20062	-0.0025127			
				A2		147.12	-1.1024	0.0026902			
				A3		-99.617	0.63102	-0.0011267			
Viscosity	Sun & Teja (2004)	74	Pa*s	a	-213.16	14158	28.516	1.5232	-5.0007	0.00098106	3.2452
Thermal conductivity	Sun & Teja (2004)	74	W/m*K	a	0.19116	0.00011999	-9.2459E-07	0.3622	0.090345	-0.00020935	
Heat capacity	Project DIPPR 801	51	J/(kmol*	a	265720	1754.6	20442	-281090			

Appendix B - Uncertainty of thermophysical properties

Table 1. Uncertainty of carbon dioxide. General properties.

Property	Model	Total δ	Literature δ	Curve fit δ	Range [K]	Literature source
Vapor pressure	Project DIPPR 801	< 1 %	< 1 %	-	216.58 - 304.21	Project DIPPR 801
	3-order polynomial - Span & Wagner (1996) - Pressure	0.17 %	0.03 %	0.14 %	216.58 - 304.21	Span & Wagner (1996)
	6-order polynomial - Span & Wagner (1996) - Temperature	0.06 %	0.03 %	0.03 %	216.58 - 304.21	Span & Wagner (1996)
Enthalpy of vaporization	Project DIPPR 801 - Original parameters	< 1 %	< 1 %	-	216.58 - 304.21	Project DIPPR 801
	Project DIPPR 801 - Span & Wagner (1996)	0.30 %	0.15 %	0.15 %	216.58 - 304.21	Span & Wagner (1996)
Surface tension	Project DIPPR 801 - Original parameters	< 5 %	< 5 %	-	216.58 - 304.21	Project DIPPR 801
	Project DIPPR 801 - Rathjen & Straub (1977)	5.03 %	5.00 %	0.03 %	216.58 - 304.21	Rathjen & Straub (1977)

Table 2. Uncertainty of carbon dioxide. Saturated Liquid.

Property	Model	Total δ	Literature δ	Curve fit δ	Range [K]	Literature source
Density	Span & Wagner (1996) - Vapor	0.05 %	0.05 %	-	216.58 - 304.21	Span & Wagner (1996)
Thermal conductivity	Project DIPPR 801	< 3 %	< 3 %	-	216.58 - 304.21	Project DIPPR 801
	Equation 59 - Vesovic et al. (1990)	5.74 %	5.00 %	0.74 %	216.58 - 304.21	Vesovic (1990)
Viscosity	Project DIPPR 801	< 5 %	< 5 %	-	216.58 - 304.21	Project DIPPR 801
	Equation 61 - Fenghour (1998)	2.29 %	2.00 %	0.29 %	216.58 - 304.21	Fenghour (1998)
Heat capacity	Project DIPPR 801	< 1 %	< 1 %	-	216.58 - 304.21	Project DIPPR 801
	Equation 63 - Span & Wagner (1996)	0.26 %	0.15 %	0.11 %	216.58 - 304.21	Span & Wagner (1996)

Table 3. Uncertainty of carbon dioxide. Saturated Vapor.

Property	Model	Total δ	Literature δ	Curve fit δ	Range [K]	Literature source
Density	Span & Wagner (1996) - Vapor	0.05 %	0.05 %	-	216.58 - 304.21	Span & Wagner (1996)
Thermal conductivity	Project DIPPR 801	< 3 %	< 3 %	-	216.58 - 304.21	Project DIPPR 801
	Equation 59 - Vesovic et al. (1990)	5.74 %	5.00 %	0.74 %	216.58 - 304.21	Vesovic (1990)
Viscosity	Project DIPPR 801	< 5 %	< 5 %	-	216.58 - 304.21	Project DIPPR 801
	Equation 61 - Fenghour (1998)	2.29 %	2.00 %	0.29 %	216.58 - 304.21	Fenghour (1998)
Heat capacity	Project DIPPR 801	< 1 %	< 1 %	-	216.58 - 304.21	Project DIPPR 801
	Equation 63 - Span & Wagner (1996)	0.26 %	0.15 %	0.11 %	216.58 - 304.21	Span & Wagner (1996)

Table 4. Uncertainty of ice.

Property	Model	Total δ	Literature δ	Curve fit δ	Range [K]	Literature source
Density	Linear - Feister & Wagner (2006)	0.01 %	0.01 %	0.00 %	233.15 - 273.15	Feister & Wagner (2006)
	Linear - Project DIPPR 801	< 1 %	< 1 %	-	233.15 - 273.15	Project DIPPR 801
Thermal conductivity	2-order polynomial - Choi & Okos (1986)	0.79 %	0.79 %	-	233.15 - 273.15	Choi & Okos (1986)
Heat capacity	Linear - Feister & Wagner (2006)	2.01 %	2.00 %	0.01 %	233.15 - 273.15	Feister & Wagner (2006)
	Linear - Project DIPPR 801	< 3 %	< 3 %	-	233.15 - 273.15	Project DIPPR 801

Table 5. Uncertainty of liquid water.

Property	Model	Total δ	Literature δ	Curve fit δ	Range [K]	Literature source
Density	4-order polynomial - Wagner et al. (2008)	0.00 %	0.00 %	0.00 %	273.15 - 373.15	Wagner et al. (2000)
	3-order polynomial - Project DIPPR 801	< 0.2 %	< 0.2 %	-	273.15 - 373.15	Project DIPPR 801
Thermal conductivity	3-order polynomial - Huber et al. (2011)	0.74 %	0.70 %	0.04 %	273.15 - 373.15	Huber et al. (2011)
	3-order polynomial - Project DIPPR 801	< 1 %	< 1 %	-	273.15 - 373.15	Project DIPPR 801
Viscosity	5-order polynomial - Huber et al. (2009)	1.19 %	1.00 %	0.19 %	273.15 - 373.15	Huber et al. (2009)
	Project DIPPR 801 - Original Parameters	< 3 %	< 3 %	-	273.15 - 373.15	Project DIPPR 801
Heat capacity	5-order polynomial - Wagner et al. (2000)	0.21 %	0.20 %	0.01 %	273.15 - 373.15	Wagner et al. (2000)
	4-order polynomial - Project DIPPR 801	< 1 %	< 1 %	-	273.15 - 373.15	Project DIPPR 801

Table 6. Uncertainty of dry air.

Property	Model	Total δ	Literature δ	Curve fit δ	Range [K]	Literature source
Thermal conductivity	Project DIPPR 801 - Stephan & Laeseke (1985)	1.23 %	1.00 %	0.23 %	200 - 360	Stephan & Laesecke (1985)
	Project DIPPR 801 - Original parameters	< 3 %	< 3 %	-	200 - 360	Project DIPPR 801
Viscosity	Project DIPPR 801 - Kadoya et al. (1985)	2.33 %	2.00 %	0.33 %	85 - 650	Kadoya et al. (1985)
	Project DIPPR 801 - Original parameters	< 3 %	< 3 %	-	85 - 650	Project DIPPR 801
Heat capacity	3-order polynomial - Toulokian & Makita (1970)	0.01 %	0.01 %	-	263.15 - 573.15	Toulokian & Makita (1970)
	Project DIPPR 801	< 5 %	< 5 %	-	250 - 400	Project DIPPR 801
	2-order polynomial - Lemmon et al. (1999)	1.01 %	1.00 %	0.01 %	250 - 400	Lemmon et al. (1999)

Table 7. Uncertainty of steam.

Property	Model	Total δ	Literature δ	Curve fit δ	Range [K]	Literature source
Vapor pressure	Buck (2012) - Water	0.03 %	0.03 %	-	263.15 - 273.15	Buck (2012) - Water
	Buck (1981) - Ice	0.06 %	0.06 %	-	240 - 273.15	Buck (1981) - Ice
Thermal conductivity	Project DIPPR 801	< 1 %	< 1 %	-	273.15 - 373.15	Project DIPPR 801
	2-order polynomial - Huber et al. (2011)	0.75 %	0.70 %	0.05 %	273.15 - 373.15	Huber et al. (2011)
	Project DIPPR 801	< 1 %	< 1 %	-	273.15 - 373.15	Project DIPPR 801
Viscosity	3-order polynomial - Huber et al. (2009)	0.17 %	0.17 %	0.00 %	273.15 - 373.15	Huber et al. (2009)
	Project DIPPR 801	< 1 %	< 1 %	-	273.15 - 373.15	Project DIPPR 801
Heat capacity	4-order polynomial - Wagner et al. (2000)	0.20 %	0.20 %	0.00 %	273.15 - 373.15	Wagner et al. (2000)

Table 8. Uncertainty of concrete.

Property	Model	Total δ	Literature δ	Curve fit δ	Range [K]	Literature source2
Heat capacity	2-order polynomial	?	?	-	Extended to 263.15 - 1073.15 from 293.15 - 1073.15	SFS-EN 1994-1-2
Thermal conductivity	2-order polynomial, Upper Limit	?	?	-	Extended to 263.15 - 1073.15 from 293.15 - 1073.15	SFS-EN 1994-1-2
	2-order polynomial, Lower Limit	?	?	-	Extended to 263.15 - 1073.15 from 293.15 - 1073.15	SFS-EN 1994-1-2

Table 9. Uncertainty of reinforcement steel.

Property	Model	Total δ	Literature δ	Curve fit δ	Range [K]	Literature source
Heat capacity	3-order polynomial	?	?	-	Extended to 263.15 - 1073.15 from 293.15 - 1073.15	SFS-EN 1994-1-2
Thermal conductivity	Linear	?	?	-	Extended to 263.15 - 1073.15 from 293.15 - 1073.15	SFS-EN 1994-1-2

Table 10. Uncertainty of copper.

Property	Model	Total δ	Literature δ	Curve fit δ	Range [K]	Literature source
Thermal conductivity	3-order polynomial - RRR = 30	5.01 %	< 5 %	0.01 %	150 - 400	White & Minges (1996)
	3-order polynomial - RRR = 100	5.04 %	< 5 %	0.04 %	150 - 400	White & Minges (1996)
	3-order polynomial - RRR = 300	5.01 %	< 5 %	0.01 %	150 - 400	White & Minges (1996)
	3-order polynomial - RRR = 1000	5.10 %	< 5 %	0.10 %	150 - 400	White & Minges (1996)
	3-order polynomial - RRR = 3000	5.03 %	< 5 %	0.03 %	150 - 400	White & Minges (1996)
Heat capacity	White & Collocott 1984 (25 - 300 K)	0.30 %	0.003	-	25 - 300	White & Collocott (1984)
	White & Collocott 1984 (300 - 1300 K)	2.20 %	0.02	0.20 %	300 - 1300	White & Collocott (1984)

Table 11. Uncertainty of polyethylene.

Property	Model	Total δ	Literature δ	Curve fit δ	Range [K]	Literature source
Heat capacity	5-order polynomial - Amorphous - Chang (1974)	0.15 %	0.01 %	0.14 %	500 - 360	Chang (1974)
	5-order polynomial - Crystalline - Chang (1974)	0.37 %	0.01 %	0.36 %	500 - 360	Chang (1974)
	5-order polynomial - Average - Chang (1974)	0.20 %	0.01 %	0.19 %	500 - 360	Chang (1974)

Table 12. Uncertainty of ethylene glycol.

Property	Model	Total δ	Literature δ	Curve fit δ	Range [K]	Literature source
Density	Sun & Teja (2004)	0.08 %	0.08 %	-	Extended from 290 - 450 to 273.15 - 450	Sun & Teja (2004)
Viscosity	Sun & Teja (2004)	2.07 %	2.07 %	-	Extended from 290 - 450 to 273.15 - 450	Sun & Teja (2004)
Thermal conductivity	Sun & Teja (2004)	0.91 %	0.91 %	-	Extended from 290 - 450 to 273.15 - 450	Sun & Teja (2004)
Heat capacity	Project DIPPR 801	< 1 %	< 1 %	-	260.15 - 690.24	Project DIPPR 801

Table 13. Uncertainty of propylene glycol.

Property	Model	Total δ	Literature δ	Curve fit δ	Range [K]	Literature source
Density	Sun & Teja (2003)	0.04 %	0.04 %	-	Extended from 290 - 450 to 273.15 - 450	Sun & Teja (2003)
Viscosity	Sun & Teja (2003)	0.95 %	0.95 %	-	Extended from 290 - 450 to 273.15 - 450	Sun & Teja (2003)
Thermal conductivity	Sun & Teja (2003)	0.51 %	0.51 %	-	Extended from 290 - 450 to 273.15 - 450	Sun & Teja (2003)
Heat capacity	Project DIPPR 801	< 3 %	< 3 %	-	213.15 - 600	Project DIPPR 801

APPENDIX C – Thermophysical properties of humid air

CONTENT

Modeling the heat transfer at the interface of ice and humid air needs the evaluation of convective heat transfer coefficient by external convection. The heat transfer coefficient can be obtained by first understanding the equations of (11), (12), and (13) and by defining the temperature and velocity fields on top of the ice rink. The calculations should be carried out with numerical 3-dimensional simulations (CFD), which can take account, for example, the movement of the players on top of the ice rink and the orientation of the air blowers.

This Appendix presents the thermophysical properties of humid air. The information is required to calculate the properties of porous concrete. However, it also provides a framework for the property functions included in the thermophysical property module. The parameters of the functions are presented in Appendix A.

Humid air is treated as an ideal gas because the properties are measured in atmospheric conditions. It is a mixture of dry air and saturated steam.

$$m_{HA} = m_{DA} + m_S \tag{C.1}$$

In consequence, vapor quality is a function of partial pressures of dry air and steam

$$x = \frac{m_S}{m_{DA}} = \frac{M_S}{M_{DA}} \frac{n_S}{n_{DA}} = 0.6220 \left(\frac{p_r}{p - p_r}\right) \tag{C.2}$$

The relative vapor pressure of water is a product of relative humidity φ and vapor pressure of water at temperature T.

$$p_r = \varphi \cdot p_{sat} \tag{C.3}$$

Vapor pressure of water

The vapor pressure of water is presented by Equation (C.4) (Buck, 1981, 2012). It suits to model the vapor pressure on top of ice and water with a slight differential in parameter values.

$$p_{sat} = a_0 e^{\left(a_1 - \frac{T}{a_2}\right)\left(\frac{T}{a_3+T}\right)} \tag{C.4}$$

Besides, the data acquired from the industrial formulation of water IAPWS-IF97 supports the Equation (C.4) (Wagner and Kretzschmar, 2008). Figure 1 visualizes the property with Equation (C.4) and IAPWS-IF97. There is a precise observation of identical curves, which show a stiff consistency.
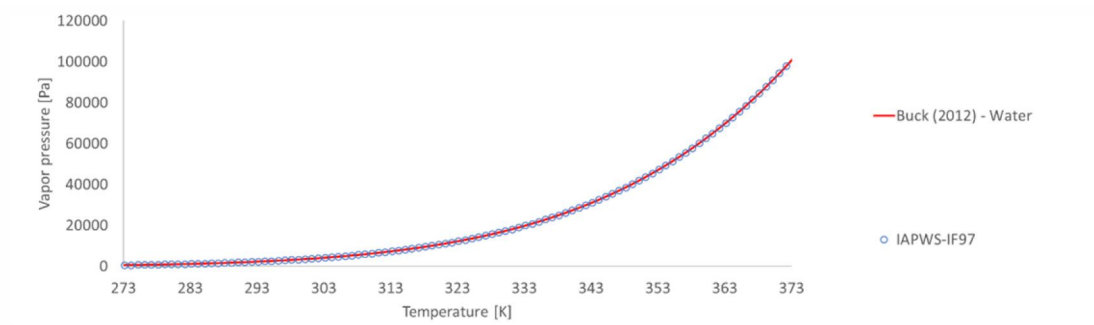

Figure 1. Vapor pressure of water as a function of temperature.

The density of humid air

It is useful to model the density of humid air by partial pressures through the ideal gas law. However, there are more advanced equations of states to calculate the density of humid air. The relation as a function pressure, and the temperature is easily obtainable with a reasonable uncertainty at low pressures ($p \approx 1$ atm). (Peng and Robinson, 1976; Lemmon *et al.*, 2000; Wagner and Kretzschmar, 2008)

$$\rho_{HA} = \frac{(p - p_{sat})M_{DA}}{\tilde{R}T} + \frac{P_{sat}M_S}{\tilde{R}T} \tag{C.5}$$

2

Thermal conductivity of humid air

Figure 2 represents the thermal conductivity of humid air as a function of temperature and relative humidity. The thermal conductivity of a gas mixture in low pressures is estimated by Wassiljeva (1904)

$$\lambda_{HA} = \sum_{i=1}^{n} \frac{y_i \lambda_i}{\sum_{j=1}^{n} y_j A_{ij}} \tag{C.6}$$

where n is the number of components and A_{ij} is obtained by the method by Lindsay and Bromley (1970) by

$$A_{ij} = \frac{1}{4} \left\{ 1 + \left[\frac{\eta_i}{\eta_j} \left(\frac{M_j}{M_i} \right)^{\frac{3}{4}} \left(\frac{T + \Omega_i}{T + \Omega_j} \right) \right]^{\frac{1}{2}} \right\}^2 \left(\frac{T + \Omega_{ij}}{T + \Omega_i} \right)$$

and

$$\Omega_{ij} = \Omega_{ji} = 0.73 \cdot \left(\Omega_i \Omega_j \right)^{\frac{1}{2}}$$

$$\Omega_i = 1.5 \cdot T_{sat_i}$$

where normal boiling points T_{sat} for dry air and water at atmospheric pressure are $78.8\ K$ and $373.15\ K$, respectively, and $A_{ii} = 0$. The method requires individual viscosities and thermal conductivities to be defined at a given temperature.

The thermal conductivity of dry air can be modeled by Equation (46). However, data by Stephan & Laesecke (1985) was used to optimize Equation (46) to reduce the total uncertainty. The study currently provides the most accurate theoretical model for the thermal conductivity of air. It evaluates the experimental data by 13 sources.

A 3-order polynomial curve was fitted to the industrial formulation of water to obtain thermal conductivity for steam (Huber *et al.*, 2012; Kretzschmar and Wagner, 2019). Alternatively, Equation (46) can be used.
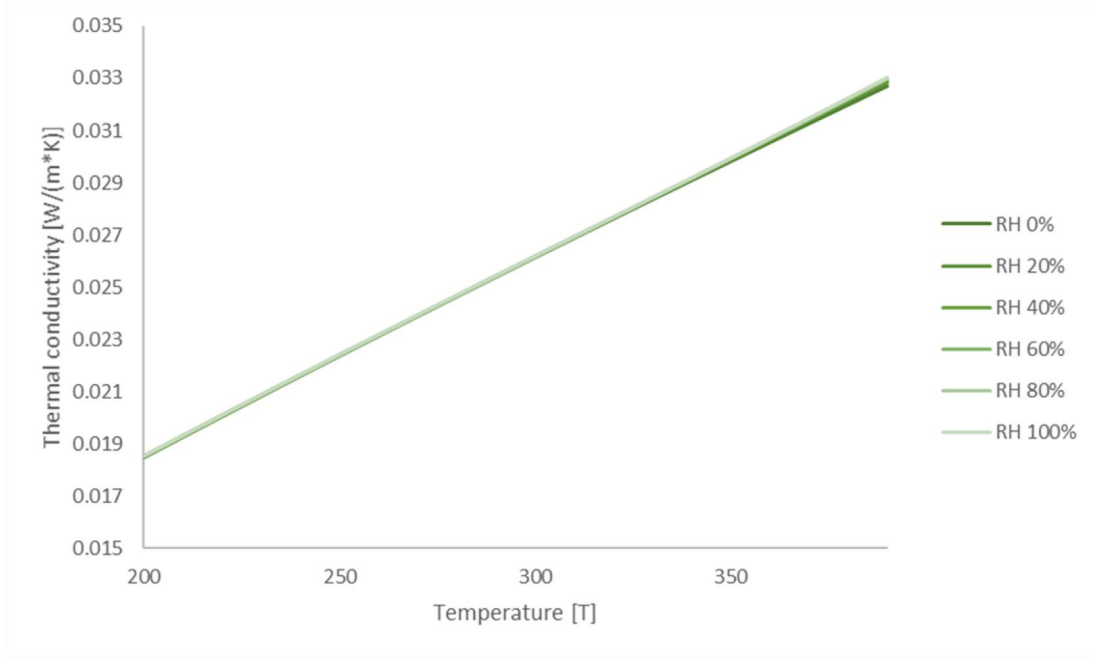
Figure 2. Thermal conductivity of humid air in atmospheric pressure as a function of temperature and relative humidity.

Dynamic viscosity of humid air

Figure 3 represents the viscosity of humid air as a function of relative humidity and temperature. A viscosity of gas mixture at low pressures is defined by Bromley & Wilke (1951) as

$$\eta_{HA} = \sum_{i=1}^{n} \frac{y_i \eta_i}{\sum_{j=1}^{n} y_j A_{ij}} \tag{C.7}$$

in which the interaction parameter A_{ij} is

$$A_{ij} = \frac{\left[1 + \left(\frac{\eta_i}{\eta_j}\right)^{\frac{1}{2}} \left(\frac{M_j}{M_i}\right)^{\frac{1}{4}}\right]^2}{\sqrt{8\left(1 + \left(\frac{M_i}{M_j}\right)\right)}}$$

where $A_{ii} = 1$. The uncertainty of the model is approximately 3 %.

By Project DIPPR 801, the viscosity for dry air is defined by Equation (46). However, the optimization for Equation (46) was made to match the EOS by Kadoya, Matsunaga, and Nagashima (1985) to minimize the error.

Moreover, the viscosity of saturated steam is defined by 4-order polynomial, fitted to the study of Huber et al. (2009). Alternatively, the dynamic viscosity can be presented by Equation (46).
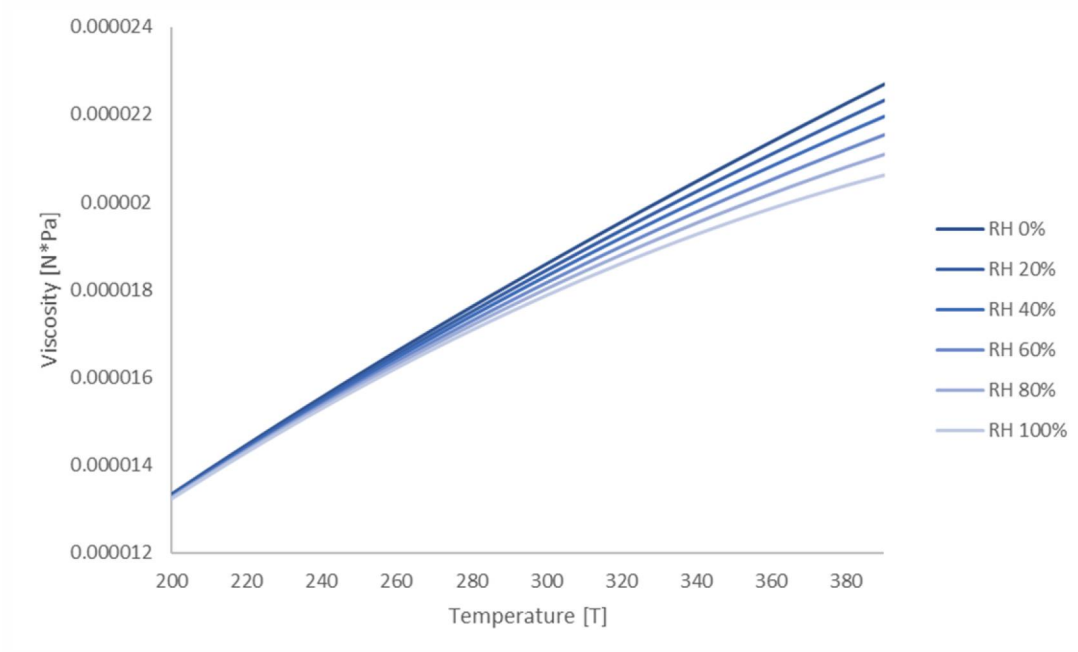

Figure 3. The viscosity of humid air at atmospheric pressure as a function of temperature and relative humidity.

Isobaric specific heat capacity of humid air

Figure 4 visualizes the isobaric heat capacity of humid air as a function of temperature and relative humidity. The law of mixtures approximates the property.

$$c_{pHA} = x \cdot c_{pS} + (1 - x) \cdot c_{pDA} \qquad (C.8)$$

The specific heat capacity of dry air can be presented by Touloukian and Makita (1970) by a 3-order polynomial equation with no additional curve-fitting or Lemmon et al. (2000) by 2-order polynomial with additional curve fitting. The uncertainty analysis shows that the error of both these models is equal. However, the selection of the model is based on minimum complexity. Thus, the model of Lemmon et al. (2000) is selected to model the heat capacity of dry air. Nevertheless, Project DIPPR 801 suggest a relation between heat capacity and temperature by Equation (48). However, the model is inconsistent with the other two.

Similarly, a specific heat capacity of saturated steam is presented as a 4-order polynomial equation, based on the industrial formulation of water IAPWS-IF97 (Wagner and Kretzschmar, 2008). Alternatively, Project DIPPR 801 presents the property by Equation (48).
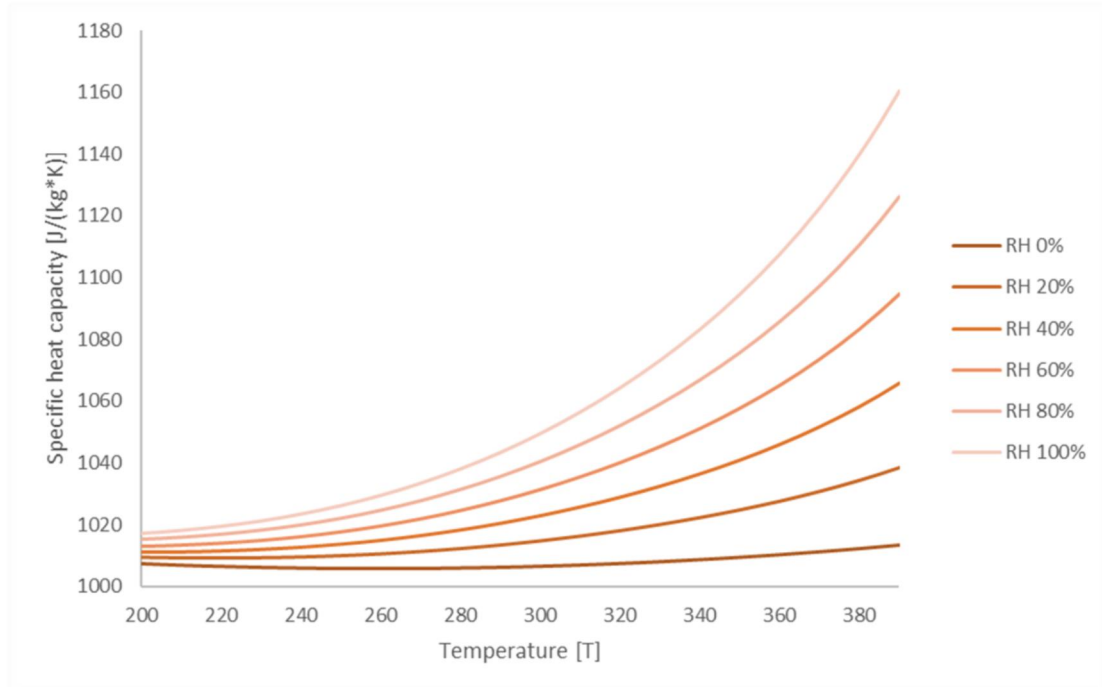

Figure 4. Isobaric specific heat capacity of humid air at atmospheric pressure as a function of temperature and atmospheric pressure. Correlations of Lemmon et al. (2000) and IAPWS-IF97 are used.

REFERENCES

Bromley, L. A., and Wilke, C. R. (1951) 'Viscosity Behavior of Gases', *Industrial & Engineering Chemistry*. American Chemical Society, 43(7), pp. 1641–1648. doi: 10.1021/ie50499a046.

Buck, A. L. (1981) 'New equations for computing vapour pressure and enhancement factor.', *Journal of Applied Meteorology*, pp. 1527–1532. doi: 10.1175/1520-0450(1981)0202.0.CO;2.

Buck, A. L. (2012) 'Buck research cr-1a user's manual', *Buck Research Instruments: Boulder, CO, USA*.

Huber, M. L. *et al.* (2009) 'New International Formulation for the Viscosity of H2O', *Journal of Physical and Chemical Reference Data*. American Institute of Physics, 38(2), pp. 101–125. doi: 10.1063/1.3088050.

Huber, M. L. *et al.* (2012) 'New International Formulation for the Thermal Conductivity of H2O', *Journal of Physical and Chemical Reference Data*. American Institute of Physics, 41(3), p. 33102. doi: 10.1063/1.4738955.

Kadoya, K., Matsunaga, N. and Nagashima, A. (1985) 'Viscosity and Thermal Conductivity of Dry Air in the Gaseous Phase', *Journal of Physical and Chemical Reference Data*. American Institute of Physics, 14(4), pp. 947–970. doi: 10.1063/1.555744.

Kretzschmar, H.-J. and Wagner, W. (2019) *International Steam Tables: Properties of Water and Steam Based on the Industrial Formulation IAPWS-IF97*. Springer.

Lemmon, E. W. *et al.* (2000) 'Thermodynamic Properties of Air and Mixtures of Nitrogen, Argon, and Oxygen From 60 to 2000 K at Pressures to 2000 MPa', *Journal of Physical and Chemical Reference Data*. American Institute of Physics, 29(3), pp. 331–385. doi: 10.1063/1.1285884.

Lindsay, A. L., and Bromley, L. A. (1970) 'Thermal Conductivity of Gas Mixtures', (10), pp. 15–18. doi: 10.1021/ie50488a017.

Peng, D. Y. and Robinson, D. B. (1976) 'A new two-constant equation of state', *Ind. Eng. Chem. Fundam.*, 15(1), pp. 59–64.

Stephan, K. and Laesecke, A. (1985) 'The Thermal Conductivity of Fluid Air', *Journal of Physical and Chemical Reference Data*. American Institute of Physics, 14(1), pp. 227–234. doi: 10.1063/1.555749.

Touloukian, Y. S. and Makita, T. (1970) *Thermophysical Properties of Matter*. Volume 6: Thermophysical and electronic properties information analysis center (The TPRC Data Series).

Wagner, W., and Kretzschmar, H.-J. (eds) (2008) 'IAPWS Industrial Formulation 1997 for the Thermodynamic Properties of Water and Steam', in *International Steam Tables: Properties of Water and Steam Based on the Industrial Formulation IAPWS-IF97*. Berlin, Heidelberg: Springer Berlin Heidelberg, pp. 7–150. doi: 10.1007/978-3-540-74234-0_3.

Wassiljewa, A. (1904) 'Heat conduction in gas mixtures', *Physikalische Zeitschrift*, pp. 737–742.